Metal and Semiconductor Nanoparticle Self-Assembly

by

G. Daniel Lilly

A dissertation submitted in partial fulfillment
of the requirements for the degree of
Doctor of Philosophy
(Chemical Engineering)
in The University of Michigan
2009

Doctoral Committee:

Professor Nicholas A. Kotov, Chair
Professor Sharon C. Glotzer
Professor Xiaoqing Pan
Assistant Professor Suljo Linic

2009

To my wife, Michelle M. Lilly, Ph.D.
To my mother and father, Nancy N. and G. Bud Lilly

ACKNOWLEDGEMENTS

I would like to thank my loving and lovely wife Michelle for her support through the process of obtaining my Ph.D. If not for her support and advice I most likely would not have finished this process. I value her as a friend and partner and am forever appreciative of her actions.

I would also like to thank my parents for laying the groundwork in my life to accomplish this. They taught me the value of hard work and persistence when reaching toward your goals, and without these lessons I most likely would not have even gone to graduate school, much less finished.

I am appreciative for all the help and support my fellow lab members have given me over the last five years. Former lab members Jaebeom Lee, Zhiyong Tang, Paul Podsiadlo, Bongsup Ship, Jungwoo Lee and Kevin Critchley helped teach me new lab techniques, NP synthesis and conjugation techniques, and numerous analysis procedures, and allowed me a venue to discuss my hypotheses concerning these approaches. Current lab members Meghan Cuddihy, Edward Jan, Peter Ho, Ashish Agarwal, Christine Andres, Jian Zhu, Huanan Zhang, Elizabeth Stewart, Yichun Wang, Inigo Alvarez, Shimei Xu, and Anna Fernandez aided with various collaborations, techniques, procedures, and experiences for which I am grateful.

I would like to thank my friends in Ann Arbor for their support through my graduate experience, both those related and unrelated to my studies. They gave me a group with similar experiences on and with whom I could lean on and share my experience.

I am indebted to my committee members, Suljo Linic, Sharon Glotzer, and Xiaoqing Pan for committing their time and effort to ensuring that my thesis is technically sound and is a contribution to my field.

Finally, I would like to thank my advisor, Nicholas A. Kotov, for supporting my research both financially and intellectually. Without both, I am sure that obtaining a Ph.D. would have been impossible. I have had invaluable experiences with all aspects of the research including collaborations, proposals, papers, etc. He is a smart and gracious person to whom I will always be indebted.

TABLE OF CONTENTS

LIST OF FIGURES

LIST OF ABBREVIATIONS

Ab	Antibody
AFM	Atomic Force Microscopy
BSA	Bovine Serum Albumin
CD	Circular Dichroism
CNT	Carbon Nanotubes
CTAB	Cetyltrimethylammonium bromide
CVD	Chemical Vapor Deposition
DLS	Dynamic Light Scattering
DMSO	Dimethyl Sulfoxide
DPN	Dip-Pen Nanolithography
EDC	1-ethyl-3(3-dimethylaminopropyl) carbodiimide hydrochloride
EDS	Energy Dispersive Spectroscopy
EHP	Electron Hole Pair
EMAL	Electron Microbeam Analytical Laboratory
FET	Field Effect Transistor
FRET	Förster Resonance Energy Transfer
HRTEM	High Resolution Transmission Electron Microscopy
LBL	Layer by Layer
LED	Light Emitting Diode
NIM	Negative Index Material
NP	Nanoparticle
NR	Nanoribbon
NW	Nanowire
OSC	Organic Semiconductor
PDDA	Poly(diallyldimethylammonium chloride)
PDMS	Polydimethylsilozane
PEG	Polyethylene Glycol
PL	Photoluminescence
QD	Quantum Dot
SEM	Scanning Electron Microscopy
SERS	Surface Enhanced Raman Scattering
SLS	Solution Liquid Solid
STEM	Scanning Transmission Electron Microscopy
Sulfo-NHS	N-hydroxysulfo-succinimide
TEM	Transmission Electron Microscopy
TGA	Thioglycolic Acid
UV	Ultraviolet
VLS	Vapor Liquid Solid

VS	Vapor Solid
XSC	Exciton Solar Cell

ABSTRACT

The field of nanotechnology is rapidly growing and faces numerous challenges to its further growth and development. Many new types of nanomaterials and applications for these materials have been developed recently; however, most of the processes by which nanomaterials and nanodevices are produced are top-down processes that are time consuming, expensive, and not practical for scale-up and commercialization. These top-down processes work by creating smaller assemblies and structures from larger ones, or physically manipulating nanomaterials using external forces. On the other hand, bottom-up synthesis and assembly techniques rely on smaller interactions between nanomaterials to guide their self-assembly. These bottom-up techniques, once properly mastered, allow for the economic scale-up of nanomaterial synthesis and nanodevice production.

The present thesis focuses on two areas of nanoparticle self-assembly, the first is the spontaneous self-assembly and subsequent recrystallization of semiconductor nanoparticles into nanowires. The self-assembly and recrystallization of CdTe nanoparticles into CdTe nanowires, as well as the effect of the solution properties on the mechanism governing this process, is investigated. Specifically, the effect of dimethyl sulfoxide on the CdTe nanoparticle reorganization into pearl necklace agglomerates, and its effect on Ostwald ripening, which triggers the recrystallization of the pearl necklace agglomerates into nanowires, is studied. The decomposition of CdTe and CdSe nanoparticles into Te and Te/Se nanowires is also studied with particular emphasis on the

effect of Se on the aspect ratio and tortuosity on the Te nanowire formation. Finally, the placement of Au nanoparticles and coatings on twisted CdTe nanoribbons by soaking the nanoribbons in $HAuCl_4$ is studied with the objective of creating metallic chiral structures for use in negative index materials. There is a particular emphasis on the effect of crystallinity of the CdTe nanoribbons and the soak time on the type of Au deposition. The second area of this thesis is the spontaneous self-assembly of various types of nanomaterials for applications; namely, the electrostatically driven self-assembly of large, positively charged Au nanoparticles and small, negatively charged CdSe/ZnS quantum dots into higher ordered core/shell assemblies whose structure and photoluminescent properties are responsive to the environment.

CHAPTER 1

INTRODUCTION

1.1 SPECIFIC AIMS

1.11 SPECIFIC AIM 1

The specific aim of the present series of studies is to use NP self-assembly to create novel NW synthesis techniques. Specifically, the focus is on recrystallization of CdTe NPs into NWs and modification of chiral, semiconductor NRs with metals to create chiral metal NRs for use in NIMs.

1.1.2 SPECIFIC AIM 2

The secondary aim is to use NP self-assembly to create hybrid nanostructures of metallic and semiconductor NPs whose PL intensity shifts upon conjugation, and in response to environmental stimuli.

1.2 SIGNIFICANCE

The use of nanomaterials offers the ability to both improve existing technologies and create new, unforeseen applications. One of the major challenges concerning NP synthesis and potential applications containing NPs is the controlled design of such systems. NPs must be synthesized to possess desired surface properties, composition,

geometry, and structure. NPs must be arranged properly for specific applications containing them to work. Two general methods exist concerning the controlled synthesis and arrangement of NPs: top-down and bottom-up methods. Top-down methods involve the creation of nanoscale objects/devices from larger ones, or the physical manipulation of nanoscale objects with larger ones; while bottom-up techniques focus on tuning the NP surface properties and their environment so that the NP synthesis/organization happens automatically. Top-down techniques are currently more common, however, bottom-up methods are desirable because they are more easily scalable, and thus cheaper than top-down options. The present research focuses on the use of bottom-up NP self-assembly techniques to 1) create novel NW synthesis techniques, and 2) create hybrid structures of metal and semiconductor NPs whose PL properties respond to environmental stimuli.

Many current NW synthesis techniques involve the use of templates or points of origin. These methods can be cumbersome and many result in polycrystalline NWs. In addition, many of the solution based NW synthesis methods use organic solvents. The series of research findings presented here offers a simple, aqueous, reproducible method to control the reorganization of semiconductor NPs into NWs. Furthermore, chiral metal nanostructures, which have potential applications as NIMs, have also proven difficult to synthesize, and often their chirality originates from chiral molecules used to stabilize the NP. Presented in this thesis is a method to coat chiral, twisted CdTe NRs with Au, creating chiral metallic nanostructures.

Common NP applications involve arrays of NPs/NWs that are arranged on substrates in specific patterns via top-down techniques. These applications are difficult to produce and rely on NPs that are tethered to a substrate and are no longer dispersed in

a medium. Other solution based NP assemblies involve cumbersome conjugation techniques that further destabilize the NP assembly and prove difficult to scale. Presented in this thesis is a solution based NP assembly method whereby metallic and semiconductor NPs self assemble into core/shell structures that are held together with electrostatic interactions, eliminating the need for complex tethers. The PL intensity of this system is dependent on the environment, allowing the NPs to be used as solution based sensors. Moreover, the semiconductor NPs used are core/shell, providing a much more robust QD that is not easily quenched and is stable in many environments.

1.3 BACKGROUND

1.3.1 NW Synthesis Techniques

NWs are synthesized using a variety of techniques, each with inherent advantages and disadvantages. Top-down NW synthesis techniques offer the ability to synthesize ordered arrays of NWs, typically by using lithographic and template based processes. Bottom-up techniques include point-oriented NW techniques and solution based techniques. Several of these NW synthesis techniques involve a combination of both top-down and bottom-up techniques. Each general technique involves many variations and can be made to produce a variety of NW types.

Top-down NW Synthesis Techniques. The most common synthesis of materials on a nanoscale is done using lithographic techniques. Generally speaking, lithography is the patterning of a substrate using a mask. Typically, a substrate (most commonly a silicon wafer) is coated with a photoresist (typically by spin coating) over which a mask with the desired pattern is placed. The substrate is then irradiated either with visible light,

ultraviolet light, x-rays, or electrons; and the substrate is rinsed in a solvent to develop the image. When a positive photoresist is used, irradiation weakens the photoresist, allowing it to be removed by rinsing. When a negative photoresist is used, irradiation strengthens the photoresist, so that washing removes the non-irradiated regions. The patterned substrate can then be exposed to various steps of etching and ion bombardment to create nanopatterned substrates[1].

NWs may be made using lithographic processes by patterning lines of photoresist onto a semiconductor substrate of the desired NW material. This substrate is then chemically etched. The photoresist protects the covered substrate, allowing the patterned NWs to be removed from substrate[2]. The resulting NWs are composed of the same material as the substrate, with common materials including Si and GaAs[2]. The smallest dimensions reported by this technique are 10nm in thickness, depending on the type of irradiation used. Typically irradiation with lower wavelengths produces patterns and/or NWs with smaller dimensions[2].

Other types of NWs may be synthesized using more exotic types of lithography or by combining lithography with other techniques, such as transfer printing, templating techniques discussed later in this section, and point-oriented NW synthesis techniques discussed in this section. Transfer printing can be used to remove patterned NWs from substrates with a polymer stamp, typically PDMS. NWs adhere to the PDMS stamp typically by Van der Waals forces[3], but the stamp surface may be tuned with plasma so that its surface can become hydrophilic and a variety of chemistries can be used to transfer the NWs to the stamp[2]. The NWs can then be deposited on numerous substrates with varied chemistries to produce ordered materials that are further discussed later in

this section. Depending on the properties of the substrate, the resulting NWs can lay in a variety of conformations, including wavy NWs[2].

Lithographic processes are the most common source of nanopatterning and nanofabrication. However, the features created by lithography are limited by the wavelength of irradiation used[1]. Lithography is also a very difficult process that requires numerous steps and a very clean environment that make it a time consuming and expensive process.

NW synthesis using templates involves the use of a template to guide the growth of a NW. The most common materials used as templates are porous membranes. Alumina template membranes are prepared from aluminum metal that is polished and anodized using a procedure that results in a thin porous alumina membrane[4]. The pores are uniform, non-intersecting, densely packed (10^{11} pore per square cm)[4], and have a range of pore diameters from 5-250 nm[4]. The thickness of alumina templates, which governs the length of the resulting NWs, can be controlled by adjusting the anodization time[5]. Polymer membranes are also used in the preparation of NWs[6]. Here, polymer membranes (usually polycarbonate or polyester), are bombarded with ions to create weak areas which are then chemically etched to create uniform pores[7]. The pores have uniform diameters, but unlike alumina membranes, they often intersect, which can make the synthesis of uniform NWs difficult[6]. Other, less common, porous membranes that are used as NW templates include glass, xeolite[7], and mesoporous silica[8].

Templates are used to make NWs using a variety of methods. The most common method is electrochemical deposition[6,9,10]. In this method, a conductive material is coated on one side of the membrane to act as a cathode. The membrane is then immersed

in a solution containing the desired materials like metals (Au, Ag, Sn, Cu, Ni, Co, Pt, Pd, Pb, Fe, Zn, Bi), conductive polymers (polypyrrole, polyaniline, poly(3-methylthiophene)), and semiconductors (ZnO, II-IV semiconductors)[6]. When an electrical current is applied to the system, the materials are deposited into the membrane pores[11]. The membrane is subsequently removed (usually by chemical dissolution), leaving the NWs in ordered arrays on the substrate[6]. The substrate onto which the NWs are grown can be patterned using techniques like lithography to create ordered arrays of NWs on the substrate[12], which can aid in device fabrication as discussed in Section 1.3.2.

Segmented NWs, which consist of two or more materials, can be synthesized using sequential electrochemical deposition with two different materials[13]. Templates can be used to make nonconducting NWs as well. Electroless deposition chemically plates a material onto a template surface, which causes the NW to grow radially instead of axially, as with electrochemical deposition[14]. Templated growth of nonconductive polymer NWs can occur by the chemical polymerization of monomers into polymers in the template membrane[7]. CVD may also be used to create NWs from templates[15]. Most of these techniques result in amorphous or polycrystalline NWs that may be unsuitable for most applications[8].

Additional templating techniques for NW synthesis include the use of carbon nanotubes to create various types of NWs including silica, vanadium pentoxide, molybdenum oxide, zirconia, silicon, boron nitride, and platinium[9]. As with previous methods, the carbon nanotubes are filled with the desired material and then the carbon nanotubes are removed, usually by heating in air. NWs that are difficult to synthesize

directly using the above techniques may be synthesized by the conversion of one type of NW into another; for example, Ag_2Se NWs are synthesized against trigonal Se NWs[16].

Bottom-Up NW Synthesis Techniques. Point oriented NW synthesis methods involve the use of a seed NP to grow NWs. The VLS process is the most common, and most commonly consists of two steps: 1) a top-down method where the substrate is covered in metal NPs and 2) a bottom-up where NWs are grown from the metal NPs. This method was pioneered by Wagner et al[17] in the 1960s[10]. In the top-down first step, metal clusters (typically gold) are placed on a clean substrate (typically semiconductor wafers), and the substrate is heated until the metal clusters liquefy. The metal clusters may be patterned on the substrate by various lithographic techniques, to prepare ordered arrays of NWs.

In the bottom-up second step, a gas containing the desired NW material is then passed over the metal droplets. The gas then diffuses into the metal droplet on the substrate. When the metal droplet is supersaturated, the NW material precipitates onto the substrate, forming a NW. As this process continues, a NW is formed that is attached at the substrate and grows at the tip containing the metal droplet. The process produces single crystalline NWs that have the same diameter as the metal droplet. The length of the NW is determined by the time and rate of the dissolution of the gas phase into the metal droplet, and subsequent precipitation of the NW material onto the substrate[8,10,18,19]. Many types of NWs can be produced using this method including Si[20], III-V semiconductors such as GaAs, InGaAs, GaP, InP, and InAs [8,21], II-IV semiconductors such as ZnS, ZnSe, CdS, and CdSe[8], and oxides such as ZnO, MgO, and SiO_2[8,22].

A similar NW synthesis method is the VS process. In this technique, a gas containing the desired NW material is produced, creating a supersaturated atmosphere. The gas is then passed over a substrate, where it precipitates at any defects in the substrate surface. The length and morphology of the NWs are determined by the level of supersaturation in the atmosphere[8,10]. This method is usually used to produce oxide NWs such as MgO, Al_2O_3, ZnO, and SnO_2[23].

Another gas phase point oriented process is oxide assisted laser ablation[8]. In this relatively new method, a laser is focused on a target of Si and SiO_2 powder. The laser evaporates the powder, creating a silicon oxide gas. The silicon oxide then decomposes into elemental silicon, which precipitates to form Si NPs. The NPs then grow into Si NWs coated with a SiO_2 shell[24-26].

There are also solution based point oriented NW synthesis procedures such as SLS and supercritical fluid procedures. The SLS method is similar to the VLS method, except the NW growth material is suspended in an organic solution instead of a vapor[8]. This procedure has been used to produce InP, InAs, and GaAs NWs[27]. In the supercritical fluid procedure, Si NWs have been grown with Au NP seeds in supercritical hexane and diphenylsilane, a silicone precursor molecule[28]. The process is similar to VLS and SLS processes in that silicon dissolves into the Au NP seeds until they are supersaturated. The silicon then precipitates into a NW with the same diameter as the Au NP[8].

Solution based NW synthesis techniques offer the ability to form NWs without the use of a template or point of origin, and most are truly bottom-up techniques. Since solution based techniques are truly bottom-up, they are usually simpler than template and

point oriented procedures[29]. However, the NWs produced using solution methods are often less homogenous and have lower aspect ratios[10]. The governing principle in solution based processes is that most NPs have a crystal face with a higher surface energy than the other faces. When exposed to the proper conditions, the higher energy face of the NP grows, reducing the overall energy of the structure and creating a NW[10]. Various methods involve using surfactants and capping agents to help direct the growth of NWs; and controlling the growth environment to help dictate the composition of the NW. The capping agents, such as biomolecular, organic amines, polymers, organic macromolecules, , organic salts, and alkane thiols, help manipulate the surface energies of the NP, which allows NWs to grow[10].

The growth of lanthanide hydroxide nanowires of the form $La(OH)_3$ occurred in this fashion by exposing $La(OH)_3$ NPs to elevated temperatures[30]. Variations of this method have allowed NWs with a variety of compositions to be synthesized. Te and Se NWs have been synthesized by the decomposition of CdTe and CdSe NPs into NWs and nanochecks[31,32]. In this procedure, a cadmium complexing agent is added to the NPs, causing Te^{2-} ions to be released into the solution. The Te^{2-} ions are then oxidized into elemental Te seeds, which subsequently grow into Te NWs and nanochecks. A similar process occurs with CdSe NP decomposition into NWs.

Another form of solution based NW synthesis is the spontaneous self-assembly of II-IV NPs into NWs and nanosheets. In NW self-assembly, presented by Tang et al[33], the stabilizers of II-IV NPs are partially removed, allowing the NPs to orient themselves into a pearl necklace arrangement which is driven by the large dipole moment of the NPs. The pearl necklace agglomerates then recrystallize into CdTe NWs. This method allows

the spontaneous, aqueous assembly of NPs into NWs. However, the resulting NWs have inconsistent growth times, short aspect ratios, and highly variable lengths. In nanosheets self-assembly, also presented by Tang et al[34], positively charged CdTe NPs arrange into fluorescent free-floating sheets. In both cases, the solution and NP properties interact to guide the NP self-assembly into NWs and nanosheets.

1.3.2 NP Assembly for Applications

NPs may be assembled using a variety of techniques. As with NW synthesis, the most common techniques for NP assembly are top-down, including previously discussed procedures such as lithography, templating, and transfer printing; as well as other procedures such as dip-pen nanolithography, fluid-assisted assembly, and LBL thin-film assembly. Bottom-up NP assembly techniques involve NP self-assembly that is guided by various methods including bioconjugation, electrostatic interactions, stearic interactions. These techniques allow the synthesis of various photonic devices, electronic devices, and sensing devices.

Top-down NP Assembly for Applications. Many top-down NP assembly techniques are two-fold. The first step involves patterning the substrate using techniques such as lithography and dip-pen; the second step involves the overlay of nanomaterials onto these patterned substrates using various methods including atomic force microscopy (AFM), fluidics, and electrical field induced alignment[8] to make useful devices. As discussed previously, the most common technique to produce ordered nanoscale structures is lithography. While still a time consuming and expensive process that is somewhat limited in the size with which nanostructures may be produced (owing to the

resolution limits in the wavelength of irradiation used to create the nanostructures), it is commonly used to prepare the backbone of many nanoscale devices.

DPN is another technique used to pattern substrates that was developed by the C. Mirkin group at Northwestern University. This technique uses an AFM tip to deliver a material directly onto a substrate, much as a fountain-tip pen delivers ink to a page[35,36]. This method allows for any molecule that will adhere to the substrate (thiols on gold surfaces for example) to be patterned onto a substrate using an AFM tip. This application tool is very small and can be controlled with resolution down to 5 nm. This technique may also be applied in parallel using multiple AFM tips simultaneously to scale up the process.

In addition to patterning substrates with molecules, as with DPN[36], AFM is also used to physically manipulate and move nanomaterials around on substrates[37]. One such method grows CNTs on an AFM tip, then using AFM, breaks the CNT off at the desired location to deposit the CNT[38]. Obviously, this is a very tedious, time consuming method that is difficult to scale up.

One of the more common and useful techniques to order nanomaterials onto patterned substrates is using fluids to carry the nanomaterials into position. This method was pioneered by the C. Lieber group at Harvard University. In this technique, a shear force generated by a laminar flowing liquid in a microfluidic device aligns NWs in a parallel orientation. The NW containing fluid is passed over a patterned substrate, where the NW adheres[39,40]. This process typically is used to suspend NWs over previously patterned electrodes in the substrate, and can be manipulated to create crossed NWs to

give various nano-circuits. This process offers quicker and more efficient NW organization than AFM assisted assembly techniques[37].

Another technique to arrange nanomaterials onto substrates is by the application of an external force, such as that generated by an electronic[41] or magnetic field[42]. In the case of magnetic fields, magnetic NWs are immobilized on substrates patterned with magnetic trapping sites. NWs can be segmented with various materials to help determine which part of the NW is immobilized on the substrate[42]. External electronic fields generated between electrodes can also allow NWs to align on a substrate[43]. Parallel NWs align between parallel electrodes[44], and by rotating the field, the NWs may be crossed.

LBL films can also be used to create layers of nanomaterials on a substrate[45]. In this technique, hybrid organic/inorganic layers of oppositely charged materials are layered onto a substrate. This is typically done by dipping the substrate into one material, rinsing, and then dipping it into the next material, rinsing, and repeating the process until the desired number of bilayers has been reached. This can be done with nanomaterials to create sandwiches of nanomaterials in other materials such as PDDA.

Finally, NW arrays may be grown onto patterned substrates to give ordered vertical arrays of NWs[46]. Such arrays are typically grown by point oriented process such as VLS.

Many types of devices can be used with one, or a combination of several, of the above techniques. For example, NWs have found uses in many electronic devices including resistors, switches, inverters, field emitters, and transistors. Many types of metal and polymer NWs are used as resistors[6] including Pt-Ni-Pt NWs[47], Ni-Au-Ni NWs[48], Au-Sn-Au NWs[49], and Au-polypyrrole NWs[6]. Au Ppy Cd-Au NWs[50] and metal

NW/carbon nanotubes/polymer/semiconductor NWs[51] have successfully been made into diodes, which work by having a junction between p-type and n-type semiconductors. Si coated Ga-ZnS NWs[52] are sensitive to electron beam irradiation, allowing them to be used as switches in electron microscopy. NWs can be applied both as bipolar junction transistors and FET. N-type Si NWs have been configured over a p-type Si NW base to give bipolar junction transistors with good current gain[53]. FET transistors have been created using p-type Si NWs and n-type GaN NWs[54], and ZnO NWs on an SiC substrate[55]. N-type and p-type Si NWs have also been arranged into inverters[53], which convert direct current into alternating current. NWs can be used as switches in the form of diodes, which allow current to flow in only one direction, and using photoconductivity, where the NW increases conductivity under electromagnetic stimulation[6]. Au-CdSe-Au NWs[56] are used as light sensitive switches because their conductivity increases when exposed to light. The Kotov group has synthesized LBL thin films containing Te NWs and PDDA[57]. These films are sensitive to light exposure and provide another method of producing light sensitive switches. One application of SiC and Si NWs has been as field emitters[58,59].

Many of these electronic devices use the unique properties of semiconductor NWs that allows them to be used in various sensing devices. Often, these devices are produced using FETs, where a semiconductor NW is suspended between two electrodes, called the source and the drain. The length over which the NW passes is called the gate. A current is then passed through the NW, allowing the conductivity of the NW to be measured. Many NWs exhibit a conductivity change when the electric field or potential at the surface of the NW is varied. For p-type semiconductor NWs, increasing the gate voltage

reduces the carriers in the NW, which decreases the conductance. Conversely, decreasing the gate voltage increases the carriers in the NW, which increases the conductance. When conductivity passing through a NWs changes, the current passing through the FET also changes. By measuring the current changes in the FET, whatever caused the changes to the electric field or surface potential of the NW, can be sensed[60]. The concentration of hydrogen ions was the first application of FETs[61]. Here, 3-aminopropyltriethoxysilane is attached to p-type Si NWs, providing amino groups which may be protonated and deprotonated depending on pH. As pH is increased, the surface charge of the Si NW decreases causing its conductance to increase. By using the strategy of modifying the surface of the NW to allow various molecules to bind to the NW and change its surface charge, many new substances may be detected with NW FETs including ethanol[62]; ATP[63]; DNA[64]; proteins such as streptavidin[61], telomerase[65], prostate-specific antigen[66]; and viruses[67].

Many types of semiconductor NWs have been used in lasing applications[8,10,68]. The most common type of NW lasers is composed of ZnO. ZnO is suitable for lasing applications because of its large band gap (3.37 eV) and high exciton binding energy (60 meV)[8]. When stimulated by high excitation intensity, ZnO NWs have been reported to generate sharp peaks (0.3 nm width) in the excitation spectra. This lasing action occurs without the use of mirrors and it has been proposed that the ZnO NWs act as natural resonance cavities[8,69]. GaN NW lasers[70] and ZnS NW lasers[71] have also been reported, which work in a similar fashion as the ZnO lasers. It has been suggested that NWs with modulated compositions may have superior lasing action to homogenous NWs[10].

Semiconducting NWs are also used in light collecting devices such as solar cells. ZnO NW arrays are used in dye-sensitized solar cells (DSSCs). The DSSCs are assembled with arrays of ZnO NWs sandwiched between F:SnO substrates. The NWs are exposed to a sensitizing dye (cis-bis(isothiocyanato)bis(2,2”-bipyridyl-4,4’-dicarboxylato)-ruthenium(II)bistetrabutlyammonium), which aids in light absorbance. The structure is then filled with a tetrabutylammonium iodide electrolyte. These ZnO NW DSSCs can have optimum overall efficiency of 0.3%[72]. Longer NWs results in an increase in efficiency because more light can be harvested as a result of the increased surface area on longer NWs. CdSe NWs have also been used in photovoltaic devices. As with the ZnO DSSCs, CdSe is arranged into arrays that are sandwiched between a conducting glass slide and an Au electrode. This device exhibited a maximum efficiency of 0.16%[73].

Semiconductor NWs have also found uses as optical waveguides, which internally guide light through a material with a lower permittivity. Flexible NWs, or nanoribbons, comprised of materials such as SnO_2 and ZnO are used to direct light[68]. In one case, SnO_2 nanoribbons with diameters between 100 and 300 nm are placed on a silica substrate. When monochromatic light is focused on one end of the nanoribbon, it is guided through the structure and exits the opposite end[74,75]. These nanoribbon waveguides can be coupled with 50% power transfer efficiencies between two nanoribbons, arranged to create color filters, and eventually may be integrated and used in integrated optical logic devices[68].

Another optical device for which semiconducting NWs may be used is light emitting diodes (LEDs). Here, a NW is connected between electrodes and a current is

passed across the NW. If an n-type NW crosses a p-type NW, or the NW has a core/shell geometry of the two types, light is emitted when current is passed through it, creating an LED[68]. InP NWs[76], ZnO NWs[77], n-GaN/InGaN/p-GaN core/shell NWs[78], and GaAs and GaP NWs have all been used in LEDs[79].

Bottom-up NP Assembly for Applications. Bottom-up NP assembly is the self assembly of NPs into superstructures. This method relies on manipulating the surface chemistry, size, charge, and composition of the nanomaterials so that they organize themselves into desired structures that are useful for various applications.

The self-organization of nanomaterials in liquid environments involves the interplay of numerous forces between the nanoparticles, including steric, osmotic, van der Waals, Coulombic, charge-dipole, dipole-dipole, and charge-induced dipole, as is seen in Eq. 1.1[80].

$$V = V_{steric} + V_{osmotic} + V_{vdW} + V_{Coulomb} + V_{charge-dipole} + V_{dipole-dipole} + V_{charge-ind.dipole} \quad (1.1)$$

Assuming this is between two NPs, A and B, the van der Waals interactions are shown in Eq. 1.2,

$$V_{vdW} = -\frac{A}{12}\left\{\frac{S}{D[1+D/2(R_A+R_B]} + \frac{1}{1+\frac{D}{S}+D^2/4R_AR_B} + 2ln\left(\frac{D[1+D/2(R_A+R_B)]}{R\left[1+\frac{D}{S}+D^2/4R_AR_B\right]}\right)\right. \quad (1.2)$$

where A is the solvent-retarded Hamaker constant, S is the reduced radius and $S=2R_AR_B/(R_A+R_B)$, D is the distance of closest approach, R_A is the radius of NP A, and R_B is the radius of NP B[80]. The Coulombic potential is shown in Eq. 1.3,

$$V_{Coulombic} = \frac{Z_AZ_Be^2}{4\pi\varepsilon\varepsilon_0R} \quad (1.3)$$

where Z_A and Z_B are the charges of NP A and B, respectively, R is the center to center interparticle distance, and ε is the dielectric constant of the medium[80]. The charge-dipole potential is listed in Eq. 1.4.

$$V_{charge-dipole} = -\frac{e}{4\pi\varepsilon\varepsilon_0 R^2}(Z_A\mu_B\cos\theta_1 - Z_B\mu_A\cos\theta_2) \quad (1.4)$$

The dipole-dipole potential is shown in Eq. 1.5.

$$V_{dipole-dipole} = \frac{\mu_A\mu_B(2\cos\theta_2\cos\theta_2 - \sin\theta_1\sin\theta_2\cos(\varphi_2-\varphi_1))}{4\pi\varepsilon\varepsilon_0 R^3} \quad (1.5)$$

The charge-induced dipole is shown in Eq. 1.6,

$$V_{charge-induced\ dipole} = -\frac{e^2}{32\pi\varepsilon\varepsilon_0 R^4}(\alpha_A Z_B^2 + \alpha_B Z_A^2) \quad (1.6)$$

where μ_A and μ_B are the dipole moments of NPs A and B, respectively, θ_1, θ_2, φ_1, and φ_2 are orientation angles, and α_A and α_B are polarizabilities of NPs A and B, respectively[80]. Typically, the Coulombic potential is the largest, followed by the charge-dipole, dipole-dipole, charge-induced dipole, and finally van der Waals potential[80]. These forces can be manipulated by varying the stabilizer of the nanomaterial, which typically consists of an end that adheres to the NP surface (such as sulfur atoms to gold), a carbon chain, and a functional group, all of which can be varied to change the forces between the nanomaterials, the shape and composition of the nanomaterial, and the liquid in which the nanomaterial is dispersed.

Lattices of NPs can be ordered on substrates by controlling these forces while NPs precipitate from solution. Two-dimensional NP lattices can be created by evaporating solvent from the NP solution and controlling the NP concentration, type of

solvent, temperature, and substrate type[80]. In these arrays, the distance between the NPs is the thickness of the stabilizing layer on the individual NPs. Three-dimensional lattices of NPs can be made by similar evaporation methods, or by destabilizing the NPs in the solution by adding a nonsolvent such as alcohol to the solution[80,81]. The type of three-dimensional structure is dependent on the various properties of the NPs and liquid. Ordered three-dimensional arrays with multiple types and sizes of NPs are also possible using this method. This method also allows for the creation ordered structures of NWs [80,82]. Similar ordered lattices produced via drying can be created in template structures made from top-down process such as lithography[83].

NP superstructures can also be formed in solution by the manipulation of the forces discussed earlier. By increasing attractive forces such as an attractive Coulombic force from oppositely charged nanostructure, superstructures such as NP spotted NTs, fullerenes, and NWs can be created[84]. Other NP structures such as NP chains may be formed by reducing the repulsive force on like charged NPs by partially removing the stabilizers and allowing the dipole moments of the NPs to drive formation of pearl necklace agglomerates[85]. Superstructures can also be created by immersing hydrophobic NPs in aqueous media[84].

Finally, NP assemblies can be formed by the chemical conjugation of their stabilizers. The stabilizers of one NP may be directly tethered to those of another NP, a substrate, or other molecules such as polymers and biomolecules to produce ordered conjugates. Typically stabilizers with specific functional groups are chosen to make further conjugation possible. A common conjugation technique involves the reaction of a amine with a carboxylic acid to produce an amide bond[86,87]. A common method used for

this conjugation is using sulfo-NHS and EDC reaction shown in Figure 1.1[88]. This is a particularly effective technique given that many biomolecules and polymers contain these functional groups, including proteins, DNA, antigens and Abs, and amino acids.

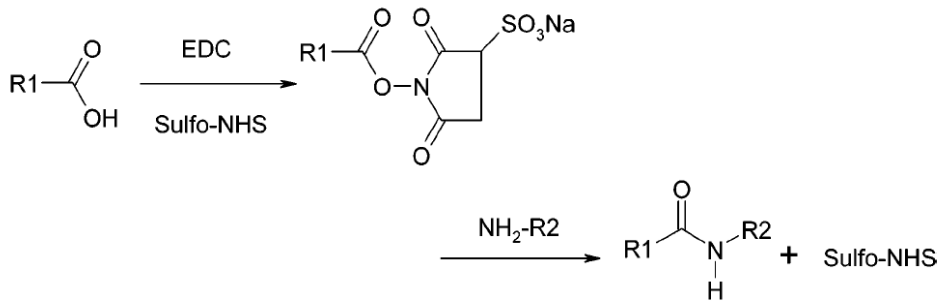

Figure 1.1. EDC/Sulfo-NHS conjugation scheme.

The Kotov group has developed several semiconductor NW assemblies whose PL properties behave differently than individual NWs. In one case, complimentary antigen/Abs are bound to l-cysteine stabilized CdTe NPs/NWs using the EDC/sulfo-NHS conjugation procedure shown in Figure 1.1. When NPs/NWs containing complimentary antigens and Abs are mixed, the proteins bind together, linking the NPs/NWs. When CdTe NPs/NWs of different sizes and PLs are closely attached, it is possible to observe FRET between the NPs/NWs. In this case, when NPs/NWs with overlapping PL spectra are bound closely, resonance dipole-dipole coupling allows an energy coupling of the NPs[88]. When green emitting CdTe NPs and red emitting CdTe NPs are linked in such a fashion using BSA and anti-BSA, the excitonic state of the green emitting CdTe NP is transferred to the red emitting CdTe NP, causing the green PL peak to decrease in intensity and the red PL peak to gain intensity[88]. Similar FRET effects have been shown with structures of CdTe NWs linked with CdTe NPs using biotin and streptavidin[89].

CdTe NW/Au NP structures have been made showing a PL enhancement and slight blue shift of the CdTe NW fluorescence[90]. Here a CdTe NW is surrounded by a shell of Au NPs using streptavidin and biotin linkage. The changes in the PL spectrum are similar to SERS and a result of a stimulation of the photon emission of the CdTe NW, which is a result of an electromagnetic field around the Au NPs. Similar structures have been produced using Ag NPs and CdTe NWs[91]. Again, a PL intensity enhancement and blue shift of the CdTe NW is seen. However, the PL changes are due to increase in absorption of the structure.

Other semiconductor NW sensors have been created based on changes in the PL of the NW. The Kotov group has created dynamic Au NP/CdTe NP assemblies that can vary their PL in response to the environment[90,92]. These assemblies consist of a CdTe NP surrounded by a shell of Au NPs. The PL intensity of the assembly is dependent on the interparticle distances of the Au NPs and the CdTe NP[93]. As the interparticle distance decreases, the PL intensity increases and the PL lifetime decreases; as the interparticle distance increases, the PL intensity decreases and the PL lifetime increases. This phenomenon is due to plasmon and exciton interactions of the Au NPs and the CdTe NPs in a similar fashion as the Au NP/CdTe NW assemblies discussed in section II.A.2. By connecting the Au NPs to the CdTe NPs with materials whose length varies in response to stimuli, these assemblies are made into sensors. A temperature sensor was produced which ties the Au NPs to the CdTe NP with PEG[92]. The radius of gyration of PEG is sensitive to temperature, so as temperatures increase the PEG relaxes and the interparticle distance increases, causing the PL intensity to decrease. As the temperature decreases, the PEG contracts, decreasing the interparticle distance, which causes the PL intensity to

increase. The Kotov group has also assembled CdTe NWs into nanocircuits on Si wafers using bovine serum albumin and anti-bovine serum albumin, complimentary antigen-Ab protein pairs[94].

1.4 EXPERIMENTAL

1.4.1 Chemicals

$Cd(ClO_4)_2 \cdot H_2O$ (cadmium perchlorate), $C_2H_4O_2S$ (thioglycolic acid, TGA), CH_3OH (methanol), $(CH_3)_2CHOH$ (2-propanol), C_2H_6OS (DMSO), $HAuCl_4$ (gold(III) chloride hydrate), CdO (cadmium oxide), H_2O_2 (hydrogen peroxide), H_2SO_4 (sulfuric acid), $(C_8H_{16}ClN)_n$ (poly(diallyldimethylammonium chloride), PDDA), $Zn(CH_3)_2$ (dimethyl zinc), $(CH_3)_3SiSSi(CH_3)_3$ (hexamethyldisilathiane, $(TMS)_2S$), $[CH_3(CH_2)_7]_3PO$ (trioctylphosphine oxide, TOPO), $[CH_3(CH_2)_3]_3P$ (tributylphosphine, TBP), Se (selenium powder), $CHCl_3$ (chloroform), $CH_3(CH_2)_{15}NH_2$ (hexadecylamine, HDA), were obtained from Sigma-Aldrich and used without further purification; Al_2Te (aluminum telluride) was obtained from Cerac, Inc and used without further purification; Na_2Se was obtained from Alfa Aesar and used without further purification; NaOH (sodium hydroxide) was obtained from Fluka and used without further purification; CH_3COCH_3 (acetone) was obtained from Fisher and used without further purification; and all water was purified using 18 MΩ deionized water (Barnstead E-pure system).

1.4.2 Equipment

AFM is performed with a Digital Instruments NanoScope IIIa surface probe microscope. AFM specimens are prepared on a silicon wafer cleaned with acetone and subsequently soaked in 0.5% PDDA. AFM images are analyzed using NanoScope ® III

software tools. Fluorospectroscopic measurements were made using a Jobin Yvon Horiba FluoroMax-3. TEM and HRTEM are conducted with a JEOL 3011 High Resolution Electron Microscope, and a JEOL 2010F High Resolution Electron Microscope. STEM is conducted with the JEOL 2010F High Resolution Electron Microscope. TEM specimens are prepared on an Ultrathin Carbon Film on Holey Carbon Support Film, 400 mesh grid supplied by Ted Pella, Inc that is soaked in 0.5% PDDA. SEM is conducted with a FEI Nova Nanolab Dualbeam Focused Ion Beam Workstation and Scanning Electron Microscope and a Philips XL30FEG. EDS is conducted with EDAX XEDS detectors on both the Philips XL30FEG SEM and the JEOL 2010F TEM. Centrifugation is performed with a Fisher Scientific Marathon 26 K M centrifuge with a Hermile 220.97.V02 rotor. Freeze drying is performed with a Labconco Freeze Dry System/Freezone 4.5. Optical micrographs are obtained with a Cytoviva dark field optical microscope.

1.5 REFERENCES

1. Internet Communication 2009.

2. Baca, A. J.; Ahn, J. H.; Sun, Y.; Meitl, M. A.; Menard, E.; Kim, H. S.; Choi, W. M.; Kim, D. H.; Huang, Y.; Rogers, J. A. Semiconductor wires and ribbons for high-performance flexible electronics. *Angew. Chem. , Int. Ed.* **2008,** *47* (30), 5524-5542.

3. Huang, Y. Y.; Zhou, W.; Hsia, K. J.; Menard, E.; Park, J. U.; Rogers, J. A.; Alleyne, A. G. Stamp Collapse in Soft Lithography. *Langmuir* **2005,** *21* (17), 8058-8068.

4. Masuda, H.; Fukuda, K. Ordered metal nanohole arrays made by a two-step replication of honeycomb structures of anodic alumina. *Science (Washington, D. C.)* **1995,** *268* (5216), 1466-1468.

5. Wade, T. L.; Wegrowe, J. E. Template synthesis of nanomaterials. *European Physical Journal: Applied Physics* **2005,** *29* (1), 3-22.

6. Hurst, S. J.; Payne, E. K.; Quin, L.; Mirkin, C. A. Multisegmented One-Dimensional Nanorods Prepared by Hard-Template Synthetic Methods. *Angewandte Chemie* **2006,** *45*, 2672-2692.

7. Martin, C. R. Nanomaterials: A Membrane-Based Synthetic Approach. *Science* **1994,** *266*, 1961-1966.

8. Yang, P.; Wu, Y.; Fan, R. Inorganic Semiconductor Nanowires. *International Journal of Nanoscience* **2002,** *1* (1), 1-39.

9. Huczko, A. Template-based synthesis of nanomaterials. *Applied Physics A* **2000,** *70*, 365-376.

10. Fan, H. J.; Werner, P.; Zacharias, M. Semiconductor nanowires: from self-organization to patterned growth. *Small* **2006,** *2* (6), 700-717.

11. Hulteen, J. C.; Martin, C. R. A general template-based method for the preparation of nanomaterials. *Journal of Materials Chemistry* **1997,** *7* (7), 1075-1087.

12. Matefi-Tempfli, S.; Matefi-Tempfli, M.; Piraux, L. Fabrication of nanowires and nanostructures: combining template synthesis with patterning methods. *Appl. Phys. A: Mater. Sci. Process.* **2009,** *96* (3), 603-608.

13. Lee, W.; Scholz, R.; Nielsch, K.; Goesele, U. A template-based electrochemical method for the synthesis of multisegmented metallic nanotubes. *Angewandte Chemie, International Edition* **2005,** *44* (37), 6050-6054.

14. Brumlik, C. J.; Menon, V. P.; Martin, C. R. Template synthesis of metal microtubule ensembles utilizing chemical, electrochemical, and vacuum deposition techniques. *Journal of Materials Research* **1994,** *9* (5), 1174-1183.

15. Cepak, V. M.; Hulteen, J. C.; Che, G.; Jirage, K. B.; Lakshmi, B. B.; Fisher, E. R.; Martin, C. R.; Yoneyama, H. Chemical Strategies for Template Syntheses of Composite Micro- and Nanostructures. *Chemistry of Materials* **1997,** *9* (5), 1065-1067.

16. Gates, B.; Wu, Y.; Yin, Y.; Yang, P.; Xia, Y. Single-Crystalline Nanowires of Ag_2Se Can Be Synthesized by Templating Against Nanowires of Trigonal Se. *J. Am. Chem. Soc.* **2001,** *123,* 11500-11501.

17. Wagner, R. S.; Ellis, W. C. The vapor-liquid-solid mechanism of crystal growth and its application to silicon. *Transactions of the American Institute of Mining, Metallurgical and Petroleum Engineers* **1965,** *233* (6), 1053-1064.

18. Yang, P.; Yan, H.; Mao, S.; Russo, R.; Johnson, J.; Saykally, R.; Morris, N.; Pham, J.; He, R.; Choi, H. J. Controlled growth of ZnO nanowires and their optical properties. *Advanced Functional Materials* **2002,** *12* (5), 323-331.

19. Banerjee, S.; Dan, A.; Chakravorty, D. Review. Synthesis of conducting nanowires. *Journal of Materials Science* **2002,** *37* (20), 4261-4271.

20. Morales, A. M.; Lieber, C. M. A laser ablation method for the synthesis of crystalline semiconductor nanowires. *Science (Washington, D. C.)* **1998,** *279* (5348), 208-211.

21. Haraguchi, K.; Katsuyama, T.; Hiruma, K.; Ogawa, K. Gallium arsenide p-n junction formed in quantum wire crystals. *Applied Physics Letters* **1992,** *60* (6), 745-747.

22. Huang, M. H.; Mao, S.; Feick, H.; Yan, H.; Wu, Y.; Kind, H.; Weber, E.; Russo, R.; Yang, P. Room-temperature ultraviolet nanowire nanolasers. *Science* **2001,** *292* (5523), 1897-1899.

23. Yang, P.; Lieber, C. M. Nanorod-superconductor composites: a pathway to materials with high critical current densities. *Science (Washington, D. C.)* **1996,** *273* (5283), 1836-1840.

24. Lee, S. T.; Wang, N.; Zhang, Y. F.; Tang, Y. H. Oxide-assisted semiconductor nanowire growth. *MRS Bulletin* **1999,** *24* (8), 36-42.

25. Lee, S. T.; Wang, N.; Lee, C. S. Semiconductor nanowires: synthesis, structure and properties. *Materials Science & Engineering, A: Structural Materials: Properties, Microstructure and Processing* **2000,** *A286* (1), 16-23.

26. Lee, S. T.; Zhang, Y. F.; Wang, N.; Tang, Y. H.; Bello, I.; Lee, C. S.; Chung, Y. W. Semiconductor nanowires from oxides. *Journal of Materials Research* **1999,** *14* (12), 4503-4507.

27. Trentler, T. J.; Suryanarayanan, R.; Sastry, S. M. L.; Buhro, W. E. Sonochemical synthesis of nanocrystalline molybdenum disilicide (MoSi2). *Materials Science & Engineering, A: Structural Materials: Properties, Microstructure and Processing* **1995,** *A204* (1-2), 193-196.

28. Holmes, J. D.; Johnston, K. P.; Doty, R. C.; Korgel, B. A. Control of thickness and orientation of solution-grown silicon nanowires. *Science (Washington, D. C.)* **2000,** *287* (5457), 1471-1473.

29. Zou, G.; Li, H.; Zhang, Y.; Xiong, K.; Qian, Y. Solvothermal/hydrothermal route to semiconductor nanowires. *Nanotechnology* **2006,** *17* (11), S313-S320.

30. Wang, X.; Li, Y. Synthesis and characterization of lanthanide hydroxide single-crystal nanowires. *Angewandte Chemie, International Edition* **2002,** *41* (24), 4790-4793.

31. Tang, Z.; Wang, Y.; Shanbhag, S.; Giersig, M.; Kotov, N. A. Spontaneous Transformation of CdTe Nanoparticles into Angled Te Nanocrystals: From Particles and Rods to Checkmarks, X-Marks, and Other Unusual Shapes. *Journal of the American Chemical Society* **2006,** *128* (20), 6730-6736.

32. Tang, Z.; Wang, Y.; Sun, K.; Kotov, N. A. Spontaneous transformation of stabilizer-depleted binary semiconductor nanoparticles into selenium and tellurium nanowires. *Advanced Materials (Weinheim, Germany)* **2005,** *17* (3), 358-363.

33. Tang, Z. Y.; Kotov, N. A.; Giersig, M. Spontaneous organization of single CdTe nanoparticles into luminescent nanowires. *Science* **2002,** *297* (5579), 237-240.

34. Zhang, Z.; Tang, Z.; Kotov, N. A.; Glotzer, S. C. Simulations and Analysis of Self-Assembly of CdTe Nanoparticles into Wires and Sheets. *Nano Letters* **2007,** *7* (6), 1670-1675.

35. Chung, S. W.; Ginger, D. S.; Morales, M. W.; Zhang, Z.; Chandrasekhar, V.; Ratner, M. A.; Mirkin, C. A. Top-down meets bottom-up: Dip-pen nanolithography and DNA-directed assembly of nanoscale electrical circuits. *Small* **2005,** *1* (1), 64-69.

36. Piner, R. D.; Zhu, J.; Xu, F.; Hong, S.; Mirkin, C. A. Dip Pen Nanolithography. *Science* **1999,** *283*, 661-663.

37. Wu, Y.; Yan, H.; Huang, M.; Messer, B.; Song, J. H.; Yang, P. Inorganic semiconductor nanowires: rational growth, assembly, and novel properties. *Chem. --Eur. J.* **2002,** *8* (6), 1260-1268.

38. Cheung, C. L.; Hafner, J. H.; Odom, T. W.; Kim, K.; Lieber, C. M. Growth and fabrication with single-walled carbon nanotube probe microscopy tips. *Appl. Phys. Lett.* **2000,** *76* (21), 3136-3138.

39. Lieber, C. M. Nanoscale science and technology: building a big future from small things. *MRS Bull.* **2003,** *28* (7), 486-491.

40. Huang, Y.; Duan, X. F.; Wei, Q. Q.; Lieber, C. M. Directed assembly of one-dimensional nanostructures into functional networks. *Science* **2001,** *291*, 630-633.

41. Lu, W.; Xie, P.; Lieber, C. M. Nanowire transistor performance limits and applications. *IEEE Trans. Electron Devices* **2008,** *55* (11), 2859-2876.

42. Hurst, S. J.; Payne, E. K.; Qin, L.; Mirkin, C. A. Multisegmented one-dimensional nanorods prepared by hard-template synthetic methods. *Angewandte Chemie, International Edition* **2006,** *45* (17), 2672-2692.

43. Smith, P. A.; Nordquist, C. D.; Jackson, T. N.; Mayer, T. S.; Martin, B. R.; Mbindyo, J.; Mallouk, T. E. Electric-field assisted assembly and alignment of metallic nanowires. *Appl. Phys. Lett.* **2000,** *77* (9), 1399-1401.

44. Duan, X.; Huang, Y.; Cui, Y.; Wang, J.; Lieber, C. M. Indium phosphide nanowires as building blocks for nanoscale electronic and optoelectronic devices. *Nature* **2001,** *409* (6816), 66-69.

45. Wang, Y.; Tang, Z.; Podsiadlo, P.; Elkasabi, Y.; Lahann, J.; Kotov, N. A. Mirror-like photoconductive layer-by-layer thin films of Te nanowires: the fusion of semiconductor, metal, and insulator properties. 18 ed.; 2006; pp 518-522.

46. He, Jr. H.; Hsu, J. H.; Wang, C. W.; Lin, H. N.; Chen, L. J.; Wang, Z. L. Pattern and Feature Designed Growth of ZnO Nanowire Arrays for Vertical Devices. *J. Phys. Chem. B* **2005,** *110* (1), 50-53.

47. Tanase, M.; Silevitch, D. M.; Hultgren, A.; Bauer, L. A.; Searson, P. C.; Meyer, G. J.; Reich, D. H. Magnetic trapping and self-assembly of multicomponent nanowires. *Journal of Applied Physics* **2002,** *91* (10, Pt. 3), 8549-8551.

48. Hangarter, C. M.; Myung, N. V. Magnetic Alignment of Nanowires. *Chemistry of Materials* **2005,** *17* (6), 1320-1324.

49. Wang, J. G.; Tian, M. L.; Mallouk, T. E.; Chan, M. H. W. Microstructure and interdiffusion of template-synthesized Au/Sn/Au junction nanowires. *Nano Letters* **2004,** *4* (7), 1313-1318.

50. Park, S.; Lim, J. H.; Chung, S. W.; Mirkin, C. A. Self-Assembly of Mesoscopic Metal-Polymer Amphiphiles. *Science (Washington, DC, United States)* **2004,** *303* (5656), 348-351.

51. Kovtyukhova, N. I.; Mallouk, T. E. Nanowire p-n heterojunction diodes made by templated assembly of multilayer carbon-nanotube/polymer/semiconductor-particle shells around metal nanowires. *Advanced Materials (Weinheim, Germany)* **2005,** *17* (2), 187-192.

52. Hu, J.; Bando, Y.; Zhan, J.; Golberg, D. Fabrication of silica-shielded Ga-ZnS metal-semiconductor nanowire heterojunctions. *Advanced Materials (Weinheim, Germany)* **2005,** *17* (16), 1964-1969.

53. Cui, Y.; Lieber, C. M. Functional nanoscale electronic devices assembled using silicon nanowire building blocks. *Science* **2001,** *291* (5505), 851-853.

54. Cui, Y. *Semiconductor nanowires for nanotechnology: synthesis, properties, nanoelectronics, nanophotonics, and nanosensors;* 2002.

55. Ng, H. T.; Han, J.; Yamada, T.; Nguyen, P.; Chen, Y. P.; Meyyappan, M. Single-crystal nanowire vertical surround-gate field-effect transistor. *Nano Letters* **2004,** *4* (7), 1247-1252.

56. Pena, D. J.; Mbindyo, J. K. N.; Carado, A. J.; Mallouk, T. E.; Keating, C. D.; Razavi, B.; Mayer, T. S. Template Growth of Photoconductive Metal-CdSe-Metal Nanowires. *Journal of Physical Chemistry B* **2002,** *106* (30), 7458-7462.

57. Wang, Y.; Tang, Z.; Podsiadlo, P.; Elkasabi, Y.; Lahann, J.; Kotov, N. A. Mirror-like photoconductive layer-by-layer thin films of Te nanowires: the fusion of semiconductor, metal, and insulator properties. *Advanced Materials (Weinheim, Germany)* **2006,** *18* (4), 518-522.

58. Pan, Z.; Lai, H. L.; Au, F. C. K.; Duan, X.; Zhou, W.; Shi, W.; Wang, N.; Lee, C. S.; Wong, N. B.; Lee, S. T.; Xie, S. Oriented silicon carbide nanowires: synthesis and field emission properties. *Advanced Materials (Weinheim, Germany)* **2000,** *12* (16), 1186-1190.

59. Zhou, X. T.; Lai, H. L.; Peng, H. Y.; Au, F. C. K.; Liao, L. S.; Wang, N.; Bello, I.; Lee, C. S.; Lee, S. T. Thin b-SiC nanorods and their field emission properties. *Chemical Physics Letters* **2000,** *318* (1,2,3), 58-62.

60. Patolsky, F.; Zheng, G.; Lieber, C. M. Nanowire-based biosensors. *Analytical Chemistry* **2006,** *78* (13), 4260-4269.

61. Cui, Y.; Wei, Q.; Park, H.; Lieber, C. M. Nanowire nanosensors for highly sensitive and selective detection of biological and chemical species. *Science (Washington, DC, United States)* **2001,** *293* (5533), 1289-1292.

62. Rout, C. S.; Hari, H. S.; Vivekchand, S. R. C.; Govindaraj, A.; Rao, C. N. R. Hydrogen and Ethanol Sensors Based on ZnO Nanorods, Nanowires and Nanotubes.
Rout, Chandra Sekhar; Hari, Krishna, S.; Vivekchand, S. R. C.; Govindaraj, A.; Rao, C. N. R. *Chemical Physics Letters* **2006,** *418*, 586-590.

63. Wang, W. U.; Chen, C.; Lin, K. h.; Fang, Y.; Lieber, C. M. Label-free detection of small-molecule-protein interactions by using nanowire nanosensors. *Proceedings of the National Academy of Sciences of the United States of America* **2005,** *102* (9), 3208-3212.

64. Hahm, J. i.; Lieber, C. M. Direct ultrasensitive electrical detection of DNA and DNA sequence variations using nanowire nanosensors. *Nano Letters* **2004,** *4* (1), 51-54.

65. Zheng, G.; Patolsky, F.; Cui, Y.; Wang, W. U.; Lieber, C. M. Multiplexed electrical detection of cancer markers with nanowire sensor arrays. *Nature Biotechnology* **2005,** *23* (10), 1294-1301.

66. MacBeath, G.; Schreiber, S. L. Printing proteins as microarrays for high-throughput function determination. *Science (Washington, D. C.)* **2000,** *289* (5485), 1760-1763.

67. Patolsky, F.; Zheng, G.; Hayden, O.; Lakadamyali, M.; Zhuang, X.; Lieber, C. M. Electrical detection of single viruses. *Proceedings of the National Academy of Sciences of the United States of America* **2004,** *101* (39), 14017-14022.

68. Sirbuly, D. J.; Law, M.; Yan, H.; Yang, P. Semiconductor Nanowires for Subwavelength Photonics Integration. *Journal of Physical Chemistry B* **2005,** *109* (32), 15190-15213.

69. Johnson, J. C.; Yan, H.; Schaller, R. D.; Haber, L. H.; Saykally, R. J.; Yang, P. Single Nanowire Lasers. *Journal of Physical Chemistry B* **2001,** *105* (46), 11387-11390.

70. Johnson, J. C.; Choi, H. J.; Knutsen, K. P.; Schaller, R. D.; Yang, P.; Saykally, R. J. Single gallium nitride nanowire lasers. *Nature Materials* **2002,** *1* (2), 106-110.

71. Ding, J. X.; Zapien, J. A.; Chen, W. W.; Lifshitz, Y.; Lee, S. T.; Meng, X. M. Lasing in ZnS nanowires grown on anodic aluminum oxide templates. *Applied Physics Letters* **2004,** *85* (12), 2361-2363.

72. Baxter, J. B.; Walker, A. M.; van Ommering, K.; Aydil, E. S. Synthesis and characterization of ZnO nanowires and their integration into dye-sensitized solar cells. *Nanotechnology* **2006,** *17* (11), S304-S312.

73. Wang, D.; Jakobson, H. P.; Kou, R.; Tang, J.; Fineman, R. Z.; Yu, D.; Lu, Y. Metal and Semiconductor Nanowire Network Thin Films with Hierarchical Pore Structures. *Chemistry of Materials* **2006,** *18* (18), 4231-4237.

74. Sirbuly, D. J.; Law, M.; Pauzauskie, P.; Yan, H.; Maslov, A. V.; Knutsen, K.; Ning, C. Z.; Saykally, R. J.; Yang, P. Optical routing and sensing with nanowire assemblies. *Proceedings of the National Academy of Sciences of the United States of America* **2005,** *102* (22), 7800-7805.

75. Law, M.; Sirbuly, D. J.; Johnson, J. C.; Goldberger, J.; Saykally, R. J.; Yang, P. Nanoribbon waveguides for subwavelength photonics integration. *Science* **2004,** *305* (5688), 1269-1273.

76. Duan, X.; Huang, Y.; Cui, Y.; Wang, J.; Lieber, C. M. Indium phosphide nanowires as building blocks for nanoscale electronic and optoelectronic devices. *Nature* **2001,** *409* (6816), 66-69.

77. Goldberger, J.; Sirbuly, D. J.; Law, M.; Yang, P. ZnO nanowire transistors. *Journal of Physical Chemistry B* **2005,** *109* (1), 9-14.

78. Qian, F.; Li, Y.; Gradecak, S.; Wang, D.; Barrelet, C. J.; Lieber, C. M. Gallium Nitride-Based Nanowire Radial Heterostructures for Nanophotonics. *Nano Letters* **2004,** *4* (10), 1975-1979.

79. Gudiksen, M. S.; Lauhon, L. J.; Wang, J.; Smith, D. C.; Lieber, C. M. Growth of nanowire superlattice structures for nanoscale photonics and electronics. *Nature* **2002,** *415* (6872), 617-620.

80. Rogach, A. L. *Semiconductor Nanocrystal Quantum Dots;* Springer-Verlag/Wien: New York, 2008.

81. Rogach, A. L. Binary superlattices of nanoparticles: self-assembly leads to "metamaterials". *Angew Chem Int Ed Engl* **2004,** *43* (2), 148-149.

82. Korgel, B. A.; Fitzmaurice, D. Self-Assembly of Silver Nanocrystals into Two-Dimensional Nanowire Arrays. *Advanced Materials* **1998,** *10* (9), 661-665.

83. Wang, D.; Moehwald, H. Template-directed colloidal self-assembly - the route to 'top-down' nanochemical engineering. *J. Mater. Chem.* **2004,** *14* (4), 459-468.

84. Yi, C.; Liu, D.; Yang, M. Building nanoscale architectures by directed synthesis and self-assembly. *Curr. Nanosci.* **2009,** *5* (1), 75-87.

85. Tang, Z.; Ozturk, B.; Wang, Y.; Kotov, N. A. Simple Preparation Strategy and One-Dimensional Energy Transfer in CdTe Nanoparticle Chains. *J. Phys. Chem. B* **2004,** *108*, 6927-6931.

86. Shenhar, R.; Rotello, V. M. Nanoparticles: Scaffolds and Building Blocks. *Acc. Chem. Res.* **2003,** *36* (7), 549-561.

87. Westerlund, F.; Bjornholm, T. Directed assembly of gold nanoparticles. *Curr. Opin. Colloid Interface Sci.* **2009,** *14* (2), 126-134.

88. Wang, S.; Mamedova, N.; Kotov, N. A.; Chen, W.; Studer, J. Antigen/antibody immunocomplex from CdTe nanoparticle bioconjugates. *Nano Letters* **2002,** *2* (8), 817-822.

89. Lee, J.; Govorov, A. O.; Kotov, N. A. Bioconjugated Superstructures of CdTe Nanowires and Nanoparticles: Multistep Cascade Foerster Resonance Energy Transfer and Energy Channeling. *Nano Letters* **2005,** *5* (10), 2063-2069.

90. Lee, J.; Govorov, A. O.; Dulka, J.; Kotov, N. A. Bioconjugates of CdTe Nanowires and Au Nanoparticles: Plasmon-Exciton Interactions, Luminescence Enhancement, and Collective Effects. *Nano Letters* **2004,** *4* (12), 2323-2330.

91. Lee, J.; Javid, T.; Skeini, T.; Govorov, A. O.; Bryant, G. W.; Kotov, N. A. Bioconjugated Ag nanoparticles and CdTe nanowires: metamaterials with field-enhanced light absorption. *Angewandte Chemie, International Edition* **2006,** *45* (29), 4819-4823.

92. Lee, J.; Govorov, A. O.; Kotov, N. A. Nanoparticle assemblies with molecular springs: A nanoscale thermometer. *Angewandte Chemie, International Edition* **2005,** *44* (45), 7439-7442.

93. Govorov, A. O.; Bryant, G. W.; Zhang, W.; Skeini, T.; Lee, J.; Kotov, N. A.; Slocik, J. M.; Naik, R. R. Exciton-Plasmon Interaction and Hybrid Excitons in Semiconductor-Metal Nanoparticle Assemblies. *Nano Letters* **2006,** *6* (5), 984-994.

94. Wang, Y.; Tang, Z.; Tan, S.; Kotov, N. A. Biological Assembly of Nanocircuit Prototypes from Protein-Modified CdTe Nanowires. *Nano Letters* **2005,** *5* (2), 243-248.

CHAPTER 2

MEDIA EFFECT ON CDTE NANOWIRE GROWTH: MECHANISM OF SELF ASSEMBLY, OSTWALD RIPENING, AND CONTROL OF NW GEOMETRY

2.1 ABSTRACT

The spontaneous self-assembly of II-IV stabilizer depleted NPs into NWs is a complex process that is only partially understood. This paper examines the mechanism governing changes in the growth pattern of CdTe NWs that are induced by the addition of DMSO to the NW growth solution. We propose that after the initial step of formation of NP pearl necklace assemblies, the assemblies recrystallize and subsequently grow into long NWs by Ostwald ripening. The addition of DMSO allows for improved control over the NW length and diameter. As the DMSO concentration in the NW growth solution is increased, the resulting NW length and diameter increases. When DMSO concentrations are raised above 70%, there is no NW formation, which is attributed to inhibition of the formation of pearl necklace assemblies. DMSO influence on NW morphology is attributed to its effect on the electrostatic interactions between the nanoparticles and mass exchange between the growing nuclei.

2.2 INTRODUCTION

Semiconductor NWs have many unique optical and electronic properties that make them desirable for use in new sensing, electronic, and photonic devices[1]. Semiconductor NW assemblies have been engineered to sense temperature[2,3], chemicals[4], and pH[5]. They are used in photonic devices such as those used for light detection[6] and collection[7]; as well as used to further decrease the size of electronic devices, helping establish nano-electronics[8,9].

Most NWs produced today are made using point growth processes[10-12], the most common of which is the VLS process. In this technique, NWs are grown by diffusion of the growth material from a gas into metal droplets[13]. Additional point growth techniques include the SLS process[14] and the VS methodologies[15]. Less common NW synthesis techniques include templating [16,17], microwave assisted reactions[18,19], and solution based reactions[20-24]. The latter manipulate the surface energies of NP crystal faces to guide constituent ions to the higher energy face of the NP, which results in a NW[25]. One of the promising methods of solution based processes is the spontaneous self-assembly of NPs into NWs[22,24]. The aqueous self-assembly of CdTe NPs into luminescent NWs by the partial removal of the organic stabilizer layer[24,26] stands out because of the uniqueness and complexity of interparticle interactions in water, which allows unique architectures of the nanoscale assemblies. Aqueous methods are also convenient for subsequent processing of the NWs into composite structures, for instance by layer-by-layer assembly with polyelectrolytes[27,28]. Finally, these reactions can also be scalable to large quantities of the product.

Until now, the groups working with this technique focused mostly on the control of NW diameter and/or its morphology that has been linked to the precursor NP diameter. There has been no systematic study on the control over NW length that is quite variable and is needed for many technological aspects of NW utilization. Additionally, we want to point to an important question about the mechanism of NP-to-NW transformation. It is well-documented that the original CdTe NPs are in a cubic crystal lattice, while the resulting NWs are in a hexagonal lattice. If NWs are growing by oriented attachment, then there must be a spontaneous recrystallization of the crystal from a cubic phase into the hexagonal phase that is likely to have a quite high activation barrier. However, if NW growth is the result of Ostwald ripening, the change of the crystal lattice might occur via ion/monomer exchange. Several authors also report the formation of NWs in a cubic crystal lattice[29,30], which indicates that under some conditions the recrystallization does not occur. We need to understand what is happening with NPs during their transformation into NWs and the first step is to understand how intense the Ostwald ripening process is.

We propose a modification of the procedure presented by Tang et al[24] to investigate the use of DMSO in the NW growth solution as a method to establish control over NW length and diameter. We show a direct correlation between DMSO concentration in the NW growth solution (stabilizer depleted CdTe NPs in pH 9 water) and the resulting CdTe NW length and diameter. Furthermore, we use this correlation to hypothesize that the mechanism governing NW formation involves a stage of NP recrystallization into NWs by Ostwald ripening that takes place parallel to particle self-

assembly. Altogether, this growth mechanism is consistent with both the media effect and other data previously published by our and other groups.

2.3 SYNTHESIS

TGA stabilized CdTe NPs were prepared according to literature[31,32]. The average diameter of the CdTe NPs, as measured with AFM, was 2.6 ± 1.1 nm, with a wavelength of maximum fluorescence (λ_{max}) of 541 nm. The average diameter was calculated using the NanoScope ® III software tool Particle Analysis. The error margins represent the standard deviation in the sample. CdTe NWs were prepared according to a modified procedure outlined by Tang et al[24]. Briefly, 1 mL of CdTe NP solution was mixed with 0.5 mL methanol and 0.5 mL 2-propanol to partially remove TGA stabilizer from the CdTe NP surface. The resulting turbid solution was shaken and centrifuged until all NPs had precipitated and the solution was clear. The supernatant was decanted. In order to ensure all excess liquid had been removed from the NPs, the moist NPs were freeze dried overnight. The dry, stabilizer depleted CdTe NPs were reconstituted to 1 mL with a mixture of pH 9 water and DMSO. The DMSO concentration was varied from 0 to 100% by volume. The resulting suspension of stabilizer depleted CdTe NPs in DMSO and pH 9 water was placed in an 80 ^{o}C oven from 40 minutes to 3 hours. The solutions were removed and studied.

2.4 RESULTS AND DISCUSSION

2.4.1 NW Length and Diameter Control

The general format of all experiments is the same as in previous papers except that we add various amounts of DMSO to the growth solution and incubate it at elevated temperature (80°C) over a certain period of time, after which physical parameters of the NWs are evaluated. As one can see from the AFM images (Figure 2.2) and the cumulative graphs plotted on their basis (Figure 2.1 A, B), both diameter and length of the NWs are strongly dependent on DMSO concentration in the growth solution, and, of course, on the time that the growth solution is held at 80°C.

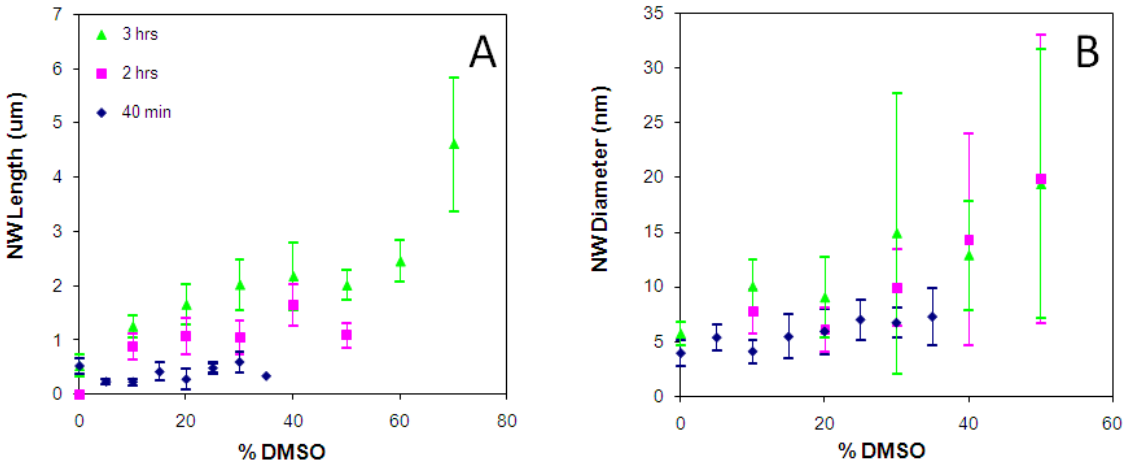

Figure 2.1 Dependences of CdTe NW (A) length, and (B) diameter. Each data point in (A) and (B) represents the average of 20 NWs from 5 separate runs using AFM and Nanoscope IIIa software. The error bars represent the standard deviation in the 5 runs.

The data obtained from AFM are averaged over several separate NW batches that are prepared independently and analyzed in the same manner.

NW growth initially occurs after 40 minutes and after 3 hours the NWs precipitate into large agglomerates that cannot be re-dispersed. Overall, the growth rate is much faster with DMSO than in the previous procedure without it[21]. Both the length and the

diameter of NWs strongly increase with DMSO concentration for the same time point. The distribution of length is quite narrow for most of the conditions, while the distribution of diameters becomes wider as the DMSO content increases. Interestingly, as soon as DMSO concentration reaches above 70% (v/v), little or no NW growth can be observed. This presents an obvious discontinuity of the trend because we see the increase in NW length and diameter (Figure 2.1-2.2) for increasing DMSO contents. Such an unusual step-function behavior requires special attention because it can reveal details of the NW growth mechanisms.

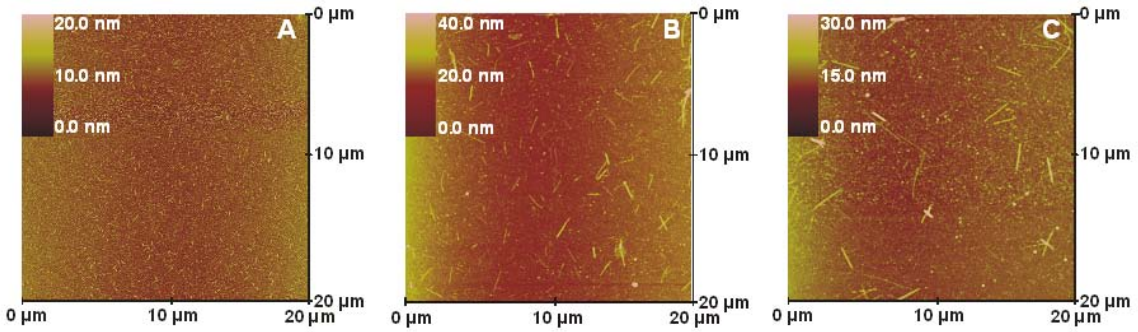

Figure 2.2. AFM images of CdTe NWs grown in (A) 0% DMSO, (B) 40% DMSO, and (C) 60% DMSO.

2.4.2 NP "Pearl Necklace" Formations

Tang et al[24] proposes the mechanism of NW formation involves the formation of NP pearl-necklace assemblies that subsequently re-crystallize into NWs. Overall, DMSO in the NW growth solution inhibits the formation of pearl necklace assemblies (Figure 2.3), which explains the cessation of NW formation for solutions with greater than 60% DMSO. While explaining the step function behavior, this observation also presents a paradox because we see the increase in NW length and diameter at the same time (Figure 2.1), which might be associated with the increase in length of particle chains.

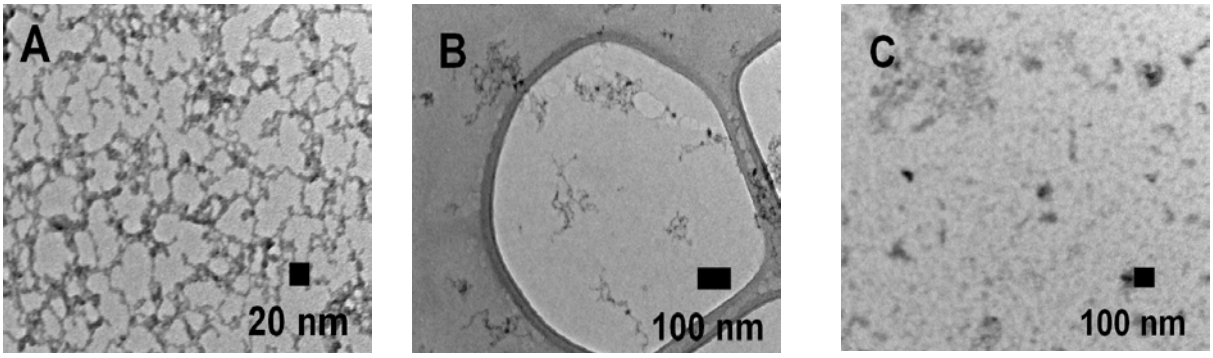

Figure 2.3. TEM images of NP assemblies for (A) 0% DMSO in growth solution, (B) 40% DMSO in growth solution (C) 60% DMSO in growth solution.

One explanation of the mechanism governing DMSO's inhibition of pearl necklace formation may be based on the reduction of the intrinsic dipole moments of NPs due to the gradual replacement of water molecules that are coordinated to the truncated faces of CdTe tetrahedrons. It is shown by quantum mechanical calculations[42] that these water molecules greatly enhance the polarity of CdTe particles compared to thiol terminals. Consequently, their replacement may result in the reduction of dipole-dipole attraction between the NPs below the level at which they can compete with thermal motion. Similar calculations using PM3 algorithm are carried out in this work for a variety of potential replacement geometries. The calculations are done for a model of relatively small CdTe cluster to reduce the calculation costs. It is expected that the principal conclusions about dipole moment trend remain the same for bigger clusters having larger overall moments.

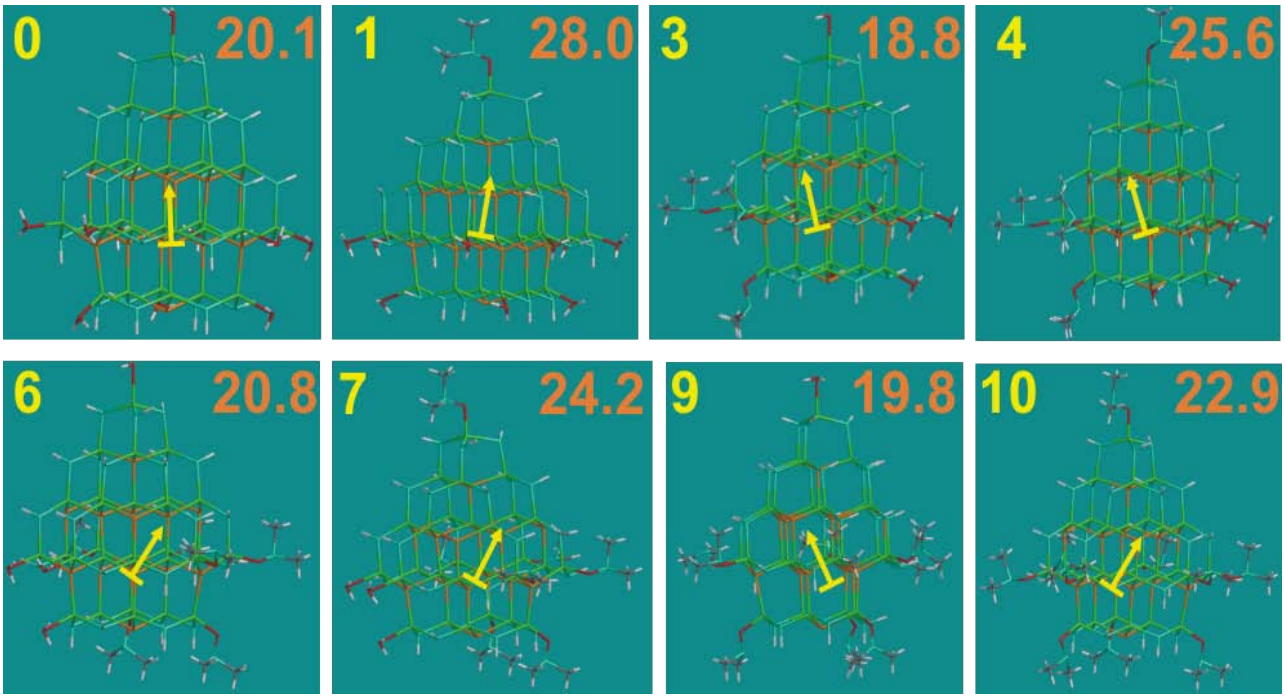

Figure 2.4. Calculations of the dipole moments of small CdTe clusters. The numbers in the top left and top right corners represent the number of DMSO molecules in the cluster and the calculated dipole moment in Debyes, respectively. Atom notations: H – light grey, Cd – green, O – red, S – blue, Te – orange, C – dark grey. The yellow arrows indicate the direction of the dipole moment in each nanoparticle.

As is seen in Figure 2.4, the replacement of water molecules by DMSO is more likely to increase rather than decrease the dipole moment. Only for the configuration in which 3 and 9 DMSO molecules replace water do we see a slight reduction of dipole moment from 20.1 to 18.8 and 19.8, respectively. In all the other tested positions of DMSO, the dipole moment increases, sometimes significantly, such as the replacement of 1 and 4 molecules of DMSO (Figure 2.4). Also note that the orientation of the moment does not significantly change, which is attributed to the similarities of the association of DMSO molecules and water molecules with Cd atoms on the CdTe surface. Based on these results, the hypothesis that pearl necklace agglomerates stop forming due to water substitution is discarded.

Let us look at the energy required to form an aggregate of NPs. The formation of linear NP pearl-necklace assemblies is defined by the Derjaguin, Landau, Verwey, and

Overbeek (DLVO) theory as an interaction of electrostatic forces (charge-dipole and dipole-dipole) and Van der Waals forces. The energy required to form an aggregate of a specific shape is described by Eq. 2.1,

$$W_{total}(r,\theta,\varphi) = W_{q-q}(r) + W_{q-\mu}(r,\theta) + W_{\mu-q}(r,\theta) + W_{\mu-\mu}(r,\theta,\varphi) + W_{VanderWaals}(r) \quad (2.1)$$

where $W_{q-q}(r)$ is the charge-charge interaction energy, $W_{q-\mu}(r,\theta)$ and $W_{\mu-q}(r,\theta)$ are the charge-dipole and dipole charge interaction energies, $W_{\mu-\mu}(r,\theta,\varphi)$ is the dipole-dipole interaction energy, and $W_{VanderWaals}(r)$ is the Van der Waals energy[33]. The charge-charge interaction energy is defined by Eq. 2.2[33],

$$W_{q-q}(r) = \frac{q_i q_j}{4\pi\varepsilon_0 \varepsilon r_{ij}} e^{-kr_{ij}} C_0^2 \quad (2.2)$$

the charge-dipole energies are defined by Eq. 2.3[33],

$$W_{q-u}(r,\theta) + W_{u-q}(r,\theta) = 2\frac{q_{ii}\mu_j \cos(\theta_j)}{r\pi\varepsilon_0 \varepsilon r_{ij}^2} e^{-kr_{ij}} (1 + kr_{ij}) C_0 C_1 \quad (2.3)$$

and the dipole-dipole energy is defined by Eq. 2.4[33].

$$W_{\mu-\mu}(r,\theta,\varphi) = \frac{\mu_{ii}\mu_j \cos(\theta_j)}{4\pi\varepsilon_0 \varepsilon r_{ij}^3} (\cos\theta_i)(\cos\theta_j)\left[2 + 2kr_{ij} + (kr_{ij})^2\right] \quad (2.4)$$

Generally, the semiconducting NPs possess large, permanent dipole moments from 41 to 98 D[34-36]. Carboxylic groups on the TGA organic stabilizers create a high surface charge on the NPs, creating a large repulsive force between the NPs (Eq. 2)[31]. The origin and magnitude of the permanent charges on the CdTe NPs were described in our previous publication[37] This charge can be quite high and depending on the size of nanoparticles and media conditions is estimated to be 2-10 electrons. The origin of the dipole is the asymmetric truncation/growth of the nanoparticles[38]. Both types of charges are

considered to be immobile and intrinsic to the nanoparticles in aqueous media. For simplicity the permanent negative charge may be considered to be located in the middle of the NPs, while the dipole charges are located on opposite sides of the NPs similarly to the model used previously.[33,37] For closely associated particle assemblies, the Van der Waals energy was shown to be extremely significant[39,40]; however, for large separations it is much smaller than the other forces and for this case is neglected.

The attractive force between the NPs can be quite large (Eq. 2.4)[41-43]. Nevertheless, in an excess of stabilizer, the repulsive forces are typically greater than the attractive forces. As we discussed previously,[24,40] partial removal of TGA stabilizer reduces the repulsive force between the NPs, so the attractive dipole forces cause the NPs to form linear aggregates.

DMSO addition to the growth solution inhibits the formation of the pearl necklace assemblies (Figure 2.3). We believe this occurs because DMSO has a lower dielectric constant than water, ε_{DMSO} is 47.2 and ε_{water} is 80. Generally speaking, decrease of dielectric constant may result in an (a) increased dipole-dipole attraction (Equation 4), and an (b) increased charge-charge repulsion (Eq. 2.2). Stronger dipole-dipole attraction must stimulate the formation of pearl-necklace agglomerates, but the higher energy of repulsion should have an opposite effect and decrease the number of agglomerates. The entire mechanism of DMSO influence on NW formation should be considered as a competition of these two effects. At low DMSO concentrations, the dielectric constant of the suspension is high enough to minimize the repulsive Coulombic force between NPs and their large dipole moments allow the NPs to agglomerate into pearl necklace assemblies (Figure 2.3A). As DMSO concentrations rise (40% (v/v) DMSO) the

frequency of the pearl necklace assemblies decreases because the repulsive Coulombic force between the NPs increases, which inhibits pearl necklace formation (Figure 2.3B). Since the energy of dipole-dipole attraction is dependent on $1/r_{ij}^{3}$ (Eq. 2.4) while the energy of the charge repulsion has $1/r_{ij}$ distance dependence (Eq. 2.2) and the concentrations of NPs are low (i.e. distances are long), the charge-charge interactions exert stronger influence on particle behavior than dipole-dipole interactions in this system. For DMSO concentrations higher than 70% (v/v), the dielectric constant of the suspension becomes too low and the electrostatic repulsion increases, leading to separation of pearl necklace aggregates (Figure 2.3C). We believe that this competition is the primary explanation of the step function behavior.

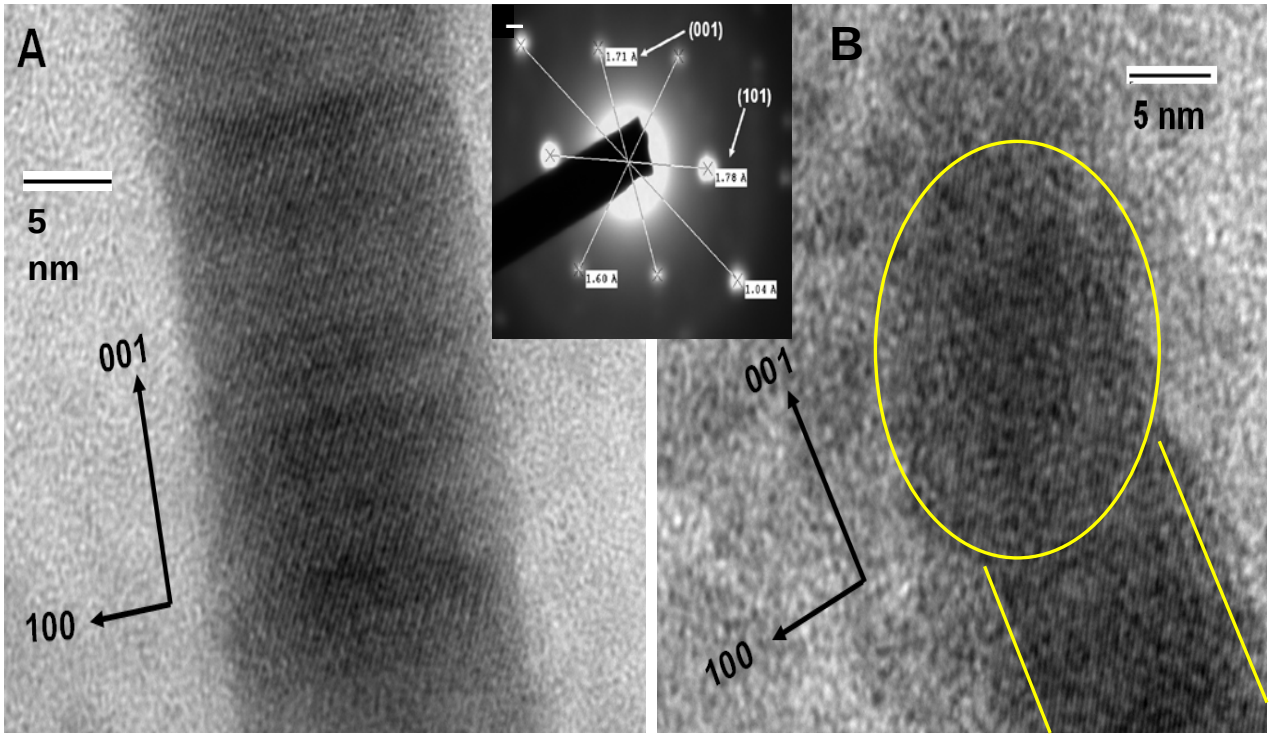

Figure 2.5. TEM of CdTe NWs grown in 20% DMSO for 2 hours, A) HRTEM of NW middle, B) HRTEM of NW end where NP is being attached to the NW. Insert: diffraction pattern of NW.

2.4.3 NW Formation by Ostwald Ripening

After some time, the pearl necklace agglomerates recrystallize into NWs. First of all, we validate previous reports by our group that this fusion is accompanied by the recrystallization of the zinc blende TGA stabilized CdTe NP pearl necklace agglomerates into hexagonal wurtzite TGA stabilized CdTe NWs[24]. We see no evidence of the formation of cubic NWs in this particular system as is verified by high-resolution TEM (Figure 2.5). The body of the NW (Figure 2.5A) has a perfect hexagonal lattice that is also confirmed by electron diffraction. Using TEM, we also investigate the tip of the NW where the NPs are supposed to attach, and find that the portion of the NW in the intermediate stages of assimilation also has hexagonal structure (Figure 2.5B). We are not able to find the presence of cubic lattice domains in the ends of the NWs, which is identified with independent NPs.

Since hexagonal NWs are also made via growth from homogeneous solution and not necessarily via particle assembly, we also question this part of the mechanism by observing the formation of NWs from two NP solutions with no DMSO. The first

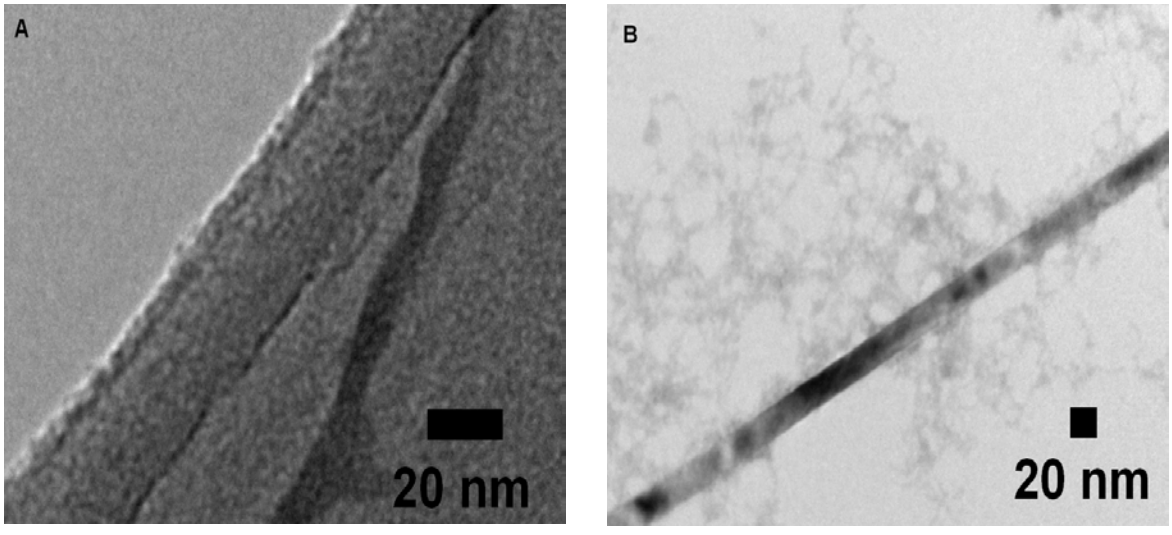

Figure 2.6. TEM images of A) NWs produced from an equimolar solution of two NP sizes, and B) NWs produced from uniform constituent NPs.

contains NPs with an average diameter of 2.396 ± 1.13 nm. The second contains an equimolar mixture of two NP sizes, those with an average diameter of 2.396 ± 1.13 nm and those with an average diameter of 5.790 ± 3.25 nm. TEM images of the resulting NWs are shown in Figure 2.6. AFM analysis confirms that the NWs from uniform constituent NPs have an average diameter variation of 0.72 ± 0.38 nm, while the NWs

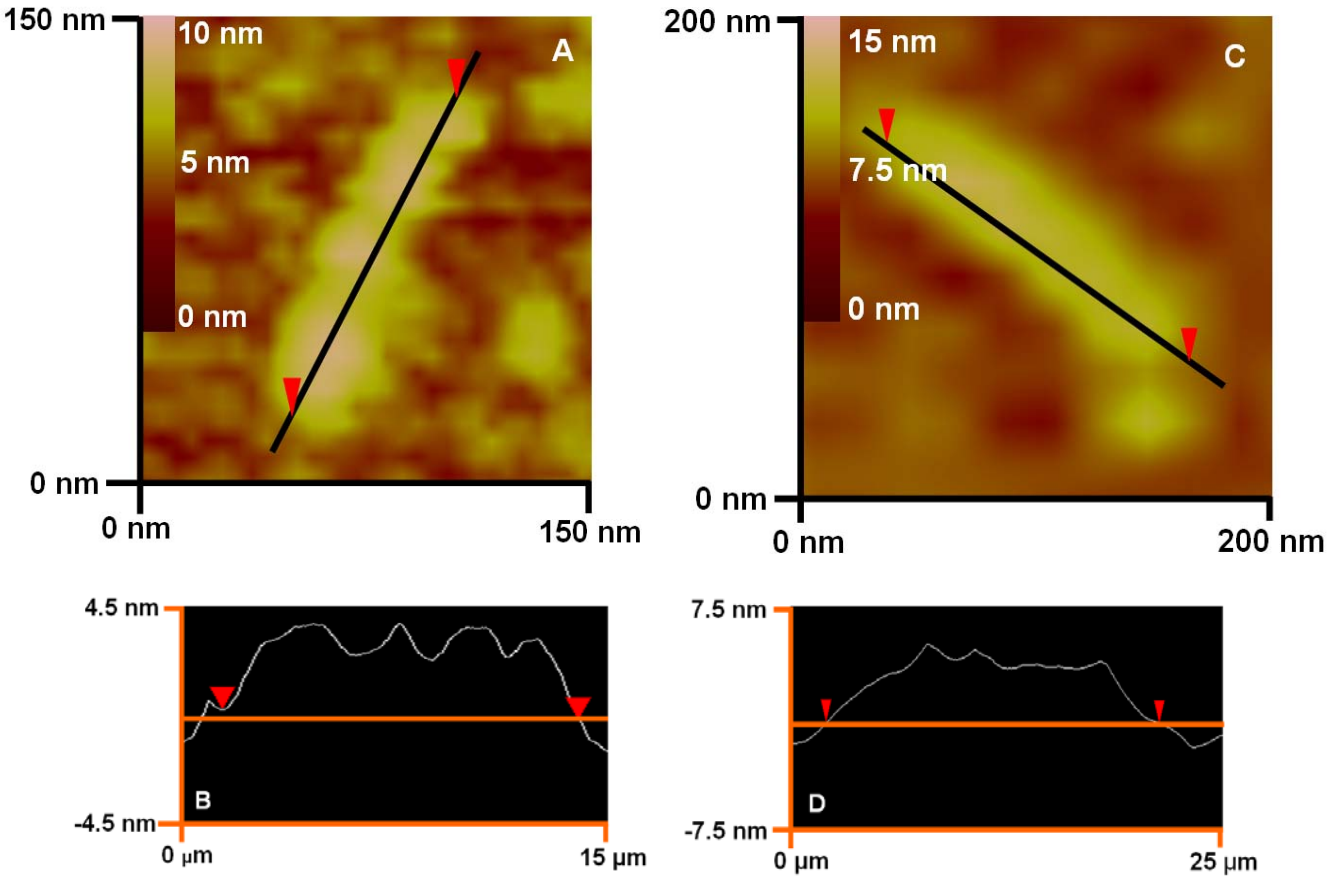

Figure 2.7. A) AFM image of NW formed from an equimolar mixture of two NP sizes, B) Topography of NW shown in A, C) AFM image of NW formed from uniform constituent NPs, D) Topography of NW shown in B.

formed from a mixture of NP sizes have an average diameter variation of 4.64 ± 4.31 nm. This confirms that there is more variation in the diameter of the NWs made from a mixture of two NP sizes. Again, the average diameter was calculated using the NanoScope ® III software tool Particle Analysis and the error margins represent the

standard deviation in the sample. AFM images and AFM analysis are given in Figure 2.7. For the NWs made from uniform constituent NPs, all of the NPs in the pearl necklace agglomerate are relatively uniform, so when the chain recrystallizes, the resulting NWs are more uniform. For NWs made from two constituent NP suspensions, the pearl necklace agglomerates contain both large and small NPs, so when the chain recrystallizes, the resulting NWs are very rough.

We believe that this recrystallization is driven by Ostwald ripening. Generally, Ostwald ripening is the process by which larger NPs grow while smaller NPs shrink and is often used in nanoscale synthesis to control NP diameter.[32,44-47] As applied to the transition of pearl necklace NP agglomerates into NWs, Cd^{2+} and Te^{2-} dissociate from smaller NPs within and surrounding the agglomerates. The ions then diffuse to the NP chains inside of the agglomerates and attach to them, filling in the voids between the NPs in the chain. The Cd^{2+} and the Te^{2-} ions preferentially attach to the ends on the NWs because the TGA stabilizer helps direct the growth along the wurtzite (001) axis. The carbonyl functional group of the TGA electrostatically attract Cd^{2+} ions and thus guide them to Te sites, creating ABAB stacking[48]. This makes Ostwald ripening in the case of NP chains direction specific that leads to eventual formation of the monocrystalline NWs (Figure 2.1). We want to point out that treating mass exchange process as diffusion of Cd^{2+} and Te^{2-} ions is a simplification. While there is no doubt that Cd^{2+} ions do exist in CdTe NP dispersions, Te^{2-} is easily oxidized in solutions by dissolved oxygen. It is quite possible that the actual species of Te diffusing from one particle to the other are some intermediates consisting of the ions of Cd, Te and one or more molecules of stabilizers (in this case thiols).

According to the general equation of Ostwald ripening in NP suspensions[49]

$$\frac{dr^*}{d\tau} = \frac{S - \exp\left[\frac{1}{r^*}\right]}{r^* + K\exp\left[\frac{\alpha}{r^*}\right]} \tag{2.5}$$

where r^* is a dimensionless radius term according to Eq. 2.6[49],

$$r^* = \frac{RT}{2\gamma V_m} r \tag{2.6}$$

τ is a dimensionless time according to Eq. 2.7[49],

$$\tau = \frac{R^2 T^2 D C_{flat}^0}{4\gamma^2 V_m} t \tag{2.7}$$

K is a dimensionless parameter that describes the ratio between diffusion and reaction rate constants according to Eq. 2.8, such that K<<1 is a diffusion limited process and K>>1 is a reaction limited process[49],

$$K = \frac{RT}{2\gamma V_m} \frac{D}{k_g^{flat}} \tag{2.8}$$

while S is a dimensionless variable that describes the oversaturation of monomer in solution and is described in Eq. 2.9.

$$S = [M]_{bulk} / C_{flat}^0 \tag{2.9}$$

In Eq. 2.5-2.9, C_{flat}^0 is the equilibrium for the dissolution of the bulk material, $C_{flat}^0 = k_d^{flat} / k_g^{flat}$, V_m is the molar volume of the solid, γ is the surface tension, D is the diffusion coefficient of the monomer, k_g^{flat} is the first-order reaction rate constant for addition of monomer to a flat surface, r is the NP radius, t is the time, T is the

temperature, $[M]_{bulk}$ is the monomer concentration in the bulk solution, and α is the transfer coefficient of the activated complex.

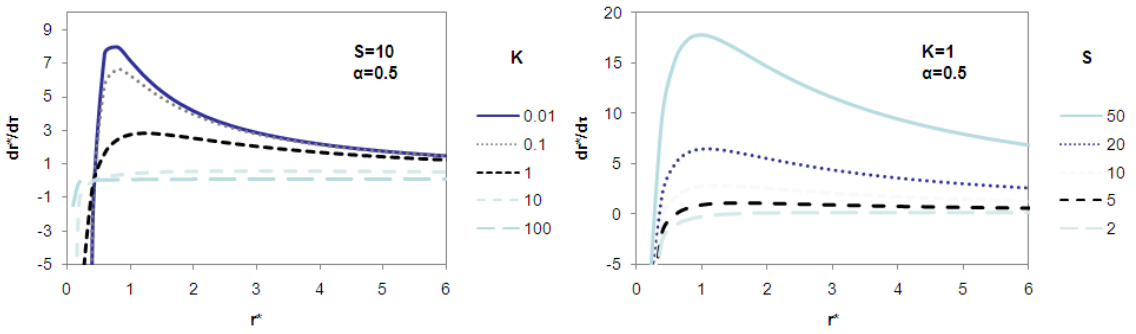

Figure 2.8. NP growth rate as it depends on K and S dimensionless variables.

As is seen in Figure 2.8, low values of K and high values of S result in larger NP growth rates; for DMSO to increase the rate of Ostwald ripening, it should either create high values of K or lower values of S, or both. The only variables that DMSO should affect in the K parameter are D, γ, and k_g^{flat} . Literature shows that DMSO lowers γ and D, so to increase K, DMSO must raise k_g^{flat}. Unfortunately, k_g^{flat} is unknown for this system and has not been calculated. Similarly, to raise S, DMSO must either increase $[M]_{bulk}$ or decrease C_{flat}^0. $[M]_{bulk}$ can only be measured experimentally, and it is not known the extent that DMSO alters it; however to lower C_{flat}^0, the k_g^{flat} must be raised in relation to k_d^{flat}. For both K and S, in order for DMSO to increase the rate of Ostwald ripening, it must increase k_g^{flat}, which is unknown for this system and would be a useful calculation for further studies of DMSO on the rate of Ostwald ripening.

While the rate of Ostwald ripening increase is not shown directly, there is significant empirical evidence to suggest that this system enhances the rate of Ostwald ripening. For example, when we synthesize NWs at 80°C (0% DMSO), their diameter is

6.1 nm (Figure 2.5), while the room temperature synthesis results in NWs approximately equal to the diameter of the particles, i.e. 2.6 nm.[24] Also, at 25°C the growth takes several weeks while the NWs grown at 80°C form in only 3 hours. The high Cd^{2+} and Te^{2-} concentrations in the growth solution cause the short hexagonal wurtzite NWs to grow much faster and less discriminately in respect to the crystal face, resulting in a greater diameter of the NWs.

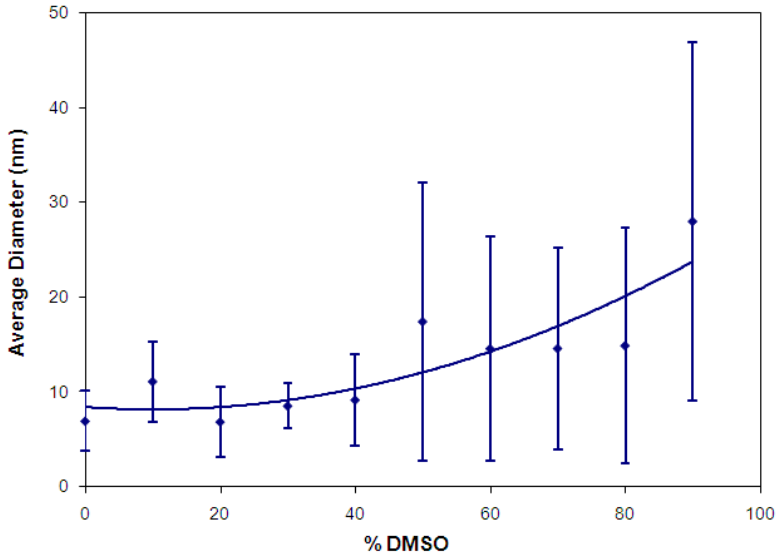

Figure 2.9. Average diameter dependence of CdTe NPs in growth solution on DMSO. The measurements were made at 80 °C and after 3 hours. Data were obtained using the particle analysis tool on the Nanoscope III AFM software. The error bars represent the standard deviation as determined using the NanoScope ® III software tool Particle Analysis.

To further show that DMSO enhances Ostwald processes in CdTe nanostructures, the average diameter of CdTe NPs is measured after growth in various DMSO concentrations. The larger NPs in the growth solution should grow, while the smaller ones shrink, causing a widening of the distribution of the NPs. NP solutions at various DMSO concentrations were analyzed after 3 hours at 80°C (Figure 2.9).

As predicted by the Ostwald ripening processes, a trend is seen that shows larger average NP diameters with higher standard deviations as DMSO concentration increases. Note that when DMSO concentrations exceed 70%, the curve in Figure 2.9 does not discontinue. This confirms that although Ostwald ripening has significant effect on NW growth, this process alone cannot explain the NP-to-NW transition. The explanation of discontinuity does require the intermediate step of formation of pearl necklace agglomerates that is inhibited by DMSO due to the electrostatic reasons described earlier.

Not all aspects of the growth process can be experimentally explored at the moment. However, the fact that Ostwald ripening does play a significant role can be substantiated by several observations, including the DMSO effect. One of them is the unforeseen blue shift of fluorescence spectrum (Figure 2.10) that indicates dispersed particles become smaller as NWs grow, which is in agreement with the proposed mechanism. The optical properties of the CdTe NW solutions are directly linked to the size and shape of the structures.[50] When considering luminescence of long semiconductor NWs is primarily determined by the diameter, one would expect the PL to red-shift or at least to stay the same for solutions containing longer NWs. However, Figure 2.10 shows the opposite. The explanation is that

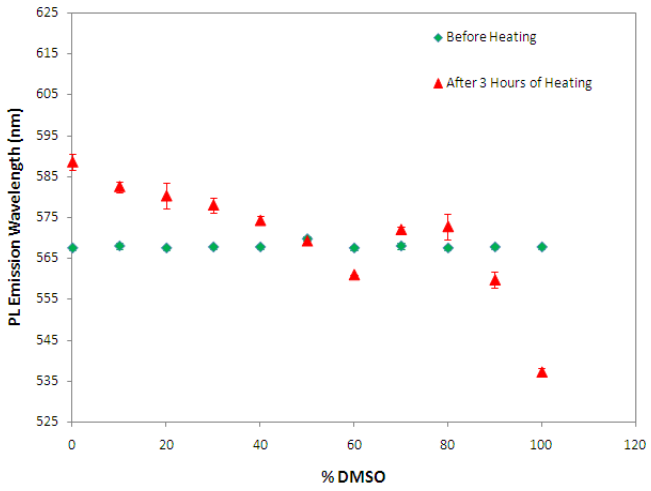

Figure 2.10. PL dependence of CdTe NW solution on DMSO concentration in the growth solution. Measurements are after 3 hours growth time in 80 ^{o}C oven.

dispersions here contain both CdTe NPs and NWs. Since NW growth occurs via Ostwald ripening, most of the NPs in the solution shrink while a few NPs and NWs grow. DMSO aids Ostwald ripening, so increased DMSO concentration in the growth solution results in longer NWs and smaller NPs. Since the PL of the solution is a cumulative effect of its contents, and since there are many more NPs than NWs and the quantum yield of NWs is typically smaller than that of NPs (due to lower probability of radiative excitonic recombination in greater volume of the particle), the PL of the solution is more dependent on the size of the NPs rather than the NWs. As a result, Figure 2.10 shows that the fluorescence of the solutions decreases with increasing DMSO concentration. As discussed earlier, DMSO concentration inhibits NW formation, with little or no NW formation above 70% DMSO. The sudden increase in PL for suspensions above 70% DMSO occurs because little or no NWs are formed in solutions above 70% DMSO. As such, Ostwald ripening results in an increase of the average diameter of the NPs (Figure 2.9).

2.5 CONCLUSIONS

We present a method to consistently control the length and diameter of TGA stabilized CdTe NPs by the addition of DMSO to the NP growth solution. This method sheds new light onto the mechanism of NW formation. After the formation of pearl necklace NP assemblies in the growth solution, Ostwald ripening causes the chains to recrystallize and grow. Experimental data suggest that the addition of DMSO inhibits the formation of the NP pearl necklace aggregates, but enhances Ostwald ripening. As such, in the concentration range when particle chains do form, the synthesis of NWs is accelerated. However, once electrostatic repulsion between the NPs from DMSO becomes too strong, the formation of NWs abruptly stops. The formation of NP pearl necklace assemblies and the direct fusion and growth of NP chains into NWs by Ostwald ripening are likely to be competing processes. The balance between these and other processes of NW assembly are affected by environmental factors, such as temperature and media composition. Once we understand these processes, we can control the morphology of the resulting NWs. Note that there are other intriguing aspects of NP-to-NW transformation process that are still difficult to rationalize at the moment, such as the nature of Te-containing species and the reasons for absent product of Te^{2-} oxidation, as well as the effects of using other solvents to vary the dielectric constant of the solution. These aspects will be a subject of ensuing research.

One can expect that similar effects may be observed for other water-miscible organic solvents that reduce dielectric constant. At the same time, we need to be careful extending these analogies because of other processes that may accompany the addition of

the solvent, such as destabilization and colloidal uncontrolled agglomeration. DMSO in that respect is very convenient solvent because it can serve as particle stabilizer by itself[51]. We expect that similar behavior can be expected for acetonitrile.

2.6 ACKNOWLEDGEMENTS

This work was published in *Journal of Physical Chemistry C*[52]. I would like to thank Jaebeom Lee, Zhiyong Tang, and Ki-Sub Kim for their help in the synthesis and characterization of these NWs. I would like to thank Kai Sun of the University of Michigan's EMAL for his assistance with electron microscopy.

2.7 REFERENCES

1. He, Jr. H.; Hsu, J. H.; Wang, C. W.; Lin, H. N.; Chen, L. J.; Wang, Z. L. Pattern and Feature Designed Growth of ZnO Nanowire Arrays for Vertical Devices. *J. Phys. Chem. B* **2005,** *110* (1), 50-53.

2. Lee, J.; Govorov, A. O.; Kotov, N. A. Nanoparticle assemblies with molecular springs: A nanoscale thermometer. *Angewandte Chemie, International Edition* **2005,** *44* (45), 7439-7442.

3. Govorov, A. O.; Bryant, G. W.; Zhang, W.; Skeini, T.; Lee, J.; Kotov, N. A.; Slocik, J. M.; Naik, R. R. Exciton-Plasmon Interaction and Hybrid Excitons in Semiconductor-Metal Nanoparticle Assemblies. *Nano Letters* **2006,** *6* (5), 984-994.

4. Rout, C. S.; Hari, H. S.; Vivekchand, S. R. C.; Govindaraj, A.; Rao, C. N. R. Hydrogen and Ethanol Sensors Based on ZnO Nanorods, Nanowires and Nanotubes.
   Rout, Chandra Sekhar; Hari, Krishna, S.; Vivekchand, S. R. C.; Govindaraj, A.; Rao, C. N. R. *Chemical Physics Letters* **2006,** *418*, 586-590.

5. Pearton, S. J.; Norton, D. P.; Heo, Y. W.; Tien, L. C.; Ivill, M. P.; Li, Y.; Kang, B. S.; Ren, F.; Kelly, J.; Hebard, A. F. ZnO Spintronics and Nanowire Devices. *Journal of Electronic Materials* **2006,** *35* (5), 862-868.

6. Hayden, O.; Agarwal, R.; Lieber, C. M. Nanoscale Avalanch Photodiodes for Highly Sensitive and Spatially Resolved Photon Detection. *Nature Materials* **2006,** *5* (5), 352-356.

7. Lee, J.; Govorov, A. O.; Dulka, J.; Kotov, N. A. Bioconjugates of CdTe Nanowires and Au Nanoparticles: Plasmon-Exciton Interactions, Luminescence Enhancement, and Collective Effects. *Nano Letters* **2004,** *4* (12), 2323-2330.

8. Wang, Y.; Tang, Z.; Tan, S.; Kotov, N. A. Biological Assembly of Nanocircuit Prototypes from Protein-Modified CdTe Nanowires. *Nano Letters* **2005,** *5* (2), 243-248.

9. Kamins, T. I.; Sharma, S.; Islam, M. S. Self-Assembled Semiconductor Nanowires on Silicon and Insulating Substrates: Experimental Behavior. *NATO Science Series, II: Mathematics, Physics and Chemistry* **2005,** *185*, 327-332.

10. Holmes, J. D.; Johnston, K. P.; Doty, R. C.; Korgel, B. A. Control of Thickness and Orientation of Solution-Grown Silicon Nanowires. *Science* **2000,** *287*, 1471-1473.

11. Martin, C. R. Nanomaterials: A Membrane-Based Synthetic Approach. *Science* **1994,** *266*, 1961-1966.

12. Gudiksen, M. S.; Wang, J.; Lieber, C. M. Synthetic Control of the Diameter and Length of Single Crystal Semiconductor Nanowires. *J. Phys. Chem. B* **2001,** *105*, 4062-4064.

13. Wagner, R. S.; Ellis, W. C. The vapor-liquid-solid mechanism of crystal growth and its application to silicon. *Transactions of the American Institute of Mining, Metallurgical and Petroleum Engineers* **1965,** *233* (6), 1053-1064.

14. Buhro, W. E.; Hickman, K. M.; Trentler, T. J. Turning down the heat on semiconductor growth. Solution-chemical syntheses and the solution-liquid-solid mechanism. 8 ed.; 1996; pp 685-688.

15. Yang, P.; Wu, Y.; Fan, R. Inorganic Semiconductor Nanowires. *International Journal of Nanoscience* **2002,** *1* (1), 1-39.

16. Gates, B.; Wu, Y.; Yin, Y.; Yang, P.; Xia, Y. Single-Crystalline Nanowires of Ag_{2Se} Can Be Synthesized by Templating Against Nanowires of Trigonal Se. *J. Am. Chem. Soc.* **2001,** *123*, 11500-11501.

17. Al-Mawlawi, D.; Liu, C. Z.; Moskovits, M. Nanowires Formed in Anodic Oxide Nanotemplates. *Journal of Materials Research* **1994,** *9* (4), 1014-1018.

18. Zhu, Y.-J.; Wang, W.-W.; Qu, R.-J.; Hu, X.-L. Microwave-Assisted Synthesis of Single-Crystalline Tellurium Nanorods and Nanowires in Ionic Liquids. *Angew. Chem. Int. Ed.* **2004,** *43*, 1410-1414.

19. Hwang, Y. K.; Chang, J.-S.; Park, S.-E.; Kim, D. S.; Kwon, Y.-U.; Jhung, S. H.; Hwang, J.-S.; Pearton, S. J. Microwave Fabrication of MFI Zeolite Crystals with a Fibrous Morphology and Their Applications. *Angew. Chem. Int. Ed.* **2005,** *44*, 556-560.

20. Wang, X.; Li, Y. Synthesis and characterization of lanthanide hydroxide single-crystal nanowires. *Angewandte Chemie, International Edition* **2002,** *41* (24), 4790-4793.

21. Fan, H. J.; Werner, P.; Zacharias, M. Semiconductor nanowires: from self-organization to patterned growth. *Small* **2006,** *2* (6), 700-717.

22. Cho, K.-S.; Talapin, D. V.; Gaschler, W.; Murray, C. M. Designing PbSe Nanowires and Nanorings Through Oriented Attachment of Nanoparticles. *J. Am. Chem. Soc.* **2005,** *127*, 7140-7147.

23. Peng, X.; Manna, L.; Yang, W.; Wickham, J.; Scher, E.; Kadavanich, A.; Alivisatos, A. P. Shape Control of CdSe Nanocrystals. *Nature* **2000,** *404*, 59-61.

24. Tang, Z.; Kotov, N. A.; Giersig, M. Spontaneous organization of single CdTe nanoparticles into luminescent nanowires. *Science* **2002,** *297* (5579), 237-240.

25. Yin, Y.; Alivisatos, A. P. Colloidal nanocrystal synthesis and the organic-inorganic interface. *Nature (London, United Kingdom)* **2005,** *437* (7059), 664-670.

26. Volkov, Y.; Mitchell, S.; Kelleher, D.; Gaponik, N.; Rakovich, Y. P.; Donegan, J. F.; Rogach, A. L. Highly Emissive Nanowires Grown from CdTe Nanocrystals in a Phosphate Buffer Solution. *Proc. of SPIE* **2005,** *5824*, 123-128.

27. Crisp, M. T.; Kotov, N. A. Preparation of Nanoparticle Coatings on Surfaces of Complex Geometry. *Nano Letters* **2003,** *3* (2), 173-177.

28. Rogach, A. L.; Kotov, N. A.; Koktysh, D. S.; Susha, A. S.; Caruso, F. II-VI semiconductor nanocrystals in thin films and colloidal crystals. *Colloids and Surfaces, A: Physicochemical and Engineering Aspects* **2002,** *202* (2-3), 135-144.

29. Xu, L.; Yuan, Z.; Zhang, X. Fabrication of multi-level branched metal nanowires by AAO template electro-deposition. *Chinese Science Bulletin* **2006,** *51* (17), 2055-2058.

30. Zong, F.; Ma, H.; Ma, J.; Du, W.; Zhang, X.; Xiao, H.; Ji, F.; Xue, C. Structural properties and photoluminescence of zinc nitride nanowires. *Applied Physics Letters* **2005,** *87* (23), 233104-1-233104/3.

31. Gaponik, N.; Talapin, D. V.; Rogach, A. L.; Hoppe, K.; Shevchenko, E. V.; Kornowski, A.; Eychmuller, A.; Weller, H. Thiol-Capping of CdTe Nanocrystals: An Alternative to Organometallic Synthetic Routes`. *J. Phys. Chem. B* **2002,** *106*, 7177-7185.

32. Talapin, D. V.; Rogach, A. L.; Shevchenko, E. V.; Kornowski, A.; Haase, M.; Weller, H. Dynamic Distribution of Growth Rates within the Ensembles of Colloidal II - IV and III - V Semiconductor Nanocrystals as a Factor Governing Their Photoluminescence Efficiency. *J. Am. Chem. Soc.* **2002,** *124*, 5782-5790.

33. Sinyagin, A. Y.; Belov, A.; Tang, Z.; Kotov, N. A. Monte carlo computer simulation of chain formation from nanoparticles. *J Phys Chem B* **2006,** *110* (14), 7500-7507.

34. Blanton, S. A.; Leheny, R. L.; Hines, M. A.; Guyot-Sionnest, P. ielectric Dispersion Measurements of CdSE Nanocrystal Colloids: Observation of a Permanent Dipole Moment. *Physical Review Letters* **1997,** *79* (5), 865-868.

35. Rabani, E.; Hetenyi, B.; Berne, B. J. Electronic Properties of CdSe Nanocrystals in the Absence and Presence of a Dielectric Medium. *Journal of Chemical Physics* **1999,** *110* (11), 5355-5369.

36. Shim, M.; Guyot-Sionnest, P. Permanent Dipole Moment and Charges in Colloidal Semiconductor Quantum Dots. *Journal of Chemical Physics* **1999,** *111* (15), 6955-6964.

37. Yaroslavov, A. A.; Sinani, V. A.; Efimova, A. A.; Yaroslavova, E. G.; Rakhnyanskaya, A. A.; Ermakov, Y. A.; Kotov, N. A. What Is the Effective Charge of TGA-Stabilized CdTe Nanocolloids? *Journal of the American Chemical Society* **2005,** *127* (20), 7322-7323.

38. Shanbhag, S.; Kotov, N. A. On the Origin of a Permanent Dipole Moment in Nanocrystals with a Cubic Crystal Lattice: Effects of Truncation, Stabilizers, and Medium for CdS Tetrahedral Homologues. *Journal of Physical Chemistry B* **2006,** *110* (25), 12211-12217.

39. Tang, Z.; Zhang, Z.; Wang, Y.; Glotzer, S. C.; Kotov, N. A. Self-Assembly of CdTe Nanocrystals into Free-Floating Sheets. *Science (Washington, DC, United States)* **2006,** *314* (5797), 274-278.

40. Zhang, Z.; Tang, Z.; Kotov, N. A.; Glotzer, S. C. Simulations and Analysis of Self-Assembly of CdTe Nanoparticles into Wires and Sheets. *Nano Letters* **2007,** *7* (6), 1670-1675.

41. Sinyagin, A.; Belov, A.; Kotov, N. Monte Carlo Simulation of Linear Aggregate Formation from CdTe Nanoparticles. *Modelling and Simulation in Materials Science and Engineering* **2005,** *13*, 389-399.

42. Rabani, E. Structure and Electrostatic Properties of Passivated CdSe Nanocrystals. *Journal of Chemical Physics* **2001,** *115* (3), 1493-1497.

43. Pradhan, N.; Xu, H.; Peng, X. Colloidal CdSe Quantum Wires by Oriented Attachment. *Nano Letters* **2006,** *6*, 720-724.

44. Talapin, D. V.; Rogach, A. L.; Haase, M.; Weller, H. Evolution of an Ensemble of Nanoparticles in a Colloidal Solution: Theoretical Study. *J. Phys. Chem. B* **2001,** *105*, 12278-12285.

45. Peng, X.; Wickham, J.; Alivisatos, A. P. Kinetics of II - IV and III - V Colloidal Semiconductor Nanocrystal Growth: "Focusing" of Size Dirstibutions. *J. Am. Chem. Soc.* **1998,** *120*, 5343-5344.

46. Brigham, E. S.; Weisbecker, C. S.; Rudzinski, W. E.; Mallouk, T. E. Stabilization of Intrazeolitic Cadmium Telluride Nanoclusters by Ion Exchange. *Chem. Mater.* **1996,** *8*, 2121-2127.

47. Peng, Z. A.; Peng, X. Mechanisms of the Shape Evolution of CdSe Nanocrystals. *J. Am. Chem. Soc.* **2001,** *123*, 1389-1395.

48. Zhang, H.; Wang, D.; Mohwald, H. Ligand-Selective Aqueous Synthesis of One-Dimensional CdTe Nanostructures. *Angew. Chem. Int. Ed.* **2006,** *45*, 748-751.

49. Talapin, D. V.; Rogach, A. L.; Haase, M.; Weller, H. Evolution of an Ensemble of Nanoparticles in a Colloidal Solution: Theoretical Study. *J. Phys. Chem. B* **2001,** *105*, 12278-12285.

50. Kovalenko, M. V.; Bodnarchuk, M. I.; Stroyuk, A. L.; Kuchmii, S. Y. Spectral, Optical, and Photocatalytic Characteristics of Quantum-Sized Particles of CdTe. *Theoretical and Experimental Chemistry* **2004,** *40* (4), 220-225.

51. Diaz, D.; Robles, J.; Ni, T.; Castillo-Blum, S. E.; Nagesha, D.; varez-Fregoso, O. J.; Kotov, N. A. Surface Modification of CdS Nanoparticles with MoS42-: A Case Study of Nanoparticle-Modifier Electronic Interaction. *Journal of Physical Chemistry B* **1999,** *103* (45), 9859-9866.

52. Lilly, G. D.; Lee, J.; Sun, K.; Tang, Z.; Kim, K.-S.; Kotov, N. A. Media effect on CdTe nanowire growth: mechanism of self-assembly, ostwald ripening, and control of NW geometry. *J. Phys. Chem. C* **2007**.

CHAPTER 3

Effect of CdSe Nanoparticles on The Growth of Te Nanowires: Greater Length and Tortuosity and Non-Monotonic Concentration Effect

3.1 ABSTRACT

Improved control over NW geometry and composition offers multiple benefits for design material and devices One example is in complex nanoelectronic circuits, whereby facilitating their organization on substrates provides more efficient charge transport over large distances, as well as greater mechanical strength. Te NWs have many interesting thermoelectric, piezoelectric, conducting, and photo-conducting properties, and these NWs are highly reactive with numerous chemicals. This allows Te NWs to be used as templates for NWs of other compositions. Te NWs in this study are made from CdTe NPs by slow oxidation. Te NWs with average lengths of 6.63±1.07 μm and aspect ratios of 50 were initially formed. Unexpectedly, the presence of CdSe NPs results in a drastic increase in the length, aspect ratio, and tortuosity of the Te NWs. We believe that Se^{2-} is being incorporated into the Te seeds as elemental Se, fouling them and reducing the number of viable Te seeds, which allows longer Te NWs to form. Excessive amounts of CdTe NPs stop the growth of Te NWs completely making the concentration dependence strongly non-monotonic. The longest tortuous NWs grown in this fashion have lengths of 15.56±4.16 μm and aspect ratios 103. This work reveals a novel process taking place

between growing NWs and NPs. These finding indicate advantages of using NPs for reaction control in preparation of NW with high practical relevance.

3.2 INTRODUCTION

One-dimensional semiconductor NWs offer small size and one dimensional quantum confinement which give them many unique optical and electronic properties. These unique properties make semiconductor NWs desirable for use in new photonic devices such as solid state lasers,[1-3] in light collecting devices such as solar cells[4], as optical waveguides that internally guide light through a material with a lower permittivity,[3,5,6] and as light emitting diodes[3,7,8,9]. NWs also find uses in many electronic devices including resistors.[10,11] diodes[10,12,13], switches[14,15], inverters[16], transistors[16,17,18], and more complex circuits[19]. The unique properties of semiconductor NWs allow them to be used in various sensors including those based on field-effect FETs[20,21] and photoluminescence[22,23].

The dimensions (length, diameter, aspect ratio) and geometry (shape, tortuosity) of the NWs play important roles in NW performance in the above applications. The formation of long, high aspect ratio NWs is desirable because it makes possible manufacturing more complex nanoelectronic circuits, for instance using on-nanowire lithography[24]. Furthermore, NWs with increasingly complex geometries offer the formation of more complex nanoelectronic circuits provided that there are simple means to control NW morphology. High aspect ratios also facilitate NW alignment on substrates[25,26] and provide more efficient charge transport over large distances by eliminating tunneling junctions between the individual wires. Contact resistance in

tunneling junctions representing significant problem for preparation of highly conductive macroscale materials from nanoscale building blocks[27-29]. Composite materials made of longer NWs have intrinsically better mechanical properties than the same materials made of shorter ones because of their ability to offer higher percolation values[30-32].

Therefore, it is important to be able to increase the aspect ratio of the NWs synthesized following the same pattern as it is being done for carbon nanotubes. We have previously presented a solution-based NW synthesis procedure governed by the oriented attachment of NPs into NWs. In this method, presented by Tang et al[33], the stabilizers of II-IV NPs are partially removed, allowing the NPs to orient themselves into pearl necklace structures which subsequently recrystallize into CdTe NWs. This method allows the spontaneous, aqueous assembly of NPs into NWs. Various refinements of this technique have allowed more precise control over the dimensions of the NWs[34], as well as the composition[35] and geometry of the resulting structures[36,37]. Interestingly, this project began with a different purpose in mind. Our desire was to produce gradient NWs whose composition and band-gap vary along the length of the NW for use in solar cells and autonomous nanosensors[38]. The aim was to synthesize NWs with CdTe middle sections that transition to CdSe ends by the formation of short CdTe NWs, then introducing CdSe NPs into the growth solution as the NW continued to grow. However, a corresponding modification of the earlier procedure[39] instead resulted in the spontaneous transformation of CdTe NPs into Te NWs. Concomitantly, the effect of added CdSe NPs was also quite different than what we expected in the beginning. Nevertheless, the results that obtained were both unexpected and quite interesting from a structural point of view, and potentially useful in practice. Te NWs have many interesting

thermoelectric, piezoelectric, conducting, and photo-conducting properties.[35,40-44] Additionally, Te is highly reactive with numerous chemicals, so Te NWs may also be used as templates for NWs of other compositions.[35] High aspect ratio Te NWs potentially have even greater significance than those made from CdTe.

There are many reported methods to synthesize nanomaterials. Most rely on the reduction of a tellurium compound (orthotrelluric acid[45], $(NH_4)_2TeS_4$[46], H_2TeO_2[47], $Te(OC_2H_5)_4$[42], and Na_2TeO_3[48] to create Te seeds which subsequently grow into Te nanomaterials. The morphology of the resulting nanomaterials can be altered from nanotubes (NTs), NWs, and nanoribbons (NRs) by changing the reducing environment including the reducing agent (ethylene glycol, hydrazine, biomolecules, surfactants), dispersing material (water, ethanol, and ethylene glycol), and temperature. One is the reduction of orthotelluric acid with hydrazine or ethylene glycol to produce Te NWs and NTs depending on the conditions[45,49] and offers a method to synthesize Te/Se NW alloys using a reduction of orthotelluric and selenious acid in the same pot. The resulting NWs have a Te:Se ratio of 1:1 with good crystallinity; however, they have relatively short aspect ratios of 5[45].

Here we report that single crystalline, straight Te NWs can be grown from CdTe without any growth modifiers to give lengths of 6.63±1.07 μm and aspect ratios of 51. The addition of CdSe NP or Se^{2-} ions into this growth solution causes the Te NWs to become more tortuous and increase in length and aspect ratio to reach maxima of 15.56±4.16 μm and 103, respectively, which correlates well with other studies on Te NWs preparations[35,41,42,49]. In this paper we also elaborate on the growth mechanism and relate to effect the incorporation of Se atoms and clusters in Te seeds and growing NWs,

which explains the strongly non-monotonic effect of added CdSe NPs and Se^{2-} on the length of Te NWs. While small amount of growth modifiers results in substantial increase in length, their excessive amount completely stops NW growth. Such behavior is explained on the basis of incomplete and complete fowling of Te seeds after incorporation of Se. Our method provides the Te seeds and subsequent growth material by the decomposition of CdTe NPs and subsequent oxidation of Te^{2-} ions, offers the ability to control the shape of the Te NWs by adjusting the growth environment, and describes a new aspect of chemical interactions between NWs and NPs.

3.3 SYNTHESIS

TGA stabilized CdTe and CdSe NPs are prepared according to the literature.[50,51] The average diameter of the CdTe NWs, as measured with AFM, is 2.6±1.1 nm with a wavelength of maximum fluorescence (λ_{max}) of 541 nm; while the average diameter of the CdSe NPs, as measured with AFM, is 2.1±0.8 nm. Error margins represent the standard deviation in the sample. The CdSe NPs exhibit no fluorescence. Te NWs are prepared according to a modified procedure outlined by Lilly et al[34]. Briefly, 1 mL of CdTe NP solution is mixed with 0.5 mL methanol and 0.5 mL 2-propanol to partially remove TGA stabilizer from the CdTe NP surface. All solutions are deoxygenated by bubbling nitrogen in an inert environment. The resulting turbid solution is shaken and centrifuged until all NPs have precipitated and the solution is clear. The supernatant is decanted. In order to ensure all excess liquid is removed from the NPs, the moist NPs are freeze dried overnight. The dry, stabilizer depleted CdTe NPs are reconstituted to 1 mL with a deoxygenated 20% (v/v) mixture of DMSO in pH 9 water. This constitutes the

CdTe NP growth solution. CdSe NP growth solutions are prepared in a similar manner, but the CdTe NPs are replaced with CdSe NPs. The CdTe NP growth solution and CdSe NP growth solution are mixed in ratios varying from 0% CdSe to 100% CdSe. Solutions containing Na_2Se are created by the addition of various volumes of 0.04 M Na_2Se to CdTe NP growth solution. The resulting mixtures are placed in an 80°C oven from 1 to 3 days at which time the solutions are removed and studied.

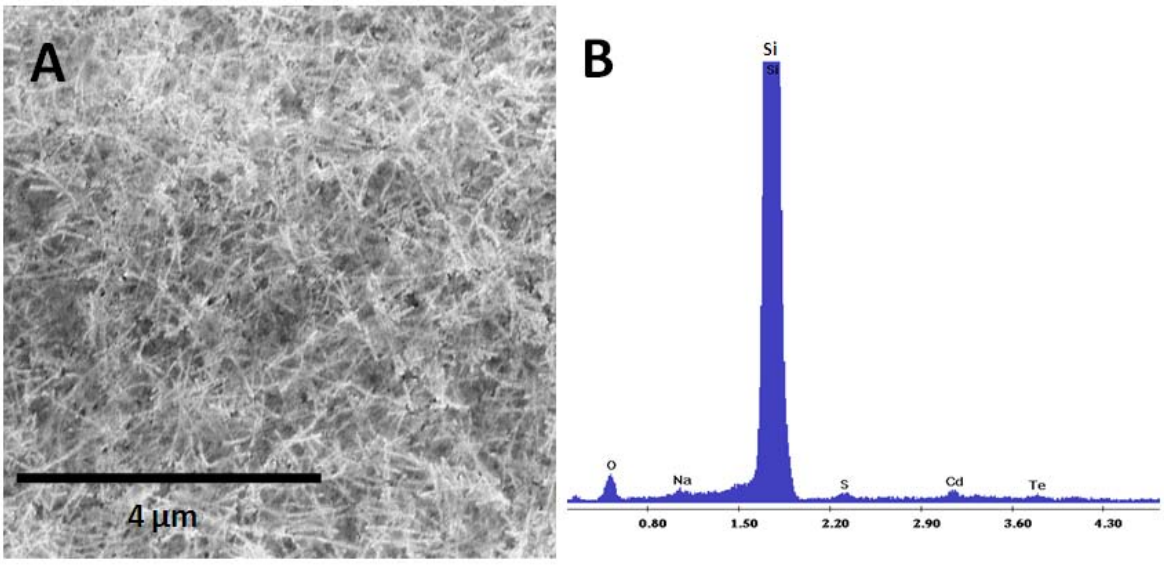

Figure 3.1. A) SEM image of a large precipitate with Te NWs fused with Cd and Te oxides, B) EDS spectra of the precipitate.

3.4 RESULTS AND DISCUSSION

3.4.1 Formation of high aspect ratio Te NWs

Long, straight, highly crystalline Te NWs result from placing a CdTe growth solution, i.e. stabilizer depleted CdTe NPs in a deoxygenated solution of 20% DMSO and pH 9 water, in an 80°C oven for 24 hours. While the solution is deoxygenated, a small quantity of oxygen persists in the solution. This small amount of oxygen and the excess DMSO in the solution oxidize Te^{2-} to create small Te atomic clusters, which serve as

seeds that allow further precipitation in the c-axis to form one dimensional 1D structures[35,52]. The relative lack of oxygen and the weak oxidization potential of DMSO limit the number Te condensation centers from forming, allowing long NWs to form. By reducing the number of Te seeds, more Te may deposit onto each, resulting in an increase in the length of the wires. In fact, when the sealed vials of growth solution are exposed to air, Te NWs along with oxides of Te and Cd precipitate from the solution immediately. Figure 3.1 shows the SEM image and corresponding EDS spectrum of the precipitate. It should be noted that the formation of new Te seeds and the growth of existing Te NWs occur simultaneously, resulting in an assortment of NW lengths.

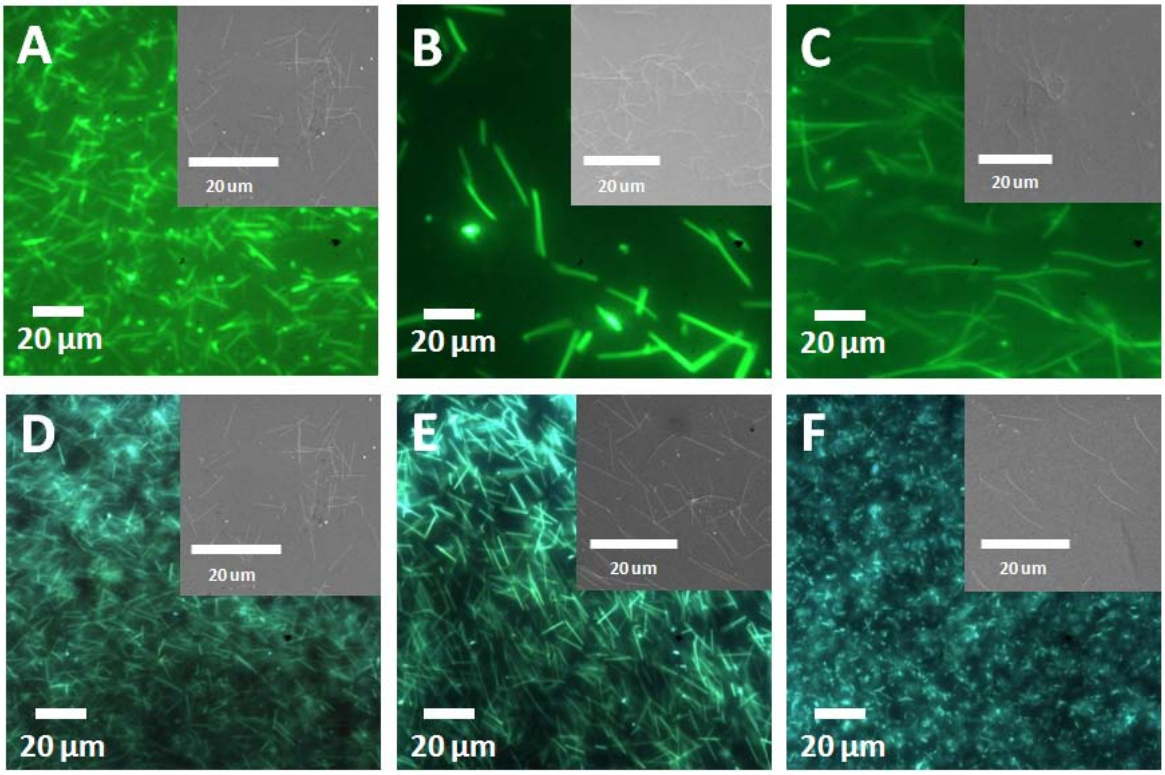

Figure 3.2. Optical michrographs and SEM images (inserts) of Te NWs synthesized from growth solutions with CdSe NP: CdTe NP ratios of A) 0:1, B) 1:1, and C) 2:1; and Se^{2-} concentrations of D) 0, E) $3.5*10^{-4}$ M, F) $6.0*10^{-4}$ M.

Te NW formation initially occurs after 6 hours, as indicated by a darkening of the suspension, and is allowed to continue an additional 24 hours, at after that the solution is removed from the oven and studied. As is clearly seen, the resulting Te NWs are long and straight, with high aspect ratios around 50 (Figure 3.2A and D). The average dimensions of the Te NWs, as measured with SEM, are 6.63±1.07 μm by 0.13±0.03 μm. Interestingly, they can be easily observed in optical microscope, which is clear demonstration of their impressive length (Figure 3.2A and D). The optical micrographs of the Te NWs are similar to the images taken with SEM. Of course the dimensions, and in particularly the width appear larger than they are in reality due to light scattering. HRTEM images (Figure 3.3A) show lattice spacing indicative of trigonal Te NWs with a 001 zone axis, as expected from previous reports[35], and an EDS spectrum (Figure 3.3B) confirms the composition of the NW as Te. No Cd or CdTe NWs are observed, and the remaining NPs in the NW suspension are rich in Cd (Figure 3.3B and D).

The formation of Te NWs can be induced from stabilizer depleted CdTe NPs by the addition of dipotassium ethylendiaminetetraacetate (EDTA) into the CdTe growth solutions.[35] There, EDTA, a Cd-complexing agent, was added to a CdTe NP solution, where it bound strongly to the Cd^{2+} ions in the CdTe NPs released free Te^{2-} ions in solution which underwent a reaction with oxygen to create Te NWs. The reaction scheme was given below as Eq. 3.1 and 3.2, where E represents either Se or Te.[35]

$$CdE + H_2EDTA^{2-} \longrightarrow Cd(EDTA)^{2-} + 2H^{+} \quad (3.1)$$

$$2E^{2-} + O_2 + 2H_2O \longrightarrow 2E + 4OH^{-} \quad (3.2)$$

In the current case, we believe that DMSO acts in a similar fashion as EDTA in the work by Z. Tang et. al.[35], which is to provide excess Te^{2-} ions in solution that are then oxidized by DMSO and traces of oxygen to become Te NWs. DMSO both serves to enhance the decomposition of the CdTe NP into Cd^{2+} and Te^{2-} ions[34] and acts as an oxidizer to assist O_2 in transforming Te^{2-} to atomic Te[52]. Similarly to EDTA, it probably complexes Cd^{2+}; and is likely to form a strong solvation shell around Te^{2-} as well.

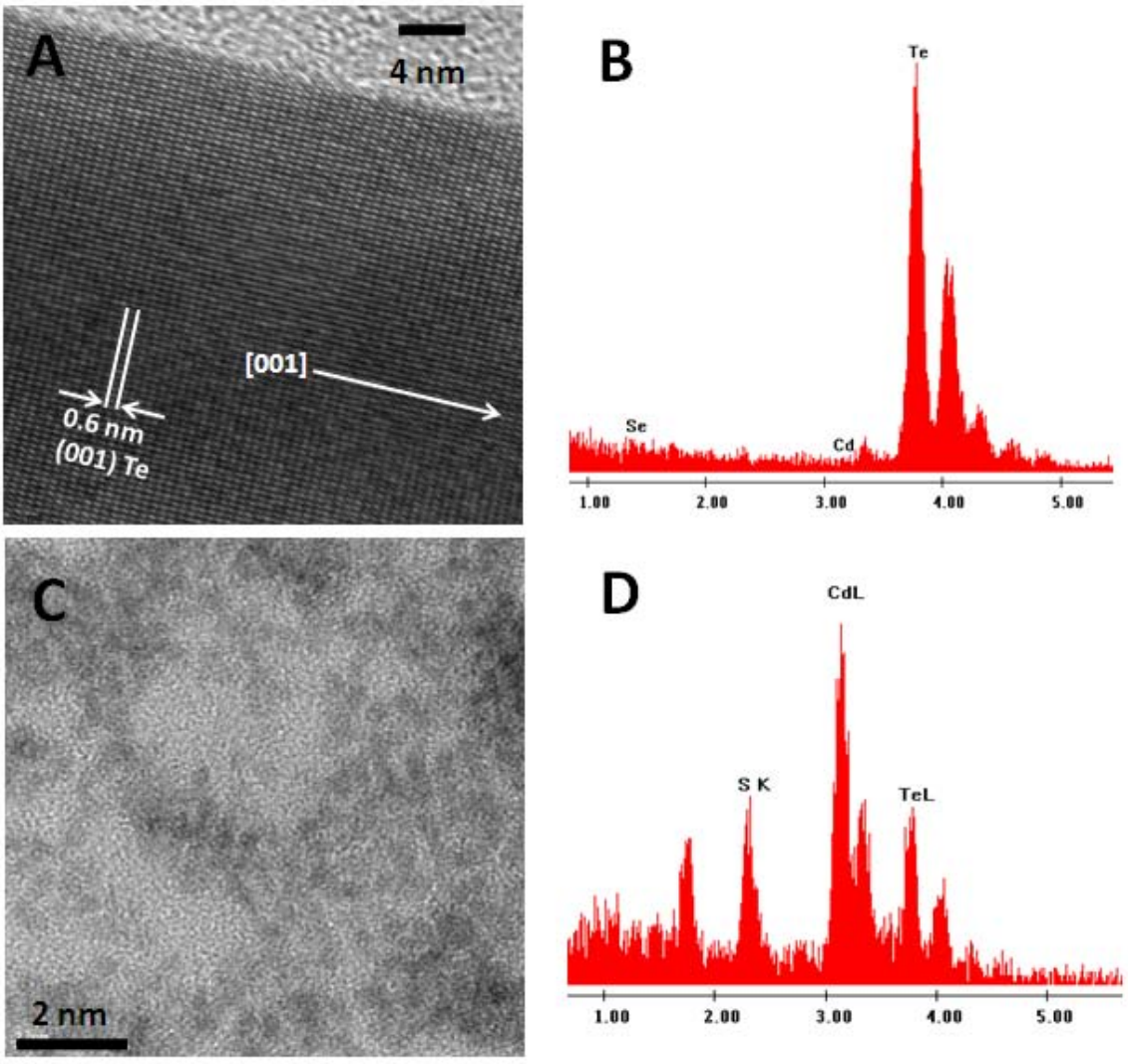

Figure 3.3. A) HRTEM and B) EDAX spectra of Te NW grown in 0:1 CdSe NP: CdTe NP ratio, C) TEM and D) EDAX of Te depleted CdTe NPs from solutions in 0:1 CdSe NP: CdTe NP ratio.

3.4.2 Effect of CdSe NPs on NW morphology

Te NWs are allowed to form from the CdTe NW growth solution for ~12 hours in the 80 ^{o}C oven as before, at which time stabilizer depleted CdSe NPs are added as growth modifier. After an additional 24 hours, the samples are removed from the 80 ^{o}C oven and studied. Optical micrographs and SEM images of NWs grown in various CdSe NP: CdTe NP ratios are shown in Figure 3.2. While the Te NWs obtained in the previous section are already quite long, their length further increases as the amount of CdSe NPs is increased. Te NWs grown in pure CdTe NP growth solutions are quite straight, while NWs grown in a 2:1 CdSe NP: CdTe NP growth solution are tortuous. Te NW average dimensions, as measured with SEM, range from 6.63±1.07 μm by 0.13±0.03 μm, aspect ratio of 51, for those grown in pure CdTe NP growth solutions to 15.56±4.16 μm by 0.15±0.02 μm, aspect ratio of 103, for those grown in a growth solution with a 2:1 CdSe NP: CdTe NP ratio.

To understand better the effect of CdSe NPs and additional series of experiments is carried out with Se^{2-} ions added to the CdTe NPs as growth modifiers. Te NWs are allowed to form from the CdTe NW growth solution for ~12 hours in the 80 ^{o}C oven, at which time Se^{2-} ions are incorporated into the CdTe growth solution by the addition of Na_2Se. Again, the samples are studied after an additional 24 hours have passed. Optical microscopy and SEM images of NWs grown in various Na_2Se concentrations are shown in Figure 3.2. We see unmistakable similarity of the effects of addition of CdSe NPs and Se^{2-}, which indicate to us an obvious chemical relationship between these two cases. Te NW length and tortuosity initially increase as the Na_2Se concentration is increased. As the Na_2Se concentration is raised further, the length of the Te NWs is stunted and large

Te and Se clusters develop. So, the effect of Se^{2-} as growth modifier on the morphology of Te NWs is strongly non-monotonic, which can also be appreciated from the optical images of Te NW dispersions (Figure 3.2). Again, Te NWs grown in pure CdTe NP growth solutions are straight, while NWs grown in higher Na_2Se concentrations are tortuous. Te NW average dimensions, as measured with SEM, range from a minimum of 6.63±1.07 μm by 0.13±0.03 μm, aspect ratio of 51, for those grown in pure CdTe NP growth solutions to 10.65±0.99 μm by 0.13±0.02 μm, aspect ratio of 82, for those grown in a growth solution with $6.0*10^{-4}$ M Na_2Se.

Both addition of CdSe NPs and Se^{2-} initially result in an increase in length and tortuosity of the Te NWs at relatively low range of Se^{2-} concentrations. However, stunting and eventual cessation of Te NWs is observed with high concentrations of Na_2Se, but not with CdSe NPs because the decomposition of CdSe NPs does not provide high enough Se^{2-} ion concentrations for this effect to occur. This is because when Na_2Se is added to the CdTe NW growth solution, it immediately dissociates into Na^+ and Se^{2-} ions; however, when CdSe NPs are added to the CdTe NW growth solution, the CdSe NPs slowly release Se^{2-} ions into solution, just as the CdTe NPs slowly release Te^{2-} ions into solution.

So, we probably need to discuss both cases from the perspective of a certain concentration of Se^{2-} present in the growth media, which acts as generic growth modifier in all experiments in the framework of this study. We believe that the length of the Te NWs is increased at low Se^{2-} concentrations because Se atoms become incorporated into some of the new Te seeds that are formed, fouling them and preventing Te NWs from forming from these seeds. Just as Te^{2-} is oxidized and becomes Te, Se^{2-} is also oxidized

to atomic Se; the redox potentials for Te^{2-}/Te and Se^{2-}/Se are -1.143 V and -0.924V, respectively.[35] This fouling is most probably the result of crystal defects in the Te seeds caused by differences in the crystal structure of Se and Te. These defects prevent 1D growth of the Te seed into a Te NW. By reducing the number of viable Te seeds, more Te may be deposited onto each active seed, which results in an increase in the length of the wires.

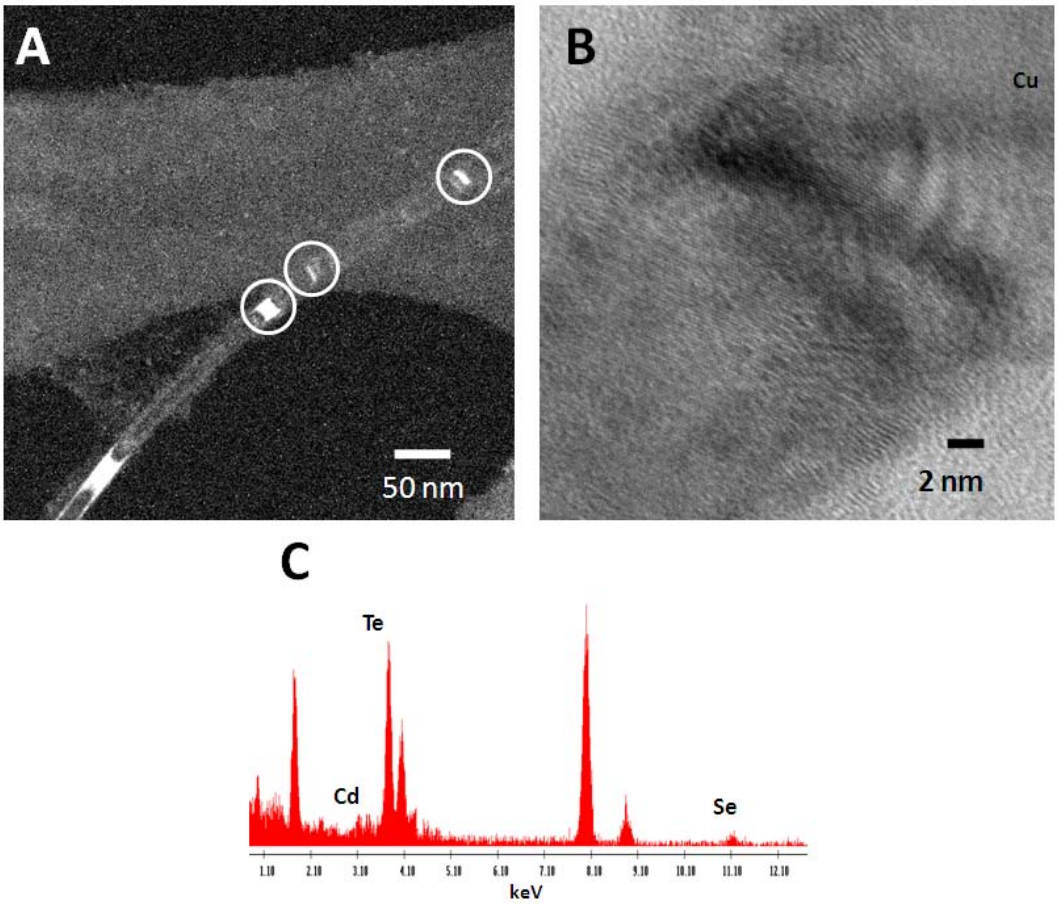

Figure 3.4. (A) Dark field TEM image of Te NW grown in a 2:1 CdSe NP: CdTe NP ratio. The defects in this wire are circled. (B) HRTEM of a defect in Te NW grown in a 2:1 CdSe NP: CdTe NP ratio. (C) EDAX of Te NW grown in a 2:1 CdSe NP: CdTe NP ratio. The Cu peak is from the copper TEM grid.

As the Se^{2-} concentration is further increased, the length of the Te NWs continues to increase and they become increasingly tortuous. Again, the further increase in length is the result of fewer Te seeds. The increase in tortuosity is the result of Se atoms

becoming incorporated into the Te NWs, as is seen in Figure 3.4C, which shows an EDAX spectrum of a NW grown in a growth solution in a 2:1 CdSe NP: CdTe NP ratio. As expected, very little Se is incorporated into the NWs. The NWs are made of predominantly from Te with minute amounts of Se. The lattice parameters of trigonal $P3_121$ Te are a=4.46Å and c=5.93Å, while those of trigonal $P3_121$ Se are a=4.37Å and c=4.96Å. They are fairly close so that the incorporation of Se into the Te NWs can occur. At the same time, the difference in c lattice constants apparently creates crystal defects that cause the NW to curve. Figure 3.4A, a dark field image of a tortuous NW, helps identify crystal defects in the NW that cause it to curve. Figure 3.4B shows a likely HRTEM image of such a defect.

Once the Se^{2-} concentration is raised above a certain threshold, Te NW growth is stunted, few NWs are formed, and large Te and Se clusters appear. Few NWs are seen because Se fouls all new Te seeds, preventing any new NW formation after the introduction of Na_2Se. The same happens probably with all the growth points on NWs, which can no longer support proper crystallization pattern with selected 0001 axis, and hence, no NWs, but rather disordered agglomerates are produced.

3.5 CONCLUSION

In conclusion, we show that a deoxygenated growth solution of CdTe NPs with DMSO results in long Te NWs with lengths of 6.63±1.07 μm and high aspect ratios of ca. 50. Additionally, the presence of CdSe NPs in the growth solution results in longer, more tortuous Te NWs. The length and tortuosity of the Te NWs are related to small concentrations of Se^{2-}generated by the NPs. As was demonstrated by a part of the study

with addition of Se^{2-}, low Se^{2-} concentrations result in long, straight Te NWs; medium Se^{2-} concentrations result in long, tortuous Te NWs with lengths of 15.56±4.16 μm and aspect ratios 103; and high Se^{2-} concentrations stunt NW formation. The entire process is driven by Se incorporation into the Te seeds and NWs. Such long, high aspect ratio, variable geometry, Te NWs offer numerous uses in various thermoelectric, piezoelectric, conducting, photoconducting, and templating applications, while CdTe NPs offer a convenient means of control this highly non-monotonic reaction. The high aspect ratio and tunable geometry of the wires,[50] which are easily visible even in optical microscope, offer the promise of more complex nanocircuitry, more efficient charge transfer, easier NW alignment, and stronger mechanical properties in composite uses. Future directions of this research include growing composition gradient CdTe/CdSe NWs using the similar technique of adding CdSe into the CdTe NW growth solution, and the incorporation of these Te NWs into various devices, such as optical switches.

3.6 ACKNOWLEDGEMENTS

This work is accepted for publication with revision in the *Journal of Physical Chemistry C.* I would like to thank Yanbin Chen and EMAL for their assistance with the TEM images. I would also like to thank the following agencies for support of this research: AFOSR (Game Changer #GRT00008581/RF60012388 and MMMM program #FA9550-05-1-043, MURI #444286-P061716), ONR (# N00014-06-1-0473), NSF (#CMS-0528867 and # R8112-G1).

3.7 REFERENCES

1. Yang, P.; Wu, Y.; Fan, R. Inorganic Semiconductor Nanowires. *International Journal of Nanoscience* **2002,** *1* (1), 1-39.

2. Fan, H. J.; Werner, P.; Zacharias, M. Semiconductor nanowires: from self-organization to patterned growth. *Small* **2006,** *2* (6), 700-717.

3. Sirbuly, D. J.; Law, M.; Yan, H.; Yang, P. Semiconductor Nanowires for Subwavelength Photonics Integration. *Journal of Physical Chemistry B* **2005,** *109* (32), 15190-15213.

4. Baxter, J. B.; Walker, A. M.; van Ommering, K.; Aydil, E. S. Synthesis and characterization of ZnO nanowires and their integration into dye-sensitized solar cells. *Nanotechnology* **2006,** *17* (11), S304-S312.

5. Sirbuly, D. J.; Law, M.; Pauzauskie, P.; Yan, H.; Maslov, A. V.; Knutsen, K.; Ning, C. Z.; Saykally, R. J.; Yang, P. Optical routing and sensing with nanowire assemblies. *Proceedings of the National Academy of Sciences of the United States of America* **2005,** *102* (22), 7800-7805.

6. Law, M.; Sirbuly, D. J.; Johnson, J. C.; Goldberger, J.; Saykally, R. J.; Yang, P. Nanoribbon waveguides for subwavelength photonics integration. *Science* **2004,** *305* (5688), 1269-1273.

7. Duan, X.; Huang, Y.; Cui, Y.; Wang, J.; Lieber, C. M. Indium phosphide nanowires as building blocks for nanoscale electronic and optoelectronic devices. *Nature* **2001,** *409* (6816), 66-69.

8. Goldberger, J.; Sirbuly, D. J.; Law, M.; Yang, P. ZnO nanowire transistors. *Journal of Physical Chemistry B* **2005,** *109* (1), 9-14.

9. Gudiksen, M. S.; Lauhon, L. J.; Wang, J.; Smith, D. C.; Lieber, C. M. Growth of nanowire superlattice structures for nanoscale photonics and electronics. *Nature* **2002,** *415* (6872), 617-620.

10. Hurst, S. J.; Payne, E. K.; Quin, L.; Mirkin, C. A. Multisegmented One-Dimensional Nanorods Prepared by Hard-Template Synthetic Methods. *Angewandte Chemie* **2006,** *45*, 2672-2692.

11. Tanase, M.; Silevitch, D. M.; Hultgren, A.; Bauer, L. A.; Searson, P. C.; Meyer, G. J.; Reich, D. H. Magnetic trapping and self-assembly of multicomponent nanowires. *Journal of Applied Physics* **2002,** *91* (10, Pt. 3), 8549-8551.

12. Park, S.; Lim, J. H.; Chung, S. W.; Mirkin, C. A. Self-Assembly of Mesoscopic Metal-Polymer Amphiphiles. *Science (Washington, DC, United States)* **2004,** *303* (5656), 348-351.

13. Kovtyukhova, N. I.; Mallouk, T. E. Nanowire p-n heterojunction diodes made by templated assembly of multilayer carbon-nanotube/polymer/semiconductor-particle shells around metal nanowires. *Advanced Materials (Weinheim, Germany)* **2005,** *17* (2), 187-192.

14. Pena, D. J.; Mbindyo, J. K. N.; Carado, A. J.; Mallouk, T. E.; Keating, C. D.; Razavi, B.; Mayer, T. S. Template Growth of Photoconductive Metal-CdSe-Metal Nanowires. *Journal of Physical Chemistry B* **2002,** *106* (30), 7458-7462.

15. Wang, Y.; Tang, Z.; Podsiadlo, P.; Elkasabi, Y.; Lahann, J.; Kotov, N. A. Mirror-like photoconductive layer-by-layer thin films of Te nanowires: the fusion of semiconductor, metal, and insulator properties. *Advanced Materials (Weinheim, Germany)* **2006,** *18* (4), 518-522.

16. Cui, Y.; Lieber, C. M. Functional nanoscale electronic devices assembled using silicon nanowire building blocks. *Science* **2001,** *291* (5505), 851-853.

17. Cui, Y. *Semiconductor nanowires for nanotechnology: synthesis, properties, nanoelectronics, nanophotonics, and nanosensors;* 2002.

18. Ng, H. T.; Han, J.; Yamada, T.; Nguyen, P.; Chen, Y. P.; Meyyappan, M. Single-crystal nanowire vertical surround-gate field-effect transistor. *Nano Letters* **2004,** *4* (7), 1247-1252.

19. Huang, Y.; Duan, X.; Cui, Y.; Lauhon, L. J.; Kim, K. H.; Lieber, C. M. Logic gates and computation from assembled nanowire building blocks. *Science (Washington, DC, United States)* **2001,** *294* (5545), 1313-1317.

20. Patolsky, F.; Zheng, G.; Lieber, C. M. Nanowire-based biosensors. *Analytical Chemistry* **2006,** *78* (13), 4260-4269.

21. Cui, Y.; Wei, Q.; Park, H.; Lieber, C. M. Nanowire nanosensors for highly sensitive and selective detection of biological and chemical species. *Science (Washington, DC, United States)* **2001,** *293* (5533), 1289-1292.

22. Lee, J.; Govorov, A. O.; Kotov, N. A. Nanoparticle assemblies with molecular springs: A nanoscale thermometer. *Angewandte Chemie, International Edition* **2005,** *44* (45), 7439-7442.

23. Lee, J.; Govorov, A. O.; Dulka, J.; Kotov, N. A. Bioconjugates of CdTe Nanowires and Au Nanoparticles: Plasmon-Exciton Interactions, Luminescence Enhancement, and Collective Effects. *Nano Letters* **2004,** *4* (12), 2323-2330.

24. Tan, S.; Tang, Z.; Liang, X.; Kotov, N. A. Resonance Tunneling Diode Structures on CdTe Nanowires Made by Conductive AFM. *Nano Lett.* **2004,** *4* (9), 1637-1641.

25. Shim, B. S.; Kotov, N. A. Single-Walled Carbon Nanotube Combing during Layer-by-Layer Assembly: From Random Adsorption to Aligned Composites. *Langmuir* **2005,** *21* (21), 9381-9385.

26. Shim, B. S.; Podsiadlo, P.; Lilly, D. G.; Agarwal, A.; Lee, J.; Tang, Z.; Ho, S.; Ingle, P.; Paterson, D.; Lu, W.; Kotov, N. A. Nanostructured Thin Films Made by Dewetting Method of Layer-By-Layer Assembly. *Nano Lett.* **2007,** *7* (11), 3266-3273.

27. Nogales, A.; Broza, G.; Roslaniec, Z.; Schulte, K.; Sics, I.; Hsiao, B. S.; Sanz, A.; Garcia-Gutierrez, M. C.; Rueda, D. R.; Domingo, C.; Ezquerra, T. A. Low Percolation Threshold in Nanocomposites Based on Oxidized Single Wall Carbon Nanotubes and Poly(butylene terephthalate). *Macromolecules* **2004,** *37* (20), 7669-7672.

28. Hicks, J.; Behnam, A.; Ural, A. Resistivity in percolation networks of one-dimensional elements with a length distribution. *Phys. Rev. E: Stat. , Nonlinear, Soft Matter Phys.* **2009,** *79* (1-1), 012102-1-012102/4.

29. Sysoev, V. V.; Kiselev, I.; Schneider, T.; Bruns, M.; Sommer, M.; Habicht, W.; Musatov, V. Y.; Strelcov, E.; Kolmakov, A. The Gas-Sensing Characteristics Of Percolating 2-D SnO2 Nanowire Mats As A Platform For Electronic Nose Devices. *AIP Conf. Proc.* **2009,** *1137* (1), 403-404.

30. Bin, Y.; Chen, Q.; Tashiro, K.; Matsuo, M. Electrical and mechanical properties of iodine-doped highly elongated ultrahigh molecular weight polyethylene films filled with multiwalled carbon nanotubes. *Phys. Rev. B: Condens. Matter Mater. Phys.* **2008,** *77* (3), 035419-1-035419/7.

31. Andrews, R.; Weisenberger, M. C.; Rantell, T. Thermomechanical properties of carbon nanotube composite materials. *Proc. NATAS Annu. Conf. Therm. Anal. Appl.* **2006,** *34th*, 108.

32. Puglia, D.; Terenzi, A.; Barbosa, S. E.; Kenny, J. M. Polypropylene-natural fibre composites. Analysis of fibre structure modification during compounding and its influence on the final properties. *Compos. Interfaces* **2008,** *15* (2-3), 111-129.

33. Tang, Z. Y.; Kotov, N. A.; Giersig, M. Spontaneous organization of single CdTe nanoparticles into luminescent nanowires. *Science* **2002,** *297* (5579), 237-240.

34. Lilly, G. D.; Lee, J.; Sun, K.; Tang, Z.; Kim, K.-S.; Kotov, N. A. Media effect on CdTe nanowire growth: mechanism of self-assembly, ostwald ripening, and control of NW geometry. *J. Phys. Chem. C* **2007**.

35. Tang, Z.; Wang, Y.; Sun, K.; Kotov, N. A. Spontaneous transformation of stabilizer-depleted binary semiconductor nanoparticles into selenium and

tellurium nanowires. *Advanced Materials (Weinheim, Germany)* **2005,** *17* (3), 358-363.

36. Tang, Z.; Wang, Y.; Shanbhag, S.; Giersig, M.; Kotov, N. A. Spontaneous Transformation of CdTe Nanoparticles into Angled Te Nanocrystals: From Particles and Rods to Checkmarks, X-Marks, and Other Unusual Shapes. *Journal of the American Chemical Society* **2006,** *128* (20), 6730-6736.

37. Tang, Z.; Zhang, Z.; Wang, Y.; Glotzer, S. C.; Kotov, N. A. Self-Assembly of CdTe Nanocrystals into Free-Floating Sheets. *Science (Washington, DC, United States)* **2006,** *314* (5797), 274-278.

38. Lee, J.; Hernandez, P.; Lee, J.; Govorov, A. O.; Kotov, N. A. Exciton-plasmon interactions in molecular spring assemblies of nanowires and wavelength-based protein detection. *Nature Materials* **2007,** *6* (4), 291-295.

39. Tang, Z.; Kotov, N. A.; Giersig, M. Spontaneous organization of single CdTe nanoparticles into luminescent nanowires. *Science* **2002,** *297* (5579), 237-240.

40. Qian, H. S.; Yu, S. H.; Gong, J. Y.; Luo, L. B.; Fei, L. F. High-Quality Luminescent Tellurium Nanowires of Several Nanometers in Diameter and High Aspect Ratio Synthesized by a Poly(Vinyl Pyrrolidone)-Assisted Hydrothermal Process. *Langmuir* **2006,** *22* (8), 3830-3835.

41. Liang, F.; Qian, H. Synthesis of tellurium nanowires and their transport property. *Mater. Chem. Phys.* **2009,** *113* (2-3), 523-526.

42. Watanabe, N.; Toshima, N. Preparation and characterization of nanomaterials of tellurium, bismuth, and bismuth telluride. *Bull. Chem. Soc. Jpn.* **2007,** *80* (1), 208-214.

43. Mohanty, P.; Kang, T.; Kim, B.; Park, J. Synthesis of Single Crystalline Tellurium Nanotubes with Triangular and Hexagonal Cross Sections. *J. Phys. Chem. B* **2006,** *110* (2), 791-795.

44. Wang, W.; Sun, L.; Fang, Z.; Chen, L.; Zhang, Z. Direct Fabrication of Tellurium/Carbon Nanocables through a Facile Solution Route. *Cryst. Growth Des.* **2009,** *9* (5), 2117-2123.

45. Xia, Y.; Yang, P.; Sun, Y.; Wu, Y.; Mayers, B.; Gates, B.; Yin, Y.; Kim, F.; Yan, H. One-dimensional nanostructures: Synthesis, characterization, and applications. *Adv. Mater. (Weinheim, Ger.)* **2003,** *15* (5), 353-389.

46. Liu, Z.; Hu, Z.; Liang, J.; Li, S.; Yang, Y.; Peng, S.; Qian, Y. Size-Controlled Synthesis and Growth Mechanism of Monodisperse Tellurium Nanorods by a Surfactant-Assisted Method. *Langmuir* **2004,** *20* (1), 214-218.

47. Lu, Q.; Gao, F.; Komarneni, S. Biomolecule-assisted reduction in the synthesis of single-crystalline tellurium nanowires. *Adv. Mater. (Weinheim, Ger.)* **2004,** *16* (18), 1629-1632.

48. Mo, M.; Zeng, J.; Liu, X.; Yu, W.; Zhang, S.; Qian, Y. Controlled hydrothermal synthesis of thin single-crystal tellurium nanobelts and nanotubes. *Adv. Mater. (Weinheim, Ger.)* **2002,** *14* (22), 1658-1662.

49. Mayers, B.; Xia, Y. One-dimensional nanostructures of trigonal tellurium with various morphologies can be synthesized using a solution-phase approach. 2009; pp 1875-1881.

50. Gaponik, N.; Talapin, D. V.; Rogach, A. L.; Hoppe, K.; Shevchenko, E. V.; Kornowski, A.; Eychmuller, A.; Weller, H. Thiol-Capping of CdTe Nanocrystals: An Alternative to Organometallic Synthetic Routes`. *J. Phys. Chem. B* **2002,** *106*, 7177-7185.

51. Talapin, D. V.; Rogach, A. L.; Shevchenko, E. V.; Kornowski, A.; Haase, M.; Weller, H. Dynamic Distribution of Growth Rates within the Ensembles of Colloidal II - IV and III - V Semiconductor Nanocrystals as a Factor Governing Their Photoluminescence Efficiency. *J. Am. Chem. Soc.* **2002,** *124*, 5782-5790.

52. Epstein, W. W.; Sweat, F. W. Dimethyl Sulfoxide Oxidations. *Chemical Reviews* **2009,** *67* (3), 247-260.

CHAPTER 4

CHIRAL AU COATED CDTE TWISTED NANORIBBONS

4.1 ABSTRACT

Chiral CdTe nanoribbons (NRs) are coated with Au NP spots and Au shells by soaking substrates coated with chiral, twisted CdTe NRs in $HAuCl_4$ solutions. High energy sites along the twisted CdTe NRs that are caused by crystal defects in the NR reduce the $HAuCl_4$ to atomic Au. The deposition first results in Au NP spotted, twisted CdTe NRs. As the reaction continues, the Au spots become more numerous and eventually form a polycrystalline Au shell around the twisted NRs. These Au NPs and the Au film are studied with high resolution transmission microscopy, and energy dispersive spectroscopy. The Au NP spotted/coated chiral, twisted, CdTe NRs may have applications in negative index materials (NIMs).

4.2 INTRODUCTION

Because of their ability to refract light on the opposite side of the normal, NIMs have intriguing properties that may find application in construction of perfect lenses and cloaking devices[1-4]. The two most actively pursued approaches to NIMs are of use resonating metallic nanostructures and photonic crystals. Metallic nanostructures typically contain a combination of thin wires and resonant rings that provide the negative

permittivity and negative permeability components, respectively[5-7]. The size of the nanostructure determines the wavelengths at which the material would behave as a NIM. By scaling down the size of nanostructures, NIM could be obtained in near-IR regime[8]. However at such small dimensions, metals no longer behave as perfect conductors and further scaling down is not efficient[9]. Another major problem with this design is that operating near plasmonic resonances may lead to very high losses from metals, as well as limits the restoration of evanescent components of light. Although compensation of losses by embedding a gain material, such as CdTe NPs[10], is being explored, it still in the very early stages of development[11]. On the other hand, photonic crystals are based on the excitation of photonic band gaps with negative slope to support negative phase velocity in the medium[12], and are limited in their performance due to scattering from surface imperfections.

Recent theoretical investigations have showed that NIMs can also be realized through chiral materials under certain conditions[1,13-16]. In a chiral medium, the Maxwell's constitutive relations are given in Eq. 4.1-4.3,

$$D = \varepsilon E + \xi H \tag{4.1}$$

$$B = \zeta E + \mu H \tag{4.2}$$

$$\zeta = \xi^{*} = j \kappa \, \mathrm{sqrt}(\mu_0 \varepsilon_0) \tag{4.3}$$

where κ is the dimensionless chirality parameter. Some trivial algebra can show that one of the required conditions to achieve negative refraction is

$$|\kappa| > \sqrt{\mu\varepsilon} \tag{4.1}$$

A chiral material breaks the degeneracy between two circularly polarized waves, increasing the effective refractive index for one polarization and reducing the refractive

index for the other ($n_{\pm}= \sqrt{\mu\varepsilon} \pm\kappa$, where κ is the chirality parameter). Normal chiral materials, even at very high concentration, have the chirality parameter on the order of 10^{-3}, whereas the required magnitude is of order 1, as was recently calculated[17]. (The term $\sqrt{\mu\varepsilon}$ is effectively the refractive index of a material and such values are typically on the order of 1). Thus one of the key requirements for making a negative index material via the chiral route is to induce strong chirality for n_- to reach an effective negative value.

Zhang et al demonstrated chiral NIMs using artificially synthesized metallic chiral resonators[18] and Zheludev et al demonstrated similar results using twisted planar metal patterns in parallel planes[19,20]. The size of the resonating structures was on the order of a few hundred micrometers and the chiral response generated was observed around 1 THz. The resonating structures in both cases were made from lithographic techniques, thus the scaling down of size becomes a challenging limitation. It is also to be noted that resonating structures will have to be simplified substantially in their design as research scales down the size using lithographic techniques, effectively reducing the strength of chirality.

In this chapter, a novel method of preparing chiral metallic nanostructures is presented. These nanostructures may find applications in NIMs. Specifically, we produce twisted NRs of Au NPs by redox transformation of parent NRs from CdTe[21].

4.3 SYNTHESIS

Twisted CdTe NRs were produced according to literature[21]. The twisted NWs were produced from CdTe NPs with a reduced ratio of TGA stabilizer for the CdTe NPs in the initial synthetic step. The assembly process was allowed to proceed under ambient

light conditions, given it is known that light can cause defects such as truncations on the surface of the NPs that can change the magnitude and direction of the NP charge dipoles (leading to interesting assemblies). CdTe NP dispersions were prepared using literature[22] procedure with the fraction of TGA to Cd^{2+} close to ~1.0 in ratio. 1.095g of $Cd(ClO_4)_2 \cdot 6H_2O$ was dissolved in 200 mL of pure water. TGA was added into the solution at a molar ratio of ~1.0 against Cd^{2+}. The pH values of the solution were adjusted to 11.4 by the drop-wise addition of 1 M NaOH solution. The solution was de-oxygenated by bubbling N_2 through the solution for 60 minutes. Under stirring, H_2Te gas was passed through the solution with a slow nitrogen flow for 60 minutes. The precursors were converted to CdTe NPs by refluxing at approximately 100 ºC for 50 min. Dispersions with a luminescence peak of 550 nm were obtained. The CdTe NPs were then precipitated by addition of methanol and centrifuged for 20 minutes. The CdTe NPs were redispersed in pure water at pH 9 (modified by the addition of NaOH). The dispersion was exposed to ambient light and aged. The orange solution of NPs turned dark green in ~48 hours, which differs from previous studies were the dispersions turned dark brown[21]. Upon analysis, the samples showed distinctive helical structures and straight NWs. NRs twisting in both right and left oriented rotations were observed. Upon evaluating ~100 NWs, 52 NRs were right oriented and 48 NRs had left oriented twist[21]. The resulting NRs consist primarily of Cd and S enriched CdTe NRs[21].

The twisted CdTe NRs are then immobilized by modified layer by layer deposition[23]. For SEM characterization, piranha cleaned Si wafers (Si wafers are soaked in a mixture of 30 % (v/v) H_2O_2 and 70 % (v/v) H_2SO_4 for 30 minutes and rinsed) are used as substrates; for TEM characterization, carbon on holey carbon TEM grids supplied

by Ted Pella, Inc are used as substrates. The substrate is then soaked in 0.5 % (v/v) PDDA for 5 minutes, rinsed in water and air dried to create a thin, positively charged film on the substrate for the negatively charged twisted NRs to adhere. The substrate is then soaked in the twisted NR solution for 1 minute, rinsed in water and air dried. The resulting substrates give a good dispersion of the twisted CdTe NRs on the substrate (Figures 1 and 2). Once the twisted CdTe NRs are immobilized, the substrate is soaked in 0.01M $HAuCl_4$ for between 30 seconds and 5 minutes, at which time it is rinsed in water and air dried.

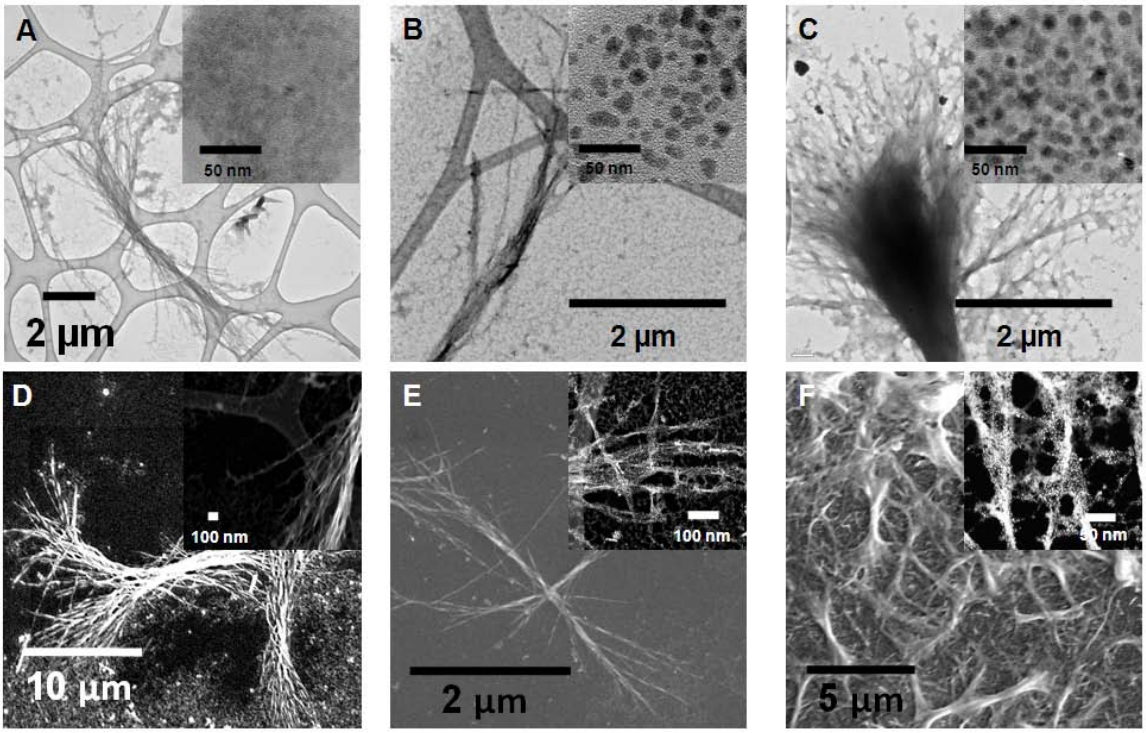

Figure 4.1. TEM images and HRTEM inserts of twisted NRs of A) CdTe NRs, B) Au NRs formed after 30 second soak of CdTe NR in $HAuCl_4$, and C) Au NRs formed after 2.5 minute soak of CdTe NR in $HAuCl_4$. SEM images and STEM inserts of D) CdTe NRs, E) Au NRs formed after 30 second soak of CdTe NR in $HAuCl_4$, and F) Au NRs formed after 2.5 minute soak of CdTe NR in $HAuCl_4$.

4.4 RESULTS AND DISCUSSION

Au NP patterned substrates are synthesized by the reaction of $HAuCl_4$ with chiral, twisted CdTe NR templates that have been immobilized on substrates (Figure 4.1). The reaction is rapid and occurs in an aqueous environment, and results in the formation of Au NPs that are patterned on the substrate in a similar geometry as the CdTe NR. The reaction can be controlled such that the Au NP patterning retains the pitch (pitch length of 240 ± 50 nm before[21], and 220 ± 30 nm after Au plating, as calculated using SEM in Figure 4.1B and E) and chirality (equal number of left and right hand helices) of the twisted CdTe NR. Since the CdTe NRs are a racemic mixture of helices, neither the CdTe NR coated substrates nor the Au NP patterned substrates show any chiral signal when measured with CD (Figure 4.S.1).

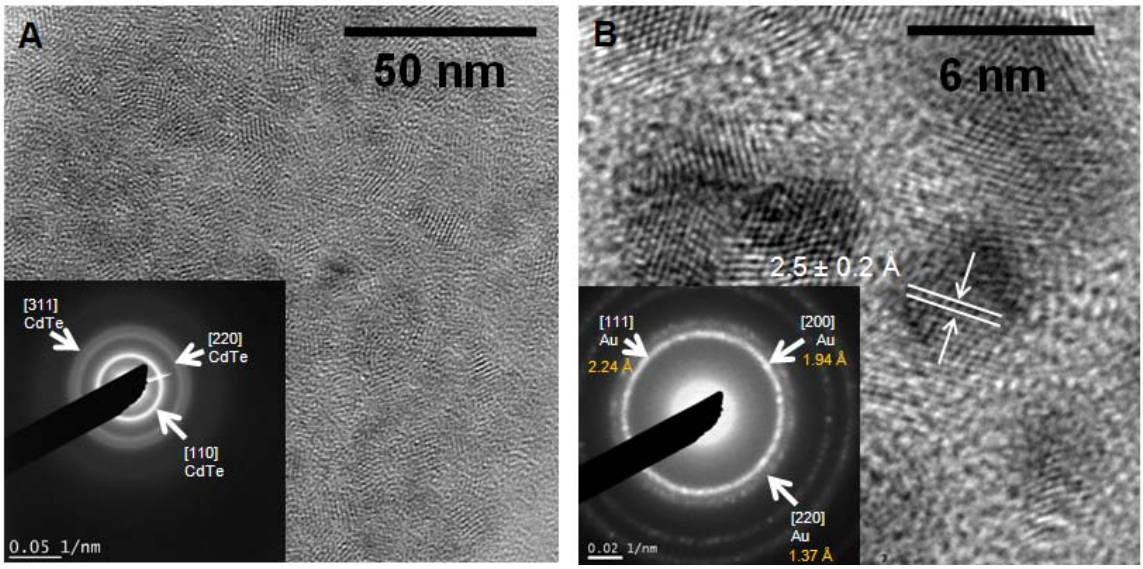

Figure 4.2. HRTEM images with electron diffraction pattern inserts of A) CdTe NRs, and B) Au NRs formed after 30 second soak of CdTe NR in $HAuCl_4$.

The probable reaction of the CdTe NRs with $HAuCl_4$ has been reported previously in literature systems with CdTe NPs[24] and in CdTe NWs[25] and is given as Rx. 4.1.

$$2AuCl_4 + 3CdTe \longrightarrow 2Au + 8Cl^- + 3Cd^{2+} + 3Te \qquad 4.1$$

Other systems have reported the formation of Au NPs on semiconductor[25-27] at high energy sites such as locations of extreme angles or defects that contain sufficient energy reduce the $HAuCl_4$ to atomic Au[28]. Since the NRs used in this study are highly polycrystalline (Figure 4.2A), they contain numerous high energy sites, so the reaction occurs simultaneously over the entire CdTe NR length, resulting in the formation Au NPs instead of a semiconductor NW with Au NPs adhered to the ends or vertices.

EDS of CdTe NR structures and Au NP structures seen in Figure 4.1 confirm the complete replacement of CdTe with Au with some residual S (Figure 4.3A and B). Electron diffraction and HRTEM of a single NR confirms that the polycrystalline zinc blende CdTe NR has been replaced by Au (Figure 4.2A and B). Note that the lattice parameters of the Au NP do not precisely match up with cubic Au as S has been incorporated into the Au NP lattice. Electron diffraction of a single NR also shows that the CdTe NRs contain many orientations of NPs in order to give a continuous circular diffraction pattern, whereas the Au NP diffraction pattern is not continuous, indicating that fewer Au NPs are present, thus creating a discontinuous circular image.

The discrete nature of the Au NPs is confirmed by EDS using STEM. Focusing the beam onto a NP gives a strong Au signal, whereas focusing between NPs gives no signal (Figure 4.3C). The Cu and Si peaks in the EDS spectra are background from the TEM grid and the EDS detector, respectively.

The discontinuous nature of the Au NPs is most likely due to the polycrystallinity of the template CdTe NRs (Figure 4.2A), as this provides numerous high energy defect

sites for Rx. 4.1 to occur. Since Au replaces CdTe at numerous sites along the NR, there are discreet Au NPs formed along the NR length. These Au NPs do not fuse along the NR length and instead result in a discontinuous layer of Au NPs adhered to the substrate in place of the CdTe NR. When the substrate is rinsed, some of Au NPs are dislodged, resulting in an Au NP pattern on the substrate in the place of the CdTe NR (Figure 4.1B and C). The S contained in the CdTe NRs is unreacted and is incorporated into the Au NPs. As the twisted NRs are exposed to the $HAuCl_4$ solution for longer periods of time, additional Au spots are seen in the NR (Figure 4.1C and F) and Au deposition occurs and fills the voids between the NRs to fill with Au (Figure 4.1C and F).

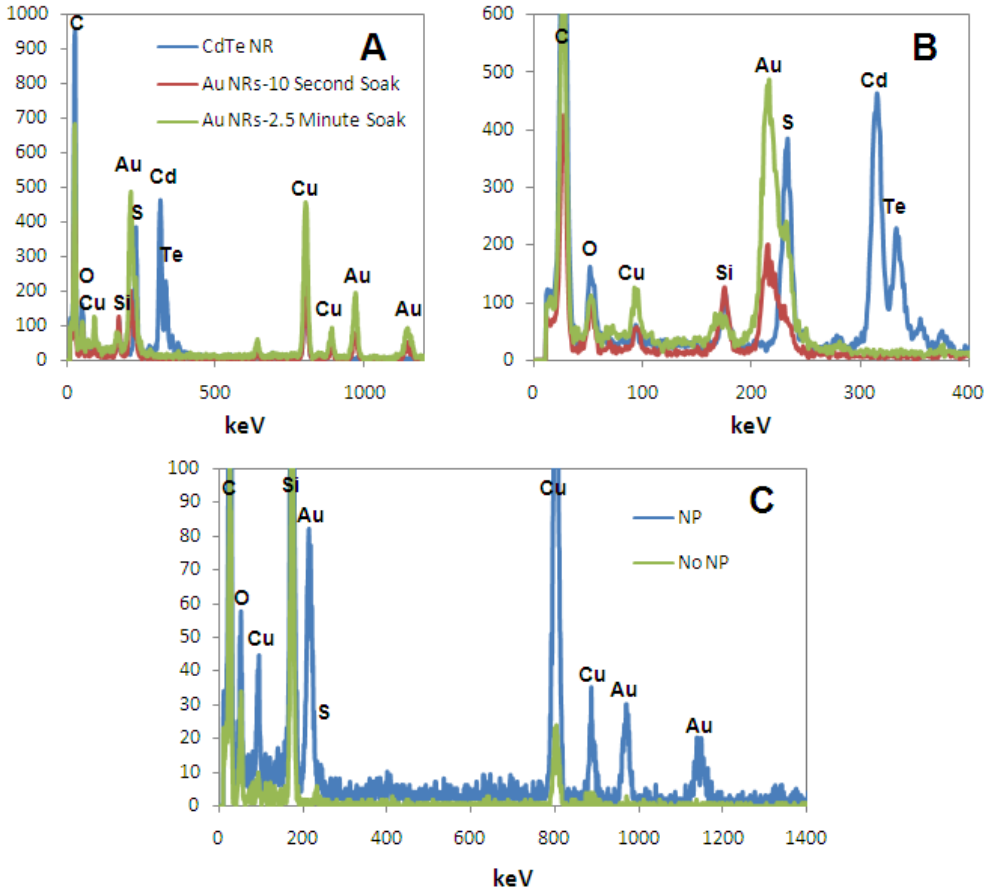

Figure 4.3. EDS spectra of A) CdTe NRs and Au NRs formed by soaking CdTe NRs in $HAuCl_4$ for 10 seconds and 2.5 minutes, B) Image A) expanded from 0-400 keV, C) an Au NP spot and between Au NP spots in a twisted Au NR formed by soaking a CdTe NR in $HAuCl_4$ for 30 seconds.

As expected, the PL and UV spectra of the CdTe NRs change dramatically upon reaction with $HAuCl_4$ (Figure 4.4). As expected, the PL signal of the CdTe NRs is quenched upon addition of $HAuCl_4$ and the formation of Au NPs. The UV absorbance of the CdTe NR coated quartz slide is also dramatically reduced upon formation of Au NPs, primarily because a substantial quantity of NR is removed by the coating process. There are no distinctive Au NP UV absorbance peaks visible in these samples because there are too few Au NPs on the quartz slide to provide a signal.

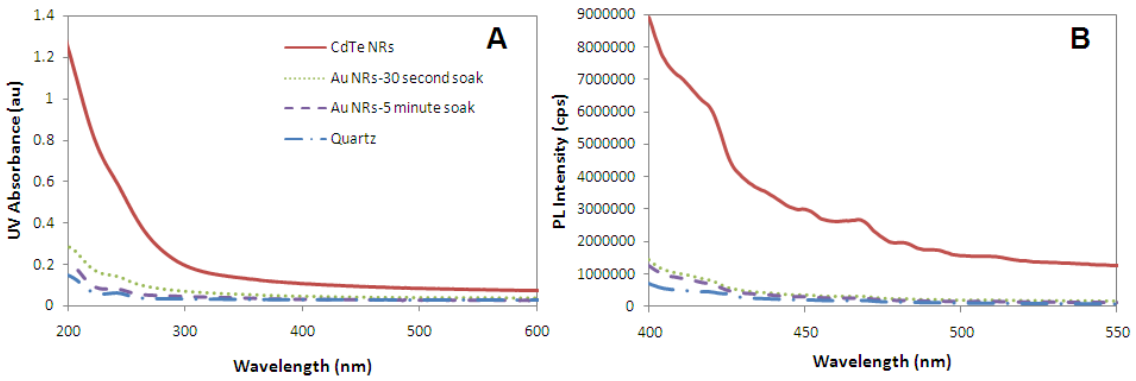

Figure 4.4. A) UV absorption spectra and PL emission spectra of CdTe NRs on a quartz slide, Au NRs formed by soaking CdTe NRs on a quartz silde in $HAuCl_4$ for 30 seconds and 5 minutes, and a clean quartz slide.

4.5 CONCLUSION

Chiral, twisted CdTe NRs are 1) surrounded by Au NP spots, and 2) coated by an Au shell by soaking substrates coated with chiral, twisted CdTe NRs in 0.01 M $HAuCl_4$ for various periods of time. Initial atomic Au deposition occurs at high energy sites along the twisted CdTe NR. Since the twisted CdTe NRs are polycrystalline and ultimately twist by strain created in the structure, there are many places for Au deposition to occur on the twisted NR. Further soaking results in an increase in Au spots along the twisted NR, until the spots eventually join to form a polycrystalline Au shell surrounding the twisted CdTe NR. If allowed to continue, the Au NP shell will begin to fill in the gaps

between the twisted NRs, much like the webbing between a duck's toes. These chiral, twisted NRs with Au spots/coating can potentially find uses in NIMs that are used as perfect lenses and cloaking devices. The next step of this research is to coat the twisted CdTe NRs in solution and verify their chiral signal.

4.6 ACKNOWLEDGEMENTS

I would like to thank Sudhanshu Srivasta and Ashish Agarwal for their help in the synthesis and characterization of these NWs. I would like to the University of Michigan's EMAL for its assistance with electron microscopy.

4.7 SUPPLEMENTAL MATERIALS

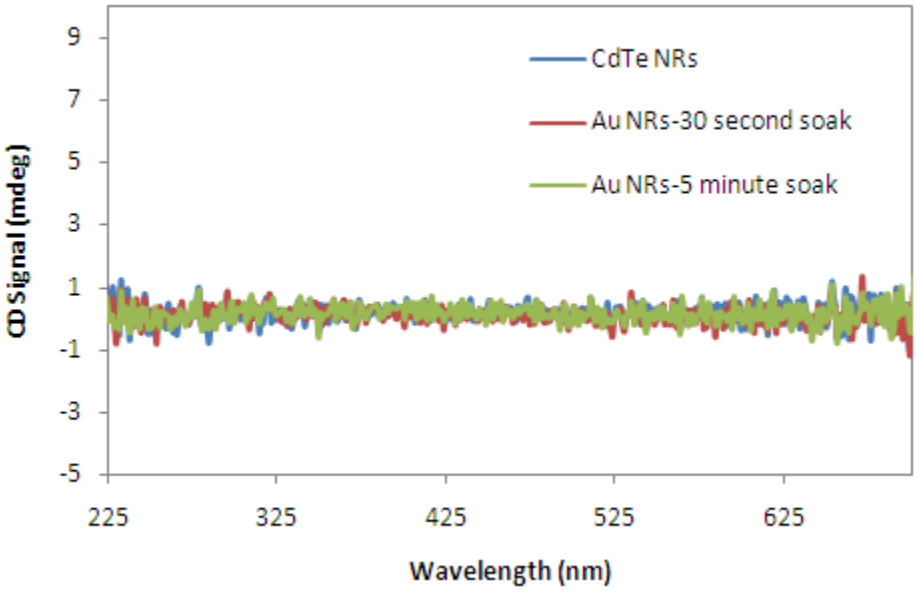

Figure 4.S.1. CD spectra of CdTe NRs on a quartz slide, Au NRs formed by soaking CdTe NRs on a quartz silde in $HAuCl_4$ for 30 seconds and 5 minutes.

4.8 REFERENCES

1. Pendry, J. B. A Chiral Route to Negative Refraction. *Science (Washington, DC, U. S.)* **2004,** *306* (5700), 1353-1355.

2. Pendry, J. B. Negative Refraction Makes a Perfect Lens. *Phys. Rev. Lett.* **2000,** *85* (18), 3966-3969.

3. Cummer, S. A.; Popa, B. I.; Schurig, D.; Smith, D. R.; Pendry, J. Full-wave simulations of electromagnetic cloaking structures. *Phys. Rev. E: Stat. , Nonlinear, Soft Matter Phys.* **2006,** *74* (3-2), 036621-1-036621/5.

4. Smolyaninov, I. I.; Hung, Y. J.; Davis, C. C. Magnifying Superlens in the Visible Frequency Range. *Science (Washington, DC, U. S.)* **2007,** *315* (5819), 1699-1701.

5. Shelby, R. A.; Smith, D. R.; Schultz, S. Experimental verification of a negative index of refraction. *Science (Washington, DC, U. S.)* **2001,** *292* (5514), 77-78.

6. Yen, T. J.; Padilla, W. J.; Fang, N.; Vier, D. C.; Smith, D. R.; Pendry, J. B.; Basov, D. N.; Zhang, X. Terahertz magnetic response from artificial materials. *Science (Washington, DC, U. S.)* **2004,** *303* (5663), 1494-1496.

7. Linden, S.; Enkrich, C.; Wegener, M.; Zhou, J.; Koschny, T.; Soukoulis, C. M. Magnetic Response of Metamaterials at 100 Terahertz. *Science (Washington, DC, U. S.)* **2004,** *306* (5700), 1351-1353.

8. Shalaev, V. M.; Cai, W.; Chettiar, U. K.; Yuan, H.; Sarychev, A. K.; Drachev, V. P.; Kildishev, A., V Negative index of refraction in optical metamaterials. *Opt Lett* **2005,** *30* (24), 3356-3358.

9. Soukoulis, C. M. Negative Refractive Index at Optical Wave-Lengths. *Science (Washington, DC, U. S.)* **2007,** *315* (5815), 1077.

10. Agarwal, A.; Lilly, G. D.; Govorov, A. O.; Kotov, N. A. Optical Emission and Energy Transfer in Nanoparticle-Nanorod Assemblies: Potential Energy Pump System for Negative Refractive Index Materials. *J. Phys. Chem. C* **2008,** *112* (47), 18314-18320.

11. Shalaev, V. M. Optical negative-index metamaterials. *Nat. Photonics* **2007,** *1* (1), 41-48.

12. Taubner, T.; Korobkin, D.; Urzhumov, Y.; Shvets, G.; Hillenbrand, R. Near-field microscopy through a SiC superlens. *Science (Washington, DC, U. S.)* **2006,** *313* (5793), 1595.

13. Cheng, Q.; Cui, T. J. Negative refractions in uniaxially anisotropic chiral media. *Phys. Rev. B: Condens. Matter Mater. Phys.* **2006,** *73* (11), 113104-1-113104/4.

14. mackay, T. G. Plane waves with negative phase velocity in isotropic chiral mediums. *Microwave and Optical Technology Letters* **2005,** *45* (2), 120-121.

15. Shen, J. Q.; He, S. L. Backward waves and negative refractive indices in gyrotropic chiral media. *Journal of Physics a-Mathematical and General* **2006,** *39* (2), 457-466.

16. Jin, J.; He, S. L. Focusing by a slab of chiral medium. *Optics Express* **2005,** *13* (13), 4974-4979.

17. Baev, A.; Samoc, M.; Prasad, P. N.; Krykunov, M.; Autschbach, J. A quantum chemical approach to the design of chiral negative index materials. *Opt. Express* **2007,** *15* (9), 5730-5741.

18. Zhang, S.; Park, Y. S.; Li, J.; Lu, X.; Zhang, W.; Zhang, X. Negative Refractive Index in Chiral Metamaterials. *Phys. Rev. Lett.* **2009,** *102* (2), 023901-1-023901/4.

19. Plum, E.; Zhou, J.; Dong, J.; Fedotov, V. A.; Koschny, T.; Soukoulis, C. M.; Zheludev, N. I. Metamaterial with negative index due to chirality. *Phys. Rev. B: Condens. Matter Mater. Phys.* **2009,** *79* (3), 035407-1-035407/6.

20. Plum, E.; Dong, J.; Zhou, J.; Fedotov, V. A.; Koschny, T.; Soukoulis, C.; Zheludev, N. I. 3D-Chiral metamaterial with artificial magnetic response. 2008; pp 3129-3130.

21. Srivastava, S.; Critchley, K.; Santos, A.; Kim, K.-S.; Podsiadlo, P.; Sun, K.; Lee, J.; Lilly, G. D.; Glotzer, S. C.; Kotov, N. A. Biomimetic Self-Assembly of Nanoparticles in Twisted Ribbons with Light Controlled Pitch. *Science* **2009**.

22. Gaponik, N.; Talapin, D. V.; Rogach, A. L.; Hoppe, K.; Shevchenko, E. V.; Kornowski, A.; Eychmuller, A.; Weller, H. Thiol-Capping of CdTe Nanocrystals: An Alternative to Organometallic Synthetic Routes`. *J. Phys. Chem. B* **2002,** *106*, 7177-7185.

23. Rogach, A. L.; Kotov, N. A.; Koktysh, D. S.; Susha, A. S.; Caruso, F. II-VI semiconductor nanocrystals in thin films and colloidal crystals. *Colloids and Surfaces, A: Physicochemical and Engineering Aspects* **2002,** *202* (2-3), 135-144.

24. Danieli, T.; Gaponik, N.; Eychmuller, A.; Mandler, D. Studying the Reactions of CdTe Nanostructures and Thin CdTe Films with Ag+ and AuCl4-. *J. Phys. Chem. C* **2008,** *112* (24), 8881-8889.

25. Carbone, L.; Kudera, S.; Giannini, C.; Ciccarella, G.; Cingolani, R.; Cozzoli, P. D.; Manna, L. Selective reactions on the tips of colloidal semiconductor nanorods. *J. Mater. Chem.* **2006,** *16* (40), 3952-3956.

26. Mokari, T.; Rothenberg, E.; Popov, I.; Costi, R.; Banin, U. Selective growth of metal tips onto semiconductor quantum rods and tetrapods. *Science (Washington, DC, U. S.)* **2004,** *304* (5678), 1787-1790.

27. Saunders, A. E.; Popov, I.; Banin, U. Synthesis of Hybrid CdS-Au Colloidal Nanostructures. *J. Phys. Chem. B* **2006,** *110* (50), 25421-25429.

28. Talapin, D. V.; Yu, H.; Shevchenko, E. V.; Lobo, A.; Murray, C. B. Synthesis of colloidal PbSe/PbS core-shell nanowires and PbS/Au nanowire-nanocrystal heterostructures. *J. Phys. Chem. C* **2007,** *111* (38), 14049-14054.

CHAPTER 5

"Cloud" Nanoassemblies: Quantum Dots Form Electrostatically Bound Diffuse Shells Around Gold Nanoparticles with Dynamic Exciton-Plasmon Coupling

5.1 ABSTRACT

Self-assembled structures of NPs can be produced by using very basic electrostatic interactions similar to ionic double electric layers in solution. Such assemblies were made from large, positively charged Au NPs surrounded by an electrostatically bound cloud of smaller, negatively charged CdSe/ZnS QDs or similarly charged CdTe QDs. Topologically, they are similar (although with lower degree of organization) to corona-like assemblies linked by polymers, and display similar PL intensity enhancement of CdSe/ZnS emission originating from quantum resonance between excitons and plasmons. The great advantages of such assemblies are (1) their highly dynamic nature compared to more rigid covalently bound assemblies; (2) simplicity of preparation, and (3) versatility of this system in respect to different NPs of any kind. Their structure is responsive to different media conditions, which can be used both for elucidation of most fundamental aspects of NP interactions, as well as for practical purposes in sensing and biology. We evaluate behavior of the "cloud" assemblies for different amounts and types of "satellite" NPs. It was demonstrated that

the behavior of these systems in media with different ionic strength can be described reasonably well by standard Gouy-Chapman formalism, which was rather unexpected considering the size of NPs compared to ions, but is very convenient for theoretical description and future studies.

5.2 INTRODUCTION

The preparation and understanding of behavior of complex nanoparticle (NP) systems are two of the most interesting aspects of nanotechnology. Recently, the ability of NPs to self-organize under intrinsic anisotropic interactions was discovered[1-4]. However, many of the resulting structures are fairly static assemblies: once the complex NP system is formed, the distances between the nanoscale components and their three-dimensional distribution becomes fairly permanent[5-8]. In general, flexible NP assemblies, such as NP polymers[9] and other conformation-rich NP superstructures, are likely to have quite interesting dynamics, but this aspect of their behavior had received limited attention. The first dynamic NP systems were made by using flexible polymeric tethers that could respond to the change of temperature[10], presence of specific biological components[11], or other parameters of the media, such as solvent composition[12]. However, the preparation of particle-on-a-rope type of structures is fairly complex and requires expensive bi-functional PEG oligomers. Notwithstanding the potential usefulness of NP assemblies connected by polymers as, for instance, nanoscale sensors reporting local chemical conditions, it would be interesting to observe a similar dynamic behavior in a much simpler system. The minimalism of the system is essential in terms of faster preparation. More importantly, however, such superstructures are expected to

be more dynamic, open, and adaptable to a larger number of NP systems, and, also, involve very fundamental aspects of inter-nanoparticle interactions.

The "cloud"-like assemblies in this work resemble the systems formed by general attractive interactions between spheres of different sizes. The nature of force can be quite different from gravitational, to magnetic[13] and electrostatic[14]. Surprisingly very little research has been done on NP structures created using purely electrostatic forces and mostly from a different perspective. Layer-by-layer assembly of oppositely charged NPs and polymers has been used to produce NP-polymer composites. However, in most cases, LBL assembly cannot be classified as purely electrostatic and, more importantly, it results in solid state material that is quite different from the purpose of this work[15-18]. Other systems are made by adsorption of metal NPs[19] and semiconductor quantum dots (QDs)[20,21] onto latex colloids. They are soluble, but not dynamic, and made primarily to impart certain properties of nanoparticles to more traditional latex colloids. Some research has been done on products of interaction of oppositely charged nanostructures with more complex dimensionality, including the pairing of NPs with cellulose fibers[22], carbon NTs[23], carbon fullerenes[24], and organic dyes[25]. Again, they are made to induce strong connection between the constituents to gain either appropriate mechanical or charge transfer characteristics. Among the variety of nanostructures made by using electrostatic forces and relevant to the assemblies described below, one study might be particularly representative[26]. This work describes electrostatic assembly of small (2 nm diameter), negatively charged Au NPs on large, positively charged SiO_2 NPs (15 nm diameter). The result is a precipitate made of both types of particles, with the relative size and connectivity of Au and SiO_2 NP in this precipitates varying with the ratio of both

components[26]. However, this work focused only on the effect of the NP ratio on the assembly geometry, and not on the dynamic properties of the system in varied environments. Just like in many examples provided above, the resulting assembly is neither dynamic, nor particularly optically active. Although, it certainly provides great flexibility in choosing the building blocks that contribute to the properties of the resulting solids.

To acquire greater optical activity and new optical properties the combination of oppositely charged semiconductor and metal NPs can be particularly fruitful[27-29]. When negative Au NPs stabilized with 3-Mercaptopropionic acid and positive CdS QDs stabilized with 2-(dimethylamino)ethanthiol at concentrations on the order of 10^{-5} m are mixed, the assemblies remain dispersed when either the NPs or QDs are in excess, and precipitate when in a 1:1 ratio[28]. This precipitate can be redispersed by changing environmental parameters such as NaCl concentration[28]. A similar system combining large, negative Ag NPs stabilized with thioglycolic acid and small, positive CdTe QDs stabilized with 2-dimethylaminoethanethiol again remain dispersed when either the NPs or QDs are in excess and precipitate when in a 1:1 ratio[27]. This system reports PL quenching of the QDs upon addition of the Ag NPs[27]. PL quenching and precipitation also occurs in mixtures of small, negative Au NPs stabilized with gallic acid and large, positive CdTe QDs stabilized with cysteamine with NP concentrations on the order of 10^{-5} [29]. None of these works describe PL enhancement upon the formation of electrostatic interactions of metal NP and semiconductor QDs, or relate the relative electrostatic potential of the NPs on the agglomerate structure.

With this in mind, we describe a seemingly simple, dynamic system held together by electrostatic attraction of large, positively charged Au NPs and smaller, negatively charged CdSe/ZnS QDs. In this system, NP concentrations are much more dilute than previous report (~10^{-7} M), so all NP solutions remain dispersed in solution and do not precipitate. Optical effects due to plasmon-exciton resonance[30] manifest in substantial PL enhancement, which are identical to those seen in covalently bound corona-like assemblies that have been observed[8,31]. The dynamic nature of these "cloud" assemblies has been demonstrated by varying the ionic strength of the media using NaCl. The behavior of the assemblies in various ionic concentrations is fairly accurately predicted using standard Gouy-Chapman theory. Although one might expect to see strong deviations from typical behavior of small Gouy-Chapman ions, this is apparently not the case for NPs. This fact is very convenient for future research.

5.3 SYNTHESIS

Aqueous l-cysteine stabilized CdSe/ZnS QDs are synthesized by a modification of current literature techniques[32,33]. Briefly, TBP/TOPO CdSe/ZnS QDs are synthesized in a single pot synthesis where 0.04 g CdO is loaded with 5.67 g HDA and 5.67 g TOPO. The solution is heated to 340^{o}C under an inert N_2 atmosphere until the CdO has dissolved and the solution is colorless. The solution is allowed to cool to 250^{o}C, at which time a Se/TBP solution (0.03 g Se and 6 mL TBP) is injected. The solution is stirred for 2-5 minutes, when a solution containing Zn and S precursors (125 μL 2M $Zn(CH_3)_2$, 130 μL $(TMS)_2S$, and 5.3 mL TBP) is injected drop wise at a rate of 0.1 mL/minute. The CdSe/ZnS QD solution is then lowered to 100^{o}C and stirred for 2 hours, at which time 60

mL of chloroform is added and the solution further cools to room temperature. Once cooled, excess TOP, HDA, and TBP are removed by multiple steps of adding methanol and centrifugation. Finally, the TOP/TBP ligands are replaced by l-cysteine by reconstituting the dry TOP/TBP NPs with 10 mL chloroform, adding 50 mL of a l-cysteine solution (50 mL H_2O, and 0.3 g l-cysteine adjusted to pH 9 with 1 M NaOH) followed by vigorous stirring and mild heating (50 ^oC) for several hours. The solution is then centrifuged to separate the organic and inorganic layers, and the organic layer is discarded. The resulting l-cysteine stabilized CdSe/ZnS QDs have an average diameter of 3.4 ± 0.6 nm.

L-cysteine stabilized CdTe QDs are synthesized according to the literature[34]. H_2Te gas, generated by the reaction of 0.5 M H_2SO_4 and Al_2Te_3 under an N_2 atmosphere, is bubbled through a 1.88 X 10^{-2} M $Cd(ClO_4)_2 \cdot H_2O$ and 4.56 X 10^{-2} M *L*-cysteine solution that has been adjusted to pH 11.4. The resulting CdTe QD solution is refluxed until the QDs have an average diameter of 2.6 ± 0.75 nm.

CTAB Au NPs are synthesized according to literature[35]. First, citrate stabilized Au seeds are formed by the reduction of 2.5 X 10^{-4} M $HAuCl_4$ with 0.1 M $NaBH_4$ in the presence of 2.5 X 10^{-4} M trisodium citrate. The Au seeds are grown by the addition of 2.5 X 10^{-4} M $HAuCl_4$ and 0.08 M CTAB growth solution. These CTAB Au NPs can be further grown by the subsequent addition of the CTAB growth solution. Excess CTAB is removed by centrifugation and subsequent redissolution of the Au NP precipitate in deionized water. The resulting Au NPs have an average diameter of 15.4 ± 1.9 nm.

TEM specimen are prepared by placing a drop of CdSe/ZnS QD and Au NP solution onto a TEM grid, flash freezing the droplet by submersion in liquid nitrogen, then freeze-drying the sample to preserve the structure of the NPs for TEM viewing.

5.4 RESULTS AND DISCUSSION

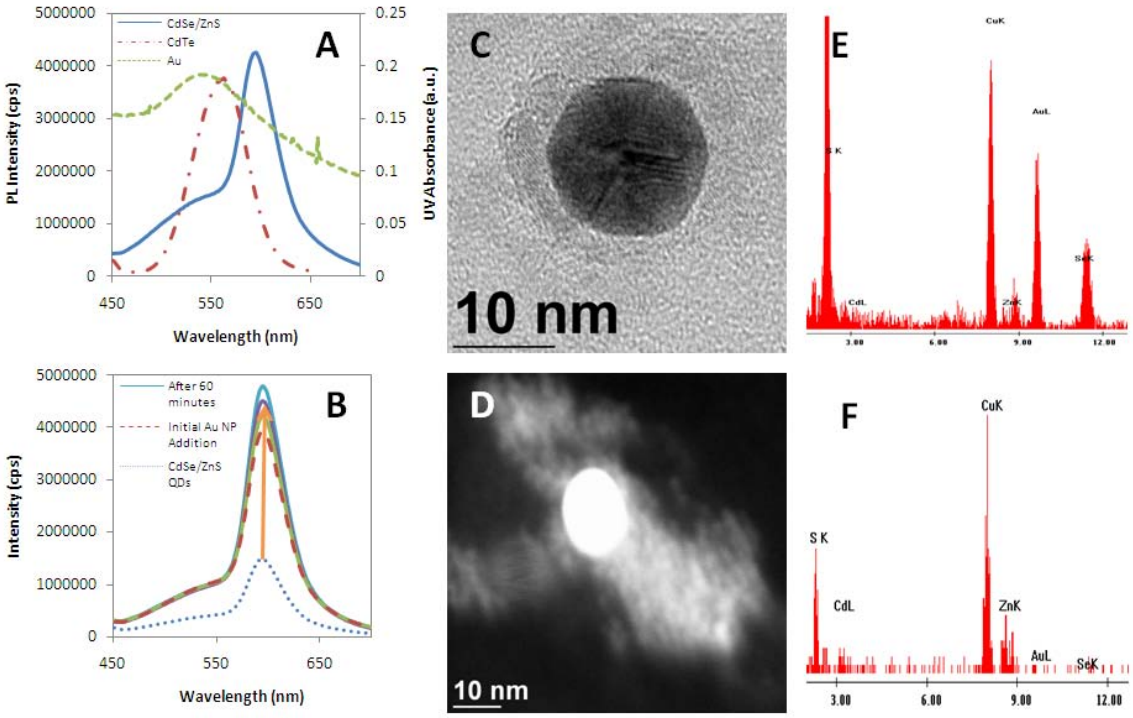

Figure 5.1. A) Au NP UV spectrum, CdTe and CdSe/ZnS QD PL spectra; B) PL enhancement of CdSe/ZnS QDs after addition of Au NPs; C) HRTEM of the assemblies formed in solution of Au NPs and CdSe/ZnS QDs; D) dark field STEM images of Au NP core with CdSe/ZnS QD cloud; E) EDAX spectra of the central part of the NP-QD electrostatic assembly; F) EDAX spectra of the peripheral part of the NP-QD electrostatic assembly QD cloud. The shape of the cloud is likely to be somewhat distorted by sample processing.

Although both metal and semiconductor particles in nanoscale dispersions can be generally described as generic NPs, in the framework of this study we will refer to Au nanocolloids as metal NPs and to semiconductor nanocolloids as QDs for better clarity of

the discussion and notations. CTAB stabilized Au NPs revealed UV-vis absorption at a peak of 535 nm, while PL spectra of *L*-cysteine-stabilized CdSe/ZnS QDs and CdTe QDs showed peaks at 590 nm and 555 nm, respectively (Figure 5.1A). These nanocolloids were chosen to achieve the spectral overlap of the Au NP plasmon and QD exciton[10,30,36]. This is necessary to achieve the quantum resonance between exciton and plasmon, which is exceptionally sensitive to the distance between the particles[10,11], so that the dynamic behavior of the nanoassemblies can be observed.

The electrokinetic zeta potential obtained by dynamic light scattering measurements, which is a measure of the potential outside of the double layer, is -75±8 mV for CdSe/ZnS QDs and +9±0.5 mV for Au NPs, respectively (Figure 5.2B). The positive Au NPs and the negative CdSe/ZnS QDs generate a strong Coulombic attraction that holds the CdSe/ZnS QDs in a shell around the Au NP core.

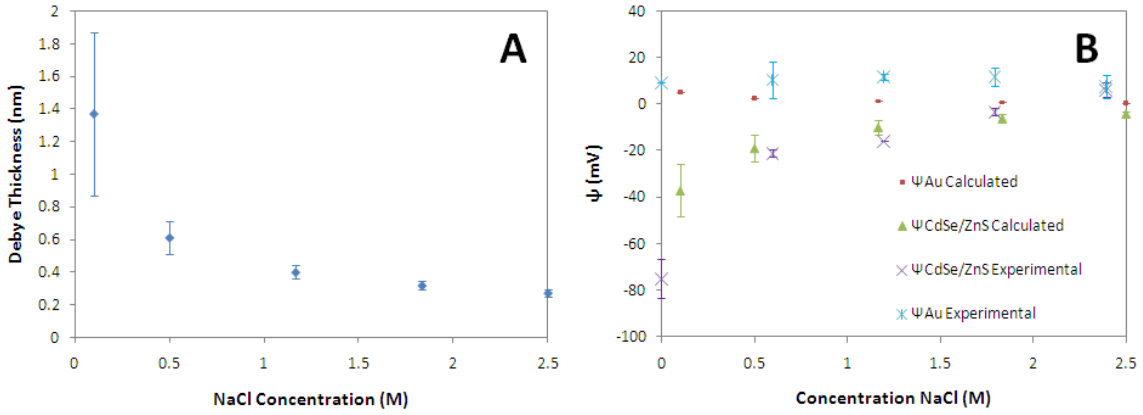

Figure 5.2. A) Calculated thickness of the Debye layer of Au NPs and CdSe/ZnS QDs with increasing NaCl concentration. This is calculated using Eq. 5 and is the same for both Au NPs, CdSe/ZnS QDs, and CdTe QDs. B) Change of the zeta potential of CdSe/ZnS QDs and Au NPs with NaCl concentration, both as calculated by Eq. 3 and 4, and as determined by zeta potential measurement.

The fact that core-satellite assemblies of the NPs and QDs form can be inferred from a number of experimental observations. The addition of Au NPs to the CdSe/ZnS QD solution results in a considerable enhancement of PL of CdSe/ZnS (Figure 5.1B). J.

Lee et. al.[8,10,11,31] reported effects that are qualitatively identical in NP assemblies made by covalent linking of QDs to metallic NPs using PEG. TEM images confirm the presence of cloud-like formations of QDs around more massive Au NP (Figure 5.1C and 5.1D). EDS spectroscopy clearly indicates that the "cloud" or satellites consists of predominantly CdSe/ZnS and virtually no Au, while the center of the assembly shows overwhelmingly strong peak of Au. The presence of Cd, Se, Zn, and S for the central part can be seen in the EDAX spectrum because the cloud of CdSe/ZnS QDs completely surrounds the Au NP core (Figure 5.1E and 5.1F). These NP structures are topologically similar to those made before by PEG tethering[10], NP assemblies held by magnetic forces[13], and gravitational assemblies of much larger objects.

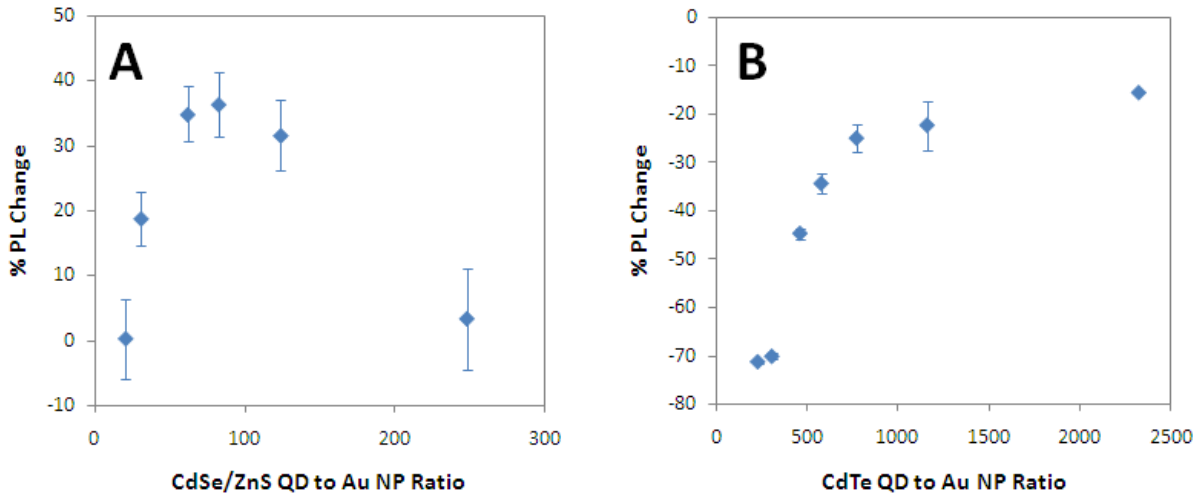

Figure 5.3. A) Percent PL change of CdSe/ZnS QDs from initial value for various Au NP:CdSe/ZnS QD ratios (v/v); B) Percent PL change of CdTe QDs from initial value for various Au NP:CdTe QD ratios (v/v). All measurements are done in water at pH 9.

As expected, the PL enhancement is dependent on the ratio of Au NPs to CdSe/ZnS QDs (Figure 5.3A). Since the PL spectrum is a cumulative property of all CdSe/ZnS QDs in the solution, at low Au NP:CdSe/ZnS QD ratios, some CdSe/ZnS QDs form associates with Au NPs and show PL enhancement; however, many excess

CdSe/ZnS QDs are free in the solution and do not form assemblies with Au NPs and hence show no PL enhancement. As the Au NP: CdSe/ZnS QD ratio is increased, more CdSe/ZnS QDs associate with Au NPs, so the PL intensity increases. As the Au NP: CdSe/ZnS QD ratio is increased further, there are insufficient CdSe/ZnS QDs to completely surround the Au NPs. Therefore, the PL intensity of the solution decreases with high Au NP: CdS/ZnS QD ratios. The maximum occurs when ***all*** CdSe/ZnS QDs form cloud-like, electrostatically bound assemblies with Au NPs.

Conspicuously, the PL of the CdSe/ZnS QDs is never quenched by mixing with Au NPs, which is quite different than observations in other systems of Au and other semiconductor QDs[29,37], which should probably be attributed to different organization of the particles.

The UV absorbance of assemblies of Au NPs and CdSe/ZnS QDs was measured for various ratios of Au NPs/CdSe/ZnS QDs to ensure that the UV absorbance (and thus the Au NP plasmon) does not shift as the number of CdSe/ZnS QD is varied (Figure 5.4). This is a concern as it has been reported that the Au NP plasmon can shift in response to changes in the dielectric constant[38,39] and refractive index[40,41] of the material surrounding the Au NP, as has been shown to happen when metal NPs are surrounded by various materials[38,39]. If the Au NP plasmons shift when surrounded by CdSe/ZnS QDs in solution, then this could be an alternative explanation to the change in PL intensity in response to Au NP and CdSe/ZnS QD ratio instead of the shape effect of the structure. However, the Au NP absorbance is constant with various CdSe/ZnS QD ratios and does not shift (Figure 5.4) because the dielectric constant of the material surrounding the Au NP is not sufficiently changed by the presence of CdSe/ZnS QDs. Most of the work

showing Au NP absorbance shifts have involved direct Au NP contact on thin films[40] and three-dimensional NP networks[38,39], whereas the system presented here of Au NPs and CdSe/ZnS QDs does not offer sufficient contact with CdSe/ZnS QDs to affect the plasmon.

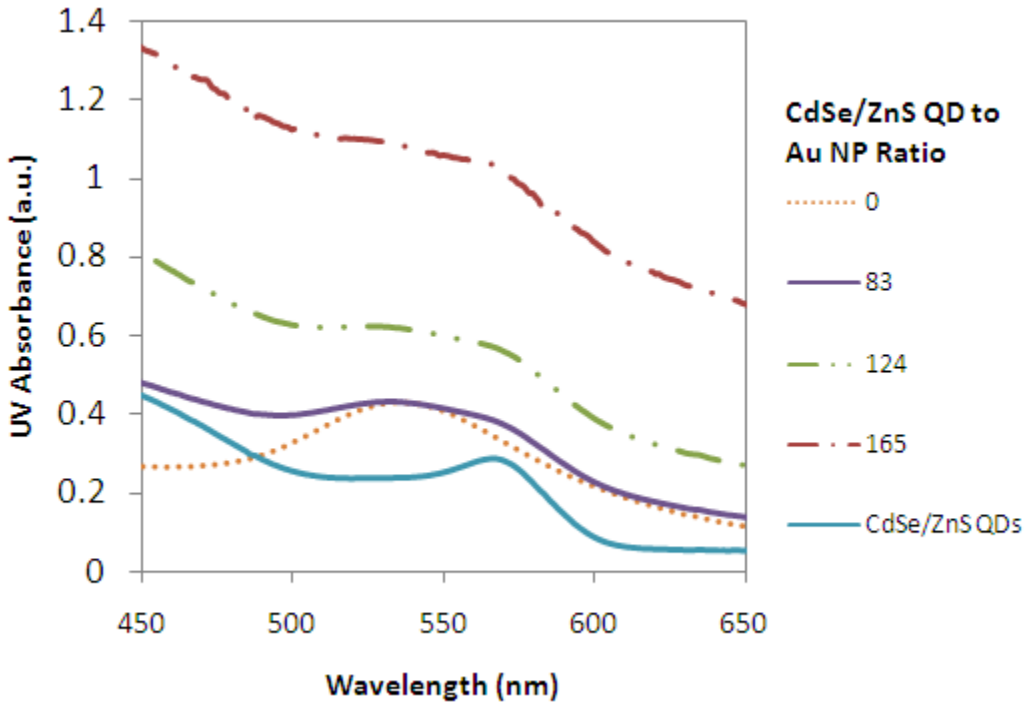

Figure 5.4. UV Absorbance of Au NPs and CdSe/ZnS QDs.

It should be noted that mixtures of CdTe QDs and Au NPs do not result in PL enhancement (Figure 5.3B) or precipitate. These assemblies serve as a negative control in the framework of this study. This is because CdTe QDs are much less negatively charged (zeta potential -20 mV) than CdSe/ZnS QDs. So, the attractive Coulombic force between the CdTe QDs and the Au NP is much smaller than that between the CdSe/ZnS QDs and the Au NPs. Therefore, CdTe QDs do not form a sufficiently closely positioned stoiciometric shell around the Au NPs, and the QD exciton and metal plasmon of Au NPs

do not resonate well and no PL enhancement is observed. This occurs even though the Au NP plasmon and the CdTe QD exciton have substantial overlap (Figure 5.1). Certainly some individual events of CdTe QDs and Au NPs approaching five- ten-fold of PL enhancement can occur, but the number of these events is relatively small and may be offset by some quenching process taking place with CdTe QDs.

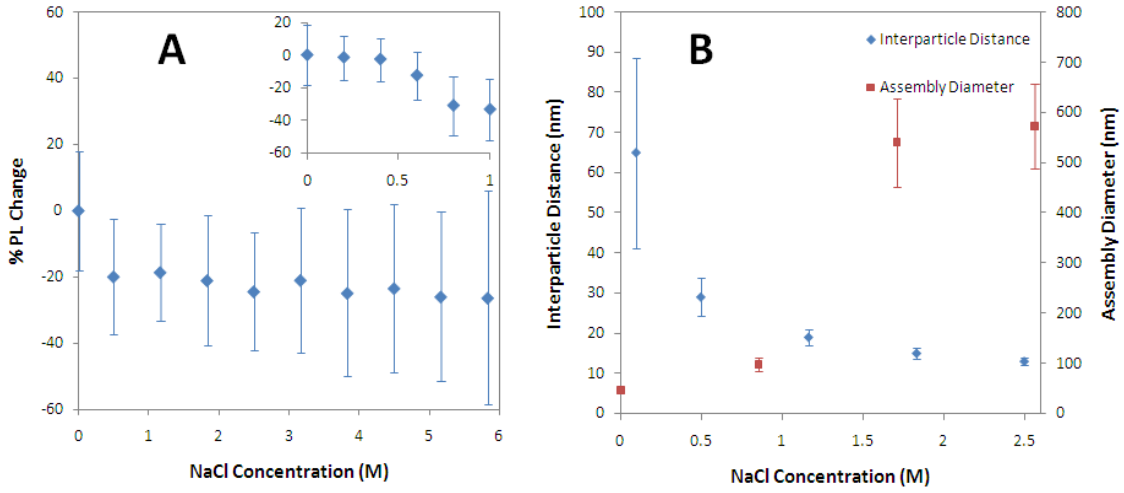

Figure 5.5. A) PL intensity dependence of Au NP and CdSe/ZnS QD cloud assemblies on ionic strength. Insert is PL dependence between 0 and 1 M NaCl. B) Theoretical calculation of the inter-particle distance of the Au NP and CdSe/ZnS QDs, and change in the diameter of the Au NP and CdSe/ZnS QD assemblies with increasing NaCl concentration as measured by DLS.

Due to the electrostatic nature of associates between two oppositely charged nanocolloids, the system should respond to variations in ionic strength (Figure 5.5A). Changes in ion strength effects can also be used to demonstrate the dynamic behavior of the Au NP and CdSe/ZnS QD structures. One can observe that PL intensity of the cloud assemblies incorporating CdSe/ZnS QDs decreases with increasing NaCl concentration (Figure 5.5). In order to rationalize these tendencies, one needs to understand how the distance between the center particle and satellites changes with environmental conditions as well as other processes in the system.

The geometrical structure of dynamic NP associates is governed mainly by two forces – Coulombic force leading to particle attraction and osmotic pressure between the particles leading to particle repulsion. Both of them are dependent on the thickness of the double layers surrounding the Au NPs and the CdSe/ZnS QDs. van der Waals forces are assumed to play an insignificant role and are neglected. At equilibrium, the attractive and repulsive forces are equal, as is shown in Eq. 5.1. This allows the equilibrium distance between the NPs to be calculated.

$$F_{Coulombic} = F_{Osmotic} \tag{5.1}$$

Coulombic force can be expressed as Eq. 5.2,

$$F_{Coulombic} = \frac{q_{Au\ NP} q_{CdSe/ZnS\ QD}}{4\pi\varepsilon\varepsilon_O R^2} \tag{5.2}$$

where $q_{Au\ NP}$ is the charge of the Au NP, $q_{CdSe/ZnS\ QD}$ is the charge of the CdSe/ZnS QD, and R is the inter-particle distance. The charge of the Au NP is related to the electrical potential around it, and can be expressed as Eq. 5.3,

$$q_{Au\ NP} = 4\pi\varepsilon\varepsilon_O r_{Au\ NP} \psi_{Au\ NP} \tag{5.3}$$

where $r_{\text{Au NP}}$ is the radius of the Au NP, and $\psi_{Au\ NP}$ is the electrical potential of the Au NP. The latter can be connected to the experimental value of zeta-potential in Eq. 5.4,

$$\psi_{Au\ NP} = \frac{4k_BT}{ze} \tanh\left(\frac{ze\psi_{o,Au\ NP}}{k_BT}\right) exp(-\kappa R) \tag{5.4}$$

where $\psi_{\text{o,Au NP}}$ is the zeta potential of the Au NP in volts and κ can be determined from the basic characteristics of the media in Eq. 5.5,

$$\kappa = \left(\frac{\varepsilon\varepsilon_o k_B T}{z^2 e^2 n^o N_{Av}}\right)^{1/2} \tag{5.5}$$

where N_{Av} is Avogadro's Number. $1/\kappa$ is the Debye length, which represents the thickness of the double layer.

The osmotic force can be calculated from Eq. 5.6,

$$F_{Osmotic} = \left(\frac{\pi d_{Au\,NP}^2}{4}\right)\left(\frac{n^o z^2 e^2 \psi_m^2 N_{Av}}{k_B T}\right) \quad (5.6)$$

where n^o is the concentration of NaCl in M, z is the charge of the electrolyte, e is the charge on an electron, k_B is the Boltzmann constant, and T is the temperature in Kelvin, and ψ_m, the electric potential at the midpoint between the NP and QD, is calculated from Eq. 5.7.

$$\psi_m = \psi_{Au\,NP} + \psi_{CdSe/ZnS\,QD} \quad (5.7)$$

Before application of this model, it was validated by calculating the electrokinetic potential of the Au NPs and CdSe/CdS QDs. As one can see the experimental results closely match those obtained by calculations (Figure 5.2B).

Using the described standard theoretical formalism, we can try to apply it to the description of the dynamic behavior of the cloud assemblies. As expected, as the ionic strength of the solution is increased, the thickness of the Debye layer decreases (Figure 5.2A).

The net result is that the Au NPs and the CdSe/ZnS QDs move closer together (Figure 5.5B) for higher values of ionic strength. However, this must result in the overall increase in intensity of exciton-plasmon resonance and, hence, luminescence enhancement, which contradicts the experimental observations. The clue to this conundrum comes from the data on DLS of the assemblies, which show that their average diameter increases with NaCl concentration (Figure 5.5B). Since the solution is very dilute (10^{-7} M), no visible precipitation is observed; however, STEM imaging confirms the formation of large agglomerates of Au NPs and CdSe/ZnS QDs when exposed to NaCl in solution (Figure 5.6). This process greatly disturbs the geometry of the

assemblies resulting in the formation of more chaotic, disorganized structures, which yield either a lower degree of enhancement or even quenching, especially when two gold NPs happen to form a rod-like structure[42,43].

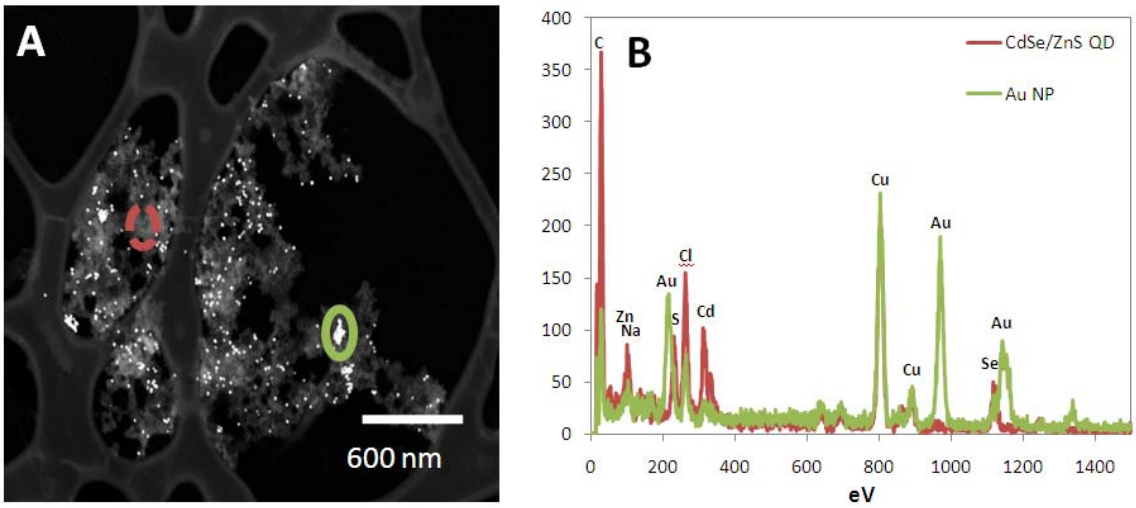

Figure 5.6. A) STEM image of large Au NP, CdSe/ZnS QD, and NaCl flocculate. B) EDS spectra of Au NP rich area, as indicated by the solid green circle; and of the CdSe/ZnS rich area, as indicated by the dashed red circle.

5.5 CONCLUSIONS

Aqueous assemblies of Au NPs surrounded by core/shell CdSe/ZnS QDs are produced by mixing positive Au NPs with negative CdSe/ZnS QDs. Upon formation, the PL is enhanced up to 40% by resonances between the Au NP plasmon and the exciton of the CdSe/ZnS QDs. The PL of the assemblies is sensitive to the Au NP: CdSe/Zns QD ratio such that low ratios gives little PL enhancement, ratios close to 100:1 give a maximum enhancement, and higher ratios give progressively less enhancement. This phenomenon occurs because the resonance between the Au NP and the CdSe/ZnS QD plasmon best occurs when there is a shell of QDs surrounding the Au NP core. The PL of the CdSe/ZnS QDs is never quenched by Au NPs because the exciton of the core/shell QD is trapped in the CdSe core by the higher bandgap ZnS shell. The formation of the

assemblies is driven by electrostatic interactions between the positive NPs and negative QDs; no PL enhancement is seen when Au NPs are mixed with CdTe QDs because the CdTe NPs are not as negatively charged as the CdSe/ZnS NPs, so the preferred assembly structure of an Au NP core surrounded by a shell of QDs does not occur. Additionally, the PL of the CdTe QDs is quenched by the presence of Au NPs. The structure, and therefore PL intensity of, the assemblies of Au NPs and CdSe/ZnS QDs are dependent on ionic strength of the solution, so the addition of sodium chloride to solutions with such assemblies causes a reduction in the PL intensity. This is caused because sodium chloride decreases the electrostatic attraction between the Au NPs and the CdSe/ZnS QDs and allows the NPs and QDs to move closer to one another. This causes large, unordered agglomerates of NPs and QDs to form. The PL dependence of the assemblies on ionic strength allows them a potential use as aqueous salinity sensors.

5.6. ACKNOWLEDGEMENTS

I would like to thank Jaebeom Lee for his assistance in the synthesis and characterization of these NPs and NP assemblies. I the University of Michigan's EMAL for its assistance with electron microscopy, and for the NSF grant #DMR-9871177 for funding for the JEOL 2010F analytical electron microscope used in this work.

5.7 REFERENCES

1. Tang, Z.; Kotov, N. A.; Giersig, M. Spontaneous organization of single CdTe nanoparticles into luminescent nanowires. *Science* **2002,** *297* (5579), 237-240.

2. Sinyagin, A. Y.; Belov, A.; Tang, Z.; Kotov, N. A. Monte carlo computer simulation of chain formation from nanoparticles. *J Phys Chem B* **2006,** *110* (14), 7500-7507.

3. Zhang, Z.; Tang, Z.; Kotov, N. A.; Glotzer, S. C. Simulations and Analysis of Self-Assembly of CdTe Nanoparticles into Wires and Sheets. *Nano Letters* **2007,** *7* (6), 1670-1675.

4. Nguyen, T. D.; Zhang, Z.; Glotzer, S. C. Molecular simulation study of self-assembly of tethered V-shaped nanoparticles. *Journal of Chemical Physics* **2009,** No.

5. Wang, S.; Mamedova, N.; Kotov, N. A.; Chen, W.; Studer, J. Antigen/antibody immunocomplex from CdTe nanoparticle bioconjugates. *Nano Letters* **2002,** *2* (8), 817-822.

6. Mamedova, N. N.; Kotov, N. A.; Rogach, A. L.; Studer, J. Albumin-CdTe Nanoparticle Bioconjugates: Preparation, Structure, and Interunit Energy Transfer with Antenna Effect. *Nano Letters* **2001,** *1* (6), 281-286.

7. Wang, Y.; Tang, Z.; Tan, S.; Kotov, N. A. Biological Assembly of Nanocircuit Prototypes from Protein-Modified CdTe Nanowires. *Nano Letters* **2005,** *5* (2), 243-248.

8. Lee, J.; Govorov, A. O.; Dulka, J.; Kotov, N. A. Bioconjugates of CdTe Nanowires and Au Nanoparticles: Plasmon-Exciton Interactions, Luminescence Enhancement, and Collective Effects. *Nano Letters* **2004,** *4* (12), 2323-2330.

9. DeVries, G. A.; Brunnbauer, M.; Hu, Y.; Jackson, A. M.; Long, B.; Neltner, B. T.; Uzun, O.; Wunsch, B. H.; Stellacci, F. Divalent Metal Nanoparticles. *Science (Washington, DC, U. S.)* **2007,** *315* (5810), 358-361.

10. Lee, J.; Govorov, A. O.; Kotov, N. A. Nanoparticle assemblies with molecular springs: A nanoscale thermometer. *Angewandte Chemie, International Edition* **2005,** *44* (45), 7439-7442.

11. Lee, J.; Hernandez, P.; Lee, J.; Govorov, A. O.; Kotov, N. A. Exciton-plasmon interactions in molecular spring assemblies of nanowires and wavelength-based protein detection. *Nature Materials* **2007,** *6* (4), 291-295.

12. Lee, J.; Orazbayev, A.; Govorov, A. O.; Kotov, N. A. Solvent effect in dynamic superstructures from Au nanoparticles and Cdte nanowires: experimental observation and theoretical description. *J. Phys. Chem.* Unpublished Work, 2009.

13. Erb, R. M.; Son, H. S.; Samanta, B.; Rotello, V. M.; Yellen, B. B. Magnetic assembly of colloidal superstructures with multipole symmetry. *Nature (London, U. K.)* **2009,** *457* (7232), 999-1002.

14. Israelachvili, J. N. *Intermolecular and Surface Forces: With Applications to Colloidal and Biological Systems;* 1985.

15. kirane-Jessel, N.; Lavalle, P.; Ball, V.; Ogier, J.; Senger, B.; Picart, C.; Schaaf, P.; Voegel, J. C.; Decher, G. Polyelectrolyte multilayer films - a general approach to functional coatings. *Macromol. Eng.* **2007,** *2*, 1249-1305.

16. Nolte, A. J.; Rubner, M. F.; Cohen, R. E. Creating Effective Refractive Index Gradients within Polyelectrolyte Multilayer Films: Molecularly Assembled Rugate Filters. *Langmuir* **2004,** *20* (8), 3304-3310.

17. Srivastava, S.; Kotov, N. A. Composite Layer-by-Layer (LBL) Assembly with Inorganic Nanoparticles and Nanowires. *Acc. Chem. Res.* **2008,** *41* (12), 1831-1841.

18. Han, Y.; Sukhishvili, S.; Du, H.; Cefaloni, J.; Smolinski, B. Layer-by-layer self-assembly of oppositely charged Ag nanoparticles on silica microspheres for trace analysis of aqueous solutions using surface-enhanced Raman scattering. *J. Nanosci. Nanotechnol.* **2008,** *8* (11), 5791-5800.

19. Qu, J. b.; Zhang, C. b.; Feng, J. y. Preparation of polystyrene-Ag latex particles and self-assembly behaviour of colloidal crystal. *Gaofenzi Cailiao Kexue Yu Gongcheng* **2008,** *24* (11), 180-183.

20. Fortuna, S.; Colard, C. A. L.; Troisi, A.; Bon, S. A. F. Packing Patterns of Silica Nanoparticles on Surfaces of Armored Polystyrene Latex Particles. *Langmuir* **2009,** ACS.

21. Sherman, R. L., Jr.; Ford, W. T. Semiconductor nanoparticles/polystyrene latex composite materials. *Polym. Prepr. (Am. Chem. Soc. , Div. Polym. Chem.)* **2003,** *44* (1), 1136-1137.

22. Dong, B. H.; Hinestroza, J. P. Metal Nanoparticles on Natural Cellulose Fibers: Electrostatic Assembly and In Situ Synthesis. *ACS Appl. Mater. Interfaces* **2009,** *1* (4), 797-803.

23. Liu, Y.; Jiang, W.; Li, S.; Li, F. Electrostatic self-assembly of Fe3O4 nanoparticles on carbon nanotubes. *Appl. Surf. Sci.* **2009,** *255* (18), 7999-8002.

24. Guldi, D. M.; Zilbermann, I.; Anderson, G.; Kotov, N. A.; Tagmatarchis, N.; Prato, M. Versatile Organic (Fullerene)-Inorganic (CdTe Nanoparticle) Nanoensembles. *J. Am. Chem. Soc.* **2004,** *126* (44), 14340-14341.

25. Halpert, J. E.; Tischler, J. R.; Nair, G.; Walker, B. J.; Liu, W.; Bulovic, V.; Bawendi, M. G. Electrostatic Formation of Quantum Dot/J-aggregate FRET Pairs in Solution. *J. Phys. Chem. C* **2009,** *113* (23), 9986-9992.

26. Galow, T. H.; Boal, A. K.; Rotello, V. M. A "building block" approach to mixed-colloid systems through electrostatic self-organization. *Adv. Mater. (Weinheim, Ger.)* **2000,** *12* (8), 576-579.

27. Wang, Y.; Li, M.; Jia, H.; Song, W.; Han, X.; Zhang, J.; Yang, B.; Xu, W.; Zhao, B. Optical properties of Ag/CdTe nanocomposite self-organized by electrostatic interaction. *Spectrochim. Acta, Part A* **2006,** *64A* (1), 101-105.

28. Kolny, J.; Kornowski, A.; Weller, H. Self-Organization of Cadmium Sulfide and Gold Nanoparticles by Electrostatic Interaction. *Nano Lett.* **2002,** *2* (4), 361-364.

29. Yang, D.; Wang, W.; Chen, Q.; Huang, Y.; Xu, S. Electrostatic assembles and optical properties of Au-CdTe QDs and Ag/Au-CdTe QDs. *Phys. E (Amsterdam, Neth.)* **2008,** *40* (10), 3072-3077.

30. Govorov, A. O.; Bryant, G. W.; Zhang, W.; Skeini, T.; Lee, J.; Kotov, N. A.; Slocik, J. M.; Naik, R. R. Exciton-Plasmon Interaction and Hybrid Excitons in Semiconductor-Metal Nanoparticle Assemblies. *Nano Letters* **2006,** *6* (5), 984-994.

31. Lee, J.; Javid, T.; Skeini, T.; Govorov, A. O.; Bryant, G. W.; Kotov, N. A. Bioconjugated Ag nanoparticles and CdTe nanowires: metamaterials with field-enhanced light absorption. *Angewandte Chemie, International Edition* **2006,** *45* (29), 4819-4823.

32. Reiss, P.; Bleuse, J.; Pron, A. Highly Luminescent CdSe/ZnSe Core/Shell Nanocrystals of Low Size Dispersion. *Nano Letters* **2002,** *2* (7), 781-784.

33. Huang, G. W.; Chen, C. Y.; Wu, K. C.; Ahmed, M. O.; Chou, P. T. One-pot synthesis and characterization of high-quality CdSe/ZnX (X, Se) nanocrystals via the CdO precursor. *Journal of Crystal Growth* **2004,** *265* (1-2), 250-259.

34. Gaponik, N.; Talapin, D. V.; Rogach, A. L.; Hoppe, K.; Shevchenko, E. V.; Kornowski, A.; Eychmuller, A.; Weller, H. Thiol-Capping of CdTe Nanocrystals: An Alternative to Organometallic Synthetic Routes`. *J. Phys. Chem. B* **2002,** *106*, 7177-7185.

35. Jana, N. R.; Gearheart, L.; Murphy, C. J. Seeding growth for size control of 5-40 nm diameter gold nanoparticles. *Langmuir* **2001,** *17* (22), 6782-6786.

36. Govorov, A. O.; Lee, J.; Kotov, N. A. Theory of plasmon-enhanced Forster energy transfer in optically excited semiconductor and metal nanoparticles. 76 ed.; 2007; pp 125308-1-125308/16.

37. Palomba, S.; Palmer, R. E. Optical coupling of core-shell quantum dots to size-selected gold clusters. *J. Appl. Phys.* **2008,** *104* (9), 094316-1-094316/6.

38. Taleb, A.; Petit, C.; Pileni, M. P. Optical Properties of Self-Assembled 2D and 3D Superlattices of Silver Nanoparticles. *J. Phys. Chem. B* **1998,** *102* (12), 2214-2220.

39. Hosoki, K.; Tayagaki, T.; Yamamoto, S.; Matsuda, K.; Kanemitsu, Y. Direct and Stepwise Energy Transfer from Excitons to Plasmons in Close-Packed Metal and Semiconductor Nanoparticle Monolayer Films. *Phys. Rev. Lett.* **2008,** *100* (20), 207404-1-207404/4.

40. Buso, D.; Pacifico, J.; Martucci, A.; Mulvaney, P. Gold-nanoparticle-doped TiO2 semiconductor thin films: optical characterization. *Adv. Funct. Mater.* **2007,** *17* (3), 347-354.

41. Underwood, S.; Mulvaney, P. Effect of the Solution Refractive Index on the Color of Gold Colloids. *Langmuir* **1994,** *10* (10), 3427-3430.

42. Li, X.; Qian, J.; Jiang, L.; He, S. Fluorescence quenching of quantum dots by gold nanorods and its application to DNA detection. *Appl. Phys. Lett.* **2009,** *94* (6), 063111-1-063111/3.

43. Nikoobakht, B.; Burda, C.; Braun, M.; Hun, M.; El-Sayed, M. A. The quenching of CdSe quantum dots photoluminescence by gold nanoparticles in solution. *Photochem. Photobiol.* **2002,** *75* (6), 591-597.

CHAPTER 6

CONCLUSIONS AND FUTURE WORK

6.1 CONCLUSIONS

Existing top-down technologies for the synthesis and organization of nanomaterials, while effective in producing evidence of concept techniques and applications, are typically time consuming, expensive, and difficult to scale-up. Furthermore, many top-down technologies have a limit on how far they can be scaled down. Therefore, NP self-assembly is of critical importance in order for devices with nano-scale components to be viable in a commercial sense. My research has focused on the self-assembly of nanomaterials for two practical purposes: 1) synthesis of higher ordered nanomaterials from the self-assembly of NPs, and 2) the assembly of metallic and semiconductor NP heterostructures to form ordered assemblies with practical applications.

Two projects presented in the previous chapters focused on the reorganization of CdTe and CdSe NPs into NWs. In the first, a method used to consistently control the length and diameter of TGA stabilized CdTe NPs by the addition of DMSO to the NP growth solution was presented. This method can shed new light onto the mechanism of NW formation. After the formation of pearl necklace NP assemblies in the growth

solution, Ostwald ripening caused the chains to recrystallize and grow. Experimental data suggest that the addition of DMSO inhibits the formation of the NP pearl necklace aggregates, but enhances Ostwald ripening. As such, in the concentration range when particle chains do form, the synthesis of NWs is accelerated. However, once electrostatic repulsion between the NPs becomes too strong (from higher DMSO concentrations), the formation of NWs abruptly stopped. The formation of NP pearl necklace assemblies and the direct fusion and growth of NP chains into NWs by Ostwald ripening are competing processes. The balance between these and other processes of NW assembly are affected by environmental factors, such as temperature and media composition.

The second project focused on the decomposition of CdTe and CdSe NPs into Te/Se NWs. It was shown that the addition of DMSO to a deoxygenated growth solution of CdTe NPs resulted in Te NWs with high aspect ratios. DMSO caused the CdTe NPs to decompose, creating Te^{2-} ions that were oxidized into Te seeds, from which Te NWs grew. Additionally, the presence of Se^{2-} ions to the growth solution resulted in longer, more tortuous Te NWs. The Se^{2-} ions may be introduced by the addition of Na_2Se salt, or by the decomposition of CdSe NPs. Low Se^{2-} concentrations resulted in long, straight Te NWs, medium Se^{2-} concentrations resulted in long, tortuous Te NWs, and high Se^{2-} concentrations stunted NW formation. The entire process is driven by Se incorporation into the Te seeds and NWs that foul them by creating crystal defects. This process prevents Te NW growth, allowing longer NWs to grow from the viable seeds. Small amounts of Se in the Te NWs resulted in point defects in the Te NW crystal lattice, which caused the NW to bend. Large Se^{2-} concentration caused fouling in all seeds and NWs, preventing further growth.

The next project focused on the placement of Au NPs onto chiral CdTe twisted NRs. Here, the twisted CdTe NRs are immobilized onto a substrate which is then soaked in an $HAuCl_4$ solution for various periods of time. Short soak times resulted in Au NP spots on the surface of the NRs. The Au deposition is caused because high energy sites on the polycrystalline NRs trigger Au reduction from Au^{3+} to atomic Au. As the soak time was increased, more Au NP spots formed, and eventually the Au NP spots merged, coating the CdTe twisted NR in an Au film. Still longer soak times caused overplating of the twisted NRs and their dog-bone structures.

The final project investigated core/shell assemblies of Au NPs surrounded by a cloud of CdSe/ZnS QDs. The PL intensity of core/shell CdSe/ZnS NPs can be enhanced by the addition of much larger Au NPs to the solution. Electrostatic interactions between the positive Au NPs and the negative CdSe/ZnS QDs drove the formation of these assemblies. Changing the ratio of Au NPs and CdSe/ZnS QDs produced different degrees of PL intensity enhancements, with the maximum PL enhancement occurring when all CdSe/ZnS QDs were used in clouds surrounding the Au NP core. Insufficient CdSe/ZnS QDs in the cloud did not provide the critical resonance of the exciton and plasmon, so the PL intensity enhancement was reduced, and excess CdSe/ZnS QDs in the solution mask the PL intensity enhancement of the assemblies. Quenching of the CdSe/ZnS QDs was not observed in this system because the exciton is trapped in the CdSe core of the CdSe/ZnS QDs and cannot escape to the Au NPs. Enhancement did not occur with CdTe QDs and Au NPs because their surface charges were not sufficiently different to cause the core and cloud assemblies to form. In fact, high ratios of Au NPs to CdTe QDs caused PL quenching because the exciton was allowed to escape the CdTe

QD. The formation of these Au NP and CdSe/ZnS QD assemblies was inhibited by changing the salinity of the solution because dissolve salts both mask the attractive electrostatic force between the Au NPs and the CdSe/ZnS QDs and reduce the thickness of the electrical double layer that surrounds the NPs and QDs. The net result is that large, unstructured agglomerates of Au NPs and CdSe/ZnS QDs form in solutions of high salinity.

6.2 FUTURE WORK

6.2.1 Synthesis of Variable Composition NWs

Variable composition NWs will be synthesized in a similar manner as the rough CdTe NWs. CdTe and CdSe NPs will be mixed, the stabilizers partially removed, and then redispersed in pH 9 water. This will allow pearl necklace agglomerates to form that contain a mixture of CdTe and CdSe NWs. Again, the synthesis will take place in room temperature with no DMSO in a deoxygenated environment. The resulting NWs should have regions rich in CdTe, and others rich in CdSe. In this manner, the chemical composition, and thus the bandgap, of the NWs will be variable.

Other composition gradient NWs of CdTe/CdSe NWs will be produced. They will occur by placing short CdTe NWs (room temperature, no DMSO, deoxygenated). A small amount of the CdSe growth solution is added to the CdTe NR solution, and the mixture is allowed to grow. Since Ostwald ripening should occur in both the CdTe and CdSe NPs, there will be Cd^{2+}, Te^{2-}, and Se^{2-} ions in the solution. It is hoped that both species will preferentially attach to the end of the CdTe NR, forming a CdTe/Se section on both ends of the CdTe NR. Additional amounts of CdSe NPs will be added over time.

As the concentration of CdSe NPs increases in the CdTe/Se NW solution, the amount of Se incorporated into the NW will increase. This will create a NW which is mostly CdTe in the middle and CdSe at the ends. NWs that are mostly CdSe in the middle and CdTe at the ends may be created by reversing the procedure. Here, CdSe NRs are first synthesized and small volumes of CdTe NP growth solutions are added with time. Since it expected that CdTe and CdSe NWs will grow at different optimal rates and conditions, it may be difficult to tune the experimental conditions to allow the gradient NWs to form. Variables that will affect the process include growth temperature, growth time, DMSO concentration in the growth solution, and the relative concentrations of the CdTe and CdSe NPs.

The second procedure to synthesize CdTe/CdSe gradient NWs is the slow addition of Na_2Se to forming CdTe NRs. In this procedure, short CdTe NRs are synthesized and Na_2Se is slowly added over time. The addition of Na_2Se will provide Se^{2-} ions to the solution, much as Ostwald ripening does. NWs grown by this procedure will have middle sections rich in CdTe with the higher concentrations of CdSe in the end of the NW.

The NWs will again be studied using AFM, SEM, and TEM techniques. Length and diameter variations will be observed using the AFM, SEM and TEM. Other TEM techniques will also be used to study the crystalline structure of the NWs, such as electron diffraction, dark field imaging, STEM, and EDS. Confocal microscopy will also be used to study the CdTe/CdSe NWs. Again, the color of fluorescence should change along the NW with the chemical gradient. CdSe has a higher bandgap than CdTe, so

sections of the NW with higher CdSe concentrations should fluoresce at lower wavelengths than CdTe rich sections.

6.2.2 Application of Variable Bandgap NWs in Wavelength Shifting Sensors

One of the most interesting properties of the variable bandgap NWs produced in Section 6.2.1 is their PL properties, which will allow them to be useful in new photonic devices. Of particular interest is the use of these gradient NWs in the metal NP/semiconductor NW assemblies used in the Kotov group. These assemblies consist of a semiconductor NW surrounded by a shell of metal NPs that are linked using streptavidin and biotin linkages. Once the NPs are attached to the NW, the PL intensity is greatly enhanced, and the PL wavelength experiences a slight blue shift (10 nm maximum) while the luminescent lifetime decreases by roughly one half. For Au NP coated CdTe NWs, the PL enhancement and decrease in luminescent lifetime are caused when plasmons in the Au NPs shell are excited during incident illumination, which produces a strong electromagnetic field surrounding the CdTe NW. This causes the PL intensity of the semiconductor to increase and the lifetime to shorten. The PL blue shift is caused because of the slight nonuniformity of the CdTe NWs used and the PL lifetime decrease. For NWs with a longer lifetime, excitons have time to diffuse to lower energy regions along the NW. The low energy regions are the areas with the lowest band gap, which are the thickest regions of the NW. When the lifetime in the NW shortens, the excitons have shorter diffusion lengths, so they get trapped in higher energy sections of the NW, which are the narrower regions with larger band gaps. Since NWs with a larger band gap fluoresce with a lower wavelength than those with shorter band gaps, the CdTe NW experiences a blue shift in fluorescence when surrounded by a shell of Au NPs[3].

The blue shift is very small because the CdTe NWs used have a uniform composition and very little surface roughness.

It is hypothesized that the use of variable bandgap NWs in these structures will increase the blue shift of the NW because there will be larger band gap variations in gradient NWs than the more homogenous CdTe NWs used in the previous work. It is hoped that PL blue shifts greater than 50 nm will be produced to allow the fluorescence of the NWs to visibly change upon conjugation with Au NPs. The procedure outlined by J. Lee et al[4] will be followed for these NWs.

The PL properties of each step of the process will be measured. Again, it is believed that the PL wavelength of the gradient NW will undergo at least a 50 nm blue shift that is observable to the eye. TEM will be used to verify the attachment of Au NPs to CdTe NWs. A recurring problem with creating these types of assemblies is agglomeration of the NWs and NPs, which leads to precipitation loss of PL. If this problem presents itself in the conjugation of these assemblies, there are several alternate pathways including using shorter NWs (less growth time), more dilute conditions, and better mixing of the solutions.

The unique PL properties of the variable bandgap NWs should similarly allow novel PL wavelength shift sensors to be created. Most current sensors are based on PL intensity, which makes their use difficult. Intensity based sensors require an even concentration gradient of the sensor, in addition to precisely calibrated equipment to accurately measure the results. PL wavelength based sensors will not require an even concentration because their PL wavelength does not depend upon concentration.

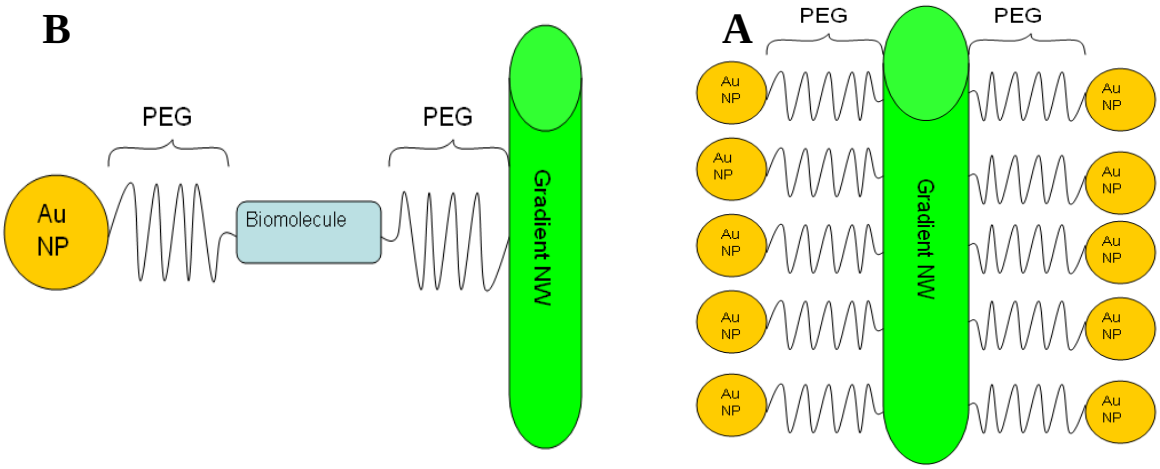

Figure 6.1. Wavelength based A) Temperature sensor, and B) antigen sensor.

The Kotov group has synthesized Au NP-PEG-CdTe NP temperature sensors in which the PL intensity varies with temperature[5]. When Au NPs enhance the PL intensity of the CdTe NP, its PL lifetime also decreases. By replacing the CdTe NPs with variable bandgap NWs, as shown in Figure 6.1A, the sensors should be useful as PL wavelength based sensors. When the temperatures are low and PEG is more tightly coiled, the Au NPs will be close to the gradient NW. This will enhance the PL intensity and decrease the PL lifetime. The exciton in the gradient NW will not have time to diffuse to lower bandgap regions of the NW, so a large blue shift should occur. When the temperature is raised, the PEG relaxes and the Au NPs move farther from the gradient NW. This will decrease the PL intensity and increase the PL lifetime. The exciton in the gradient NW will have time to diffuse to higher bandgap regions of the NW, causing a red shift.

Au NPs-PEG-variable bandgap NW temperature sensor assemblies will be made using both physical variable bandgap NWs (rough NWs) and composition variable NWs. The general structure of these sensors is shown in Figure 6.1A.

Sensor assemblies will be made using a procedure outlined by J. Lee et al[5] to make the Au NP-PEG-CdTe NP temperature sensor. The Au NPs-PEG-variable bandgap NW assemblies will then be tested for PL wavelength shifts in response to temperature fluctuations. The temperature of the solution will be varied from 20 ^{o}C to 60 ^{o}C while the PL wavelength and intensity are recorded. It is expected that both the physical gradient NW assemblies and the composition gradient NW assemblies will exhibit wavelength shift sensing. TEM will be used to verify the attachment of Au NPs to the gradient NWs.

Similar variable bandgap NW wavelength sensors can be engineered to sense a variety of substances like pH, biomolecules, other chemicals, and anything else that could change the interparticle distance between the Au NPs and the gradient NW. For example, many polymers relax in some solvents and contract in others. These polymers may be used in assemblies instead of PEG to allow solvent concentration to be determined. Biomolecules like antibodies, which change shape when they bind to specific antigens, could be incorporated into the sensor assembly as shown in Figure 6.1B. This will permit the assemblies to be used to test for specific antigens, allowing them to be used to identify cancer markers, as well as test for diseases.

The Au NPs/variable bandgap NW sensors are also solution based, allowing them to be used in many fluidic devices. Potential uses include microfluidic devices, where they can measure mixing and chemical composition. The gradient NW sensor assemblies can also be used in cell scaffolds to measure chemical gradients through the scaffolds.

6.2.3 Application of Gradient NWs in ESCs

Exciton solar cells (XSCs) work by the creation of an exciton from the absorption of photons, which diffuses to an interface where the electron and hole are separated to produce current[2].

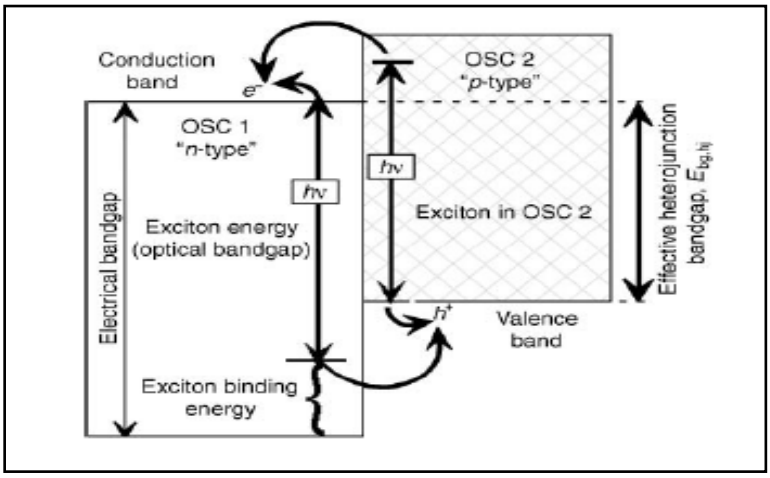

Figure 6.2: "Energy-level diagram for an excitonic solar cell at zero field. Excitons created by light absorption in OSC 1 and 2 do not possess enough energy to dissociate in the bulk (except at trap sites). But the conduction-band valence-vand offsets at the interface between OSC 1 and OSC 2 provide an exothermic pathway for dissociation of excitons in both phases, producing electrons in OSC 1 and holes in OSC 2."[2]

Excitons are bound electrons and holes that are generated when an EHP absorbs photons. Excitons are formed in materials where, when stimulated, an electron and hole are unable to separate and form an uncharged, tightly bound pair that is unaffected by electric fields[2]. This phenomenon usually occurs in organic materials and certain nanostructures. In organic materials, the exciton forms for two reasons. The first is a large Coulomb potential surrounding the electron hole pair that extends over a large volume. The second is because of weak non-covalent interactions between organic molecules, which results in a narrow bandwidth**Error! Bookmark not defined.**. Nanostructures such as NPs and NWs confine EHPs in certain dimensions. These

nanostructures create quantum confinement, which in turn creates discrete energy levels that are atom like[6]. This prevents the EHP from separating and creates an exciton.

The resulting exciton has gained an energy called the optical bandgap, E_{opt}. The optical bandgap has less energy than the energy of free EHP, which is the energy of the bandgap, E_{bg}. Figure 6.2 gives a schematic showing the optical bandgap compared to the bandgap[2].

Since the E_{opt} is less than the E_{bg}, excitons are the preferred state in certain organic and nano materials. They are free to diffuse inside of the material in much the same way free electrons and holes diffuse. The diffusion length of excitons varies with different materials. Since the exciton is uncharged, the direction of the exciton is random and is referred to as drift. To separate electrons and holes from excitons, the exciton must be exposed to a region that has a lower bandgap than the E_{opt}. This occurs at interfaces and trap sites. Trap sites exist in all types of solar cells and do not significantly affect the performance of XSCs. Here, excitons dissociate into electrons and holes, one of which is trapped in the site. The other is free to diffuse through the material. The behavior of excitons at interfaces governs the behavior of XSCs. When interfaces are created so that a material with a bandgap smaller than the E_{opt} borders the material with the excitons, the exciton will separate into an EHP[2].

When the exciton reaches an interface, it separates into electrons and holes. The electrons move to electron conducting regions (n-type) and holes to hole conducting regions (p-type). Since excitons are constantly dissociating into electrons and holes at the interface, a gradient is created where the concentration of electrons and holes is greater at the interface than the opposite end of the region. This concentration gradient drives the

flow of electrons and holes to opposite ends of the material. When the device is connected to a circuit, a current will flow because electrons are driven around the device to recombine with holes.

The materials used in inorganic nanostructured solar cells are similar to those used in today's solar cells. However, the structures of the cells, along with the way the devices work, are very different from today's solar cells. The n-conducting nanorods, nanowires, or nanoparticles can be fabricated from a number of different materials, ranging from CdS to CdSe to CdTe. The band gap size of these semiconductors must be larger but still close to the band gap size of the surrounding p-conducting material. These materials not only match the bandgap size of the n-conducting materials, but also have a close crystal lattice match with the n-conducting materials. The band gap sizes of some nanostructured materials can be seen in Table 6.1.

n - conducting		**p - conducting**	
Material	**Band Gap (eV)**	**Material**	**Band Gap (eV)**
CdS	2.6	CIS	1.04
CdSe	1.84	CIGS	1.00
CdTe	1.61		

Table 6.1: Comparison of materials and general band gap energies of those materials for both n and p type semiconductors[1].

Research has also found that large dipoles in the nanostructures help to quickly promote the electron from one electrode to the other. These dipoles are a result of the high charge difference between the two sides of the solar cell. The high crystallinity of

these structures helps to increase the mobility of the charge carriers. NW solar cell structures can be divided into three different structure types: nanorods, NWs, and NPs. Each structure has their own advantages and disadvantages, but each work in essentially the same way.

Nanorods and NWs work in a similar fashion to NPs. Nanorods and NWs avoid any high energy tunneling which may occur in a NP structure. Nanorods and NWs also excel in electron transport due to a dipole which occurs through the length of the rod. If a NR is connected between the solar cell's two electrodes, electron moves fast enough that it has no time to diffuse to the sides of the rod wall and recombine. The efficiency of electrons traveling through the NRs/NWs is dependent on the crystallinity of the NW, the density of the NWs throughout the matrix, the overall size of the NWs, and the orientation of the NWs. As with NPs, the NWs must be in tune with the matrix around it, in terms of both band gap size and crystallinity. Better crystalline interaction at the P-N junction decreases the energy requirement for charge transfer between the semiconductors.

The incorporation of gradient CdTe/CdSe NWs into these devices offers the possibility of facilitating the diffusion of the exciton to the area of the NW with the lower bandgap (the CdTe rich regions). By aligning the NWs such that the low and high bandgap regions overlap, the XSC can more efficiently convert excitons into electrons and holes, and finally, electricity. A varied bandgap will also allow for more varied wavelengths of light to be used to create electricity.

6.3 REFERENCES

1. Kittel, C. *Introduction to Solid State Physics;* 1986; Vol. 6.

2. Gregg, B. A. The photoconversion mechanism of excitonic solar cells. *MRS Bulletin* **2005,** 20-22.

3. Lee, J.; Govorov, A. O.; Dulka, J.; Kotov, N. A. Bioconjugates of CdTe Nanowires and Au Nanoparticles: Plasmon-Exciton Interactions, Luminescence Enhancement, and Collective Effects. *Nano Letters* **2004,** *4* (12), 2323-2330.

4. Lee, J.; Govorov, A. O.; Dulka, J.; Kotov, N. A. Bioconjugates of CdTe Nanowires and Au Nanoparticles: Plasmon-Exciton Interactions, Luminescence Enhancement, and Collective Effects. *Nano Letters* **2004,** *4* (12), 2323-2330.

5. Lee, J.; Govorov, A. O.; Kotov, N. A. Nanoparticle assemblies with molecular springs: A nanoscale thermometer. *Angewandte Chemie, International Edition* **2005,** *44* (45), 7439-7442.

6. Shim, M.; Wang, C.; Norris, D. J.; Guyot-Sionnest, P. Doping and charging in colloidal semiconductor nanocrystals. *MRS Bulletin* **2001,** 1005-1008.